Untersuchung eines Aerospike basierten GOX / GH2 Dual-Mode-Thruster Systems für eine kryogene Oberstufe

Investigation of an Aerospike based GOX / GH2 Dual-Mode-Thruster system for a liquid propellant upper stage

Masterthesis of
cand. aer. Malte Gradetzke
IRS-19-S-066

Examiner:
Prof. Dr. Stefan Schlechtriem

Supervisors:
Dipl.-Ing. Christian Hessel (external)
M.Sc. Marius Wilhelm (internal)

ArianeGroup, Bremen
Institute for Space Systems, University of Stuttgart
20. February, 2020

UNIVERSITÄT STUTTGART
INSTITUTE OF SPACE SYSTEMS

Pfaffenwaldring 29 · 70569 Stuttgart · Phone +49 (0) 711 685-62375 · Fax: +49 (0) 711 685-63596 · www.irs.uni-stuttgart.de

Master Thesis Work

of Mr. Malte Gradetzke

Untersuchung eines Aerospike basierten GOX/GH2 Dual-Mode Thruster Systems für eine kryogene Oberstufe

Investigation of an Aerospike-based GOX / GH2 Dual Mode Thruster System for a liquid propellant upper stage

Motivation:

On an upper stage, hot and cold gas systems are used for GNC operations (stage positioning, propellant settling, disturbance control). Cold gas systems of cryogenic upper stages use the gas or gas mixture from the ullage compartment or a separate pressure vessel, while hot gas systems use a combustion gas. Hot gas systems are utilized for impulse and thrust gain in case the firing time does not require the use of the main engine. Although cold gas systems are more likely to be used for attitude control due to their lower thrust, they are also used for thrust generation in addition to the hot gas system for certain mission scenarios. So far, however, these systems are independent of each other. Within the scope of this master thesis, a Dual-Mode Thruster System (DMTS) should therefore be developed on a system level, combining hot and cold gas in one single thruster system. Cold gas can be GOX or GH2 created during the mission through boil-off, evaporation and tank re-pressurization. The hot gas comes from a gas generator. A dedicated thrust vector control via secondary injection of gas (SITVC) should be part of the DMTS in order to compensate for arising disturbances during thrust phases. Objective is to evaluate a performance gain through reduction of structure dry mass and needed propellant mass.

Task description of the Master thesis work:

- Familiarization with the topic
- Development of a stage model that allows to parametrically analyze the design of the DMTS and to determine the propellant needs of thrust generation and SITVC
- Investigation of the suitability of an Aerospike nozzle with SITVC capability for the DMTS
- Analyzation of the design feasibility by identifying the requirements and the systems constraints
- Comparison of the mass and propellant budgets of the current upper stage configuration with the configuration modified by the DMTS to evaluate a possible gain in performance
- Documentation of model data and results

The thesis will be accomplished at Arianegroup Bremen.

Internal supervisor: Marius Wilhelm, M.Sc.

External supervisor: Christian Hessel, Dipl.-Ing.

Starting date: 01.07.2019

Submission until: 01.01.2020

Acknowledgement of receipt:
I hereby confirm that I read and understood the task of the master thesis, the juridical regulations as well as the study- and exam regulations.

Prof. Dr. S. Schlechtriem
(Responsible Professor)

External Supervisor

Signature of the student

Declaration

I, ***Gradetzke, Malte*** hereby certify that I have written this ***Master thesis*** independently with the support of the supervisor, and I did not use any resources apart from those specified. The thesis, or substantial components of it, has not been submitted as part of graded course work at this or any other educational institution.

I also declare that during the preparation of this thesis I have followed the appropriate regulations regarding copyright for the use of external content, according to the rules of good scientific and academic practice[1]. I have included unambiguous references for any external content (such as images, drawings, text passages etc.), and in cases for which approval is required for the use of this material, I have obtained the approval of the owner for the use of this content in my thesis. I am aware that I am responsible in the case of conscious negligence of these responsibilities.

Bremen, 13.02.20, M. Gradetzke

Place, Date, Sign

I hereby agree that my ***Master thesis*** with the following title:

Investigation of an Aerospike-based GOX/GH2 Dual-Mode-Thruster System for a liquid propellant upper stage

is archived and publicly available in the library of the Institute of Space Systems of the University of Stuttgart ***without blocking period*** and that the thesis is available on the website of the institute as well as in the online catalogue of the library of the University of Stuttgart. The latter means that bibliographic data of the thesis (title, author, year of publication, etc.) is permanently and worldwide available.

After finishing the work I will, for this purpose, deliver a further copy of the thesis along with the examination copy, as well as a digital version.

I transfer the proprietary of these additional copies to the University of Stuttgart. I concede that the thesis and the results generated within the scope of this work can be used free of cost and of temporal and geographical restrictions for the purpose of research and teaching to the institute of Space Systems. If there exist utilisation right agreements related to the thesis from the institute or third parties, then these agreements also apply for the results developed in the scope of this thesis.

Bremen, 13.02.20, M. Gradetzke

Place, Date, Sign

[1] Stated in the DFG recommendations for „Assurance of Good Scientific Practice" or in the statute of the University of Stuttgart for „Ensuring the Integrity of Scientific Practice and the Handling of Misconduct in Science"

Abstract

On modern upper stages like the A6 Upper Liquid Propulsion Module (ULPM) there is a self-evident need for performance increase due to increasing competition in the launcher business. Specifically, it can be translated into potential reduction of propellant and dry mass. An innovative concept to achieve this could be a Dual Mode Thruster System (DMTS). Within the scope of this master thesis, the feasibility of such a thruster concept is investigated on a system level. The general idea is to combine hot and cold gas in one single thruster system. It is first presented as a general concept with its major requirements and constraints, but a specific use-case is made up here for the A6 ULPM. The cold gas is here gaseous oxygen (GOX) and gaseous hydrogen (GH2) from the propellant tanks. The hot gas comes from an external source: A gas generator used on the ULPM for a secondary thrust system and tank (re)pressurization called APU. To analyse the potential a stage model including models based on the system simulation environment EcoSimPro and Excel are developed. It is used to evaluate the dry mass impact and propellant consumption of the system. This model is set up in a way so that it can be used for future studies. The DMTS uses an aerospike nozzle with the capability of Thrust Vector Control (TVC) via secondary fluid injection SITVC. This should be a key function to counter disturbances which have otherwise to be countered by the currently installed Cold gas reaction control system (CGRS) responsible for GNC-operations. To evaluate the potential performance gain the propellant consumption for disturbance control within a defined mission scenario is compared between the DMTS and the CGRS. The same is done for the dry mass impact under the assumption that the DMTS can partially replace the CGRS.
In the future there might be a need for a higher thrust of the secondary thrust system. A second use-case is defined as an evolution design of the Dual Mode Thruster (DMT) to investigate an additional afterburning mode using GOX. Its performance is evaluated with a comparison of the deorbiting time and propellant consumption.
The suitability of an aerospike nozzle for the DMT is investigated, because of a potentially more light-weight design and the integration of the Secondary Fluid Injection Thrust Vector Control (SITVC). The development of an aerospike nozzle is not done in this study. This work was part of a innovation project and accompanied by partners from the TU Dresden focusing on aerospike nozzle design with SITVC capability. Their expertise and delivered data served as a starting point of this investigation.
This work does not foresee a detailed design of the thruster system. The impact of the DMTS on the APU was not studied.

Kurzfassung

Moderne Oberstufen wie die der neuen Ariane 6 Trägerrakete, auch ULPM genannt, haben einen fortwährenden Bedarf nach einer Leistungssteigerung aufgrund zunehmender Konkurrenz auf dem kommerziellen Markt für Trägersysteme. Leistungssteigerung kann hier als Reduktion von Treibstoff- und Trockenmasse gesehen werden. Ein innovatives Konzept, dass das erreichen könnte ist ein Dual-Mode Thruster. Im Fokus dieser Arbeit liegt deshalb die Untersuchung der Machbarkeit um das Potential dieses Systems zu ergründen. Die generelle Idee ist dabei Heiß- und Kaltgasressourcen in einem Schubsystem zu kombinieren. Es ist zunächst als ein allgemeines Konzept mit seinen Hauptrequirements und Beschränkungen, aber der spezifische Nutzfall liegt hier bei dem ULPM. Das Kaltgas steht hier als gasförmiger Wasserstoff (GH2) und Sauerstoff (GOX) aus den Treibstofftanks zur Verfügung. Das Heißgas kommt von einer externen Quelle: Ein Gasgenerator, der als sekundäres Schubsystem und zur Tankwiederbedrückung genutzt wird und als APU bezeichnet wird. Um das Potential zu analysieren ist es Teil dieser Arbeit ein Stufenmodell zu entwerfen. Das Stufenmodell besteht dabei aus Excel-basierten Modellen und Modellen erstellt mit der Simulationsumgebung EcoSimPro. Das Stufenmodell wird genutzt um die Trockenmasse und den Treibstoffverbrauch zu evaluieren. Es ist so aufgebaut, dass es für Folgestudien genutzt werden kann. Das Dual-Mode-Thruster-System besteht aus zwei Schubdüsen, die keine konventionellen Düsen, sondern Aerospikes sind. Diese haben eine Möglichkeit der Schubvektorsteuerung mittels Seiteninjektion von Fluid, bezeichnet als SITVC. Diese soll eine Schlüsselfunktion sein um Störungen auszugleichen, die aktuell mit dem CGRS ausgeglichen werden müssen. Der Treibstoffverbrauch beider Systeme für den Ausgleich eines definierten Störmoments soll das Treibstoffeinsparpotential aufzeigen. Dies wird der Strukturmasse gegenüber gestellt unter der Annahme, dass das DMTS das CGRS teilweise ersetzen kann.
Außerdem soll noch eine Weiterentwicklung in Richtung eines höheren Schubmodus gezeigt werden, weil in Zukunft der Bedarf danach aufkommen könnte. Dies soll mit einer zusätzlicher Nachverbrennung mit GOX im DMT erreicht werden. Das Einsparpotential soll mit einem Vergleich der Zeit für das Deorbitierungsmanöver und dem Treibstoffverbrauch aufgezeigt werden. Auf eine Analyse der zusätzlichen Trockenmasse wird aber verzichtet.
Die Eignung einer Aerospike für den DMT wird untersucht, weil sie potentiell eine höheres Schub-zu-Gewicht-Verhältnis und die Integration der SITVC bietet. Die Aerospike stellt nur eine Subkomponente dar und ihre Auslegung liegt nicht im Fokus dieser Arbeit. Zurzeit begleitet ein Team der TU Dresden das Dual-Mode-Thruster-Projekt und macht eine detaillierte Entwicklung dieser Düse. Deren Expertise und Daten dienten als Ausgangspunkt für die Untersuchungen.
Diese Arbeit untersucht die Machbarkeit dieses Konzepts auf Systemebene. Eine detaillierte Auslegung des Schubsystems ist nicht vorgesehen. Ebenso können nicht alle Einflüsse auf die angrenzenden Systeme, im Besonderen der APU mituntersucht werden.

Contents

List of symbols

Latin symbols

Symbol	Unit	Description
A	$[\mathrm{m}^2]$	Cross-sectional area
A_f	$[-]$	Amplification factor
c_p	$[\mathrm{J}/(\mathrm{kg\,K})]$	Specific heat capacity at constant pressure
d	$[\mathrm{m}]$	Diameter
e	$[\mathrm{J}/\mathrm{kg}]$	Specific internal energy
F	$[\mathrm{N}]$	Force
$g = 9.806$	$[\mathrm{kg\,m}^2/\mathrm{s}]$	gravitational acceleration at earth
h	$[\mathrm{J}/\mathrm{kg}]$	Specific enthalpy
I	$[\mathrm{N\,s}]$	Impulse
L	$[\mathrm{m}]$	Length
$\dot{m}$	$[\mathrm{kg}/\mathrm{s}]$	Mass flow
m	$[\mathrm{kg}]$	Mass
M	$[\mathrm{kg}/\mathrm{mol}]$	Molecular weight
M_P	$[\mathrm{N\,m}]$	Perturbing torque
MR	$[-]$	Mixture ratio
p	$[\mathrm{Pa}]$	Static pressure
$\dot{q}$	$[\mathrm{J}/(\mathrm{kg\,s})]$	Specific heat flux
$\dot{Q}$	$[\mathrm{J}/\mathrm{s}]$	Heat flux
R	$[\mathrm{J}/(\mathrm{kg\,K})]$	Specific gas constant
Re	$[-]$	Reynolds number
t	$[\mathrm{s}]$	Time
T	$[\mathrm{K}]$	static temperature
v	$[\mathrm{m}/\mathrm{s}]$	Velocity
V	$[\mathrm{m}^3]$	Volume
x	$[\mathrm{m}]$	Horizontal axis coordinate
y	$[\mathrm{m}]$	Vertical axis coordinate

z	$[\mathrm{m}]$	Axis coordinate perpendicular to x-y-plane

Greek symbols

Symbol	Unit	Description
Δ	$[-]$	Delta / Difference
Γ	$[-]$	Function of specific heat
η	$\left[\frac{\mathrm{kg}}{\mathrm{ms}}\right]$	Kinematic viscosity
κ	$[-]$	Specific heat ratio
ϵ	$[-]$	Expansion ratio
λ	$[\mathrm{W/(m\,K)}]$	Thermal conductivity
μ	$[\mathrm{kg/(m\,s)}]$	Dynamic viscosity
ρ	$\left[\mathrm{kg/m^3}\right]$	Density
ζ	$[-]$	Pressure loss coefficient
ξ	$[-]$	Friction coefficient

Indices

0	Vessel or total quantity
c	Chamber
i	Injectant
j	Node
k	Reactant
p	Primary
s	Side
up	Upstream
t	Throat
e	Exit
oxy	Oxidizer, here: GOX
red	Reducer, here; GH2 or GH2 + water vapour

Acronyms

APU	Auxiliary Power Unit
CAD	Computer aided design

CGRS	Cold gas reaction control system
CoG	Center of gravity
DAE	Differential Algebraic Equation
DMT	Dual Mode Thruster
DMTS	Dual Mode Thruster System
EL	EcoSimPro Language
ESA	European Space Agency
ESPSS	European Space Propulsion System Simulation
GH2	Gaseous Hydrogen
GGAPU	Gas Generator of Auxiliary Power Unit
GNC	Guidance, Navigation and Control
GOX	Gaseous Oxygen
ICBM	Inter-continental ballistic missile
IVF	Integrated Vehicle Fluids
LH2	Liquid Hydrogen
LOX	Liquid Oxygen
LPRE	Liquid Propellant Rocket Engine
NASA	National Aeronautics and Space Administration
ODE	Ordinary Differential Equation
OP	Operating Point
SI3N4	Silicon Nitride
SITVC	Secondary Fluid Injection Thrust Vector Control
TAPU	APU Nozzle
TVC	Thrust Vector Control
ULPM	Upper Liquid Propulsion Module
ViTF	Vinci Thrust Frame

1. Introduction

1.1. Motivation and goals of this work

For more than two decades now, commercial competitors in the launch business have entered the market increasing the pressure for innovation and cost-effective solutions on established launch providers. In general, terms like stage re-usability and 3D-printed engine parts come into mind. For upper stages like the one of the new Ariane 6 launcher called ULPM an enhanced performance and mission flexibility is demanded. Performance can be translated into reduction of propellant and dry mass. Therefore, design philosophies like Integrated Vehicle Fluids (IVF) are being followed with the ultimate goal to reduce the amount of needed pressurization gas like Helium and the waste of propellant for non-propulsive operations as well as getting rid of extra batteries [1]. That led to the development and integration of the Auxiliary Power Unit (APU) onto the A6 upper stage, a secondary thrust system based on a gas generator with the purpose to pressurize the tanks and deliver thrust by using a part of the propellant. This secondary thrust system makes the use of the main engine obsolete for certain mission phases and is used for boost-phases, deorbiting and propellant settling. During the mission GH2 and GOX accumulate in the ullage compartment of the tank due to evaporation and repressurization. The GH2 is used by the CGRS while the GOX will be vented when the pressure increases to much through unwanted heat influx. The propellant mass used for purposes like maneuvering and counter-acting disturbances is referred to as non-propulsive resources because they are lost for gaining axial thrust with the primary or secondary thrust system or the CGRS.
During longer operating times of the APU, small perturbations occur because the thrust of both APU Nozzles (TAPUs) is not fully equal all the time due to manufacturing tolerances and temperature differences among others. Additionally the Center of gravity (CoG) of the ULPM varies with mission time, payload configuration and sloshing of the propellant in the tanks. This results in perturbations of ca. 20 N m causing deviations from the set flight path [2]. Usually the CGRS counters these disturbances, but over a long operating time of the APU the GH2 resources used up by the CGRS become exceedingly high. So a dedicated TVC is desired for the two exhaust nozzles of the APU system.
In the future, the A6 upper stage as well as future european upper stages might have a need for a higher thrust as currently possible with the APU in order to perform deorbitation faster. Also the opposite is needed: Lower thrust modes so that the propellant settling is less costly. To find new technologies to answer those needs, innovation projects get funded to conduct feasibility studies. One of those projects is the DMT. The basic idea is a thruster that can be used for expanding cold or hot gas in the same nozzle. The hope is to partially replace the CGRS and save dry mass. If the capability of using GOX is added to the concept then the ULPM could use this for axial thrust gain. Using oxygen for thrust operations is thereby not a new concept. On the A5 ESC-A upper stage oxygen was used for manoeuvring purposes in a cold gas thruster [2]. Even though it is inferior in performance the re-use of oxygen presents a chance of better propellant management at the cost of higher dry mass necessary for piping.
This use of either cold or hot gas is defined here as Dual-Mode operation. The term Dual- or Multi-Mode appears in the literature with different definitions. Usually, one can find proposals for Dual-Mode Propulsion Systems, which are used as the main propulsion for a spacecraft [3]. Applications are widespread: From tri-propellant use-cases to a hydrazine based propulsion for thrust and attitude control. Those concepts do not necessarily use the same nozzle for all propellants.

More exotic ones can be used for the propulsion of cube satellites. The Dual Mode can consist hereby of electric acceleration of an ionized gas where the two modes are either with the electric circuit switched on or off. [4]
Moreover, the DMT shall have a dedicated TVC. Such can be realized by means of mechanical deflection of the exhaust jet or gimbals. The former comes with a performance loss, the latter involves a substantial increase in dry mass. Alternatively, there is the possibility of injecting fluid perpendicular into the primary flow called SITVC. A special advantage is that fluid dynamic phenomena due to interaction of the two flows lead to a higher side force than the one only from pure injection momentum. Instead of using it on a conventional bell-nozzle an aerospike is part of the DMT. While in the former the fluid is injected from the wall, here the injection is done laterally from the central cone or spike giving the aerospike its name. This presents a unique opportunity. Because the injection orifices point outwards away from the nozzle axis they can also be used in a stand-alone mode without the primary flow active [5]. This could be exploited to use the side injection for additional Guidance, Navigation and Control (GNC)-operations. Even though its main advantage of altitude-adaptability is abundant for a pure vacuum application, the aerospike promises the same performance as a conventional bell-nozzle, but with a more compact sizing.
DMT is defined as the thruster, DMTS includes two thrusters and the peripheral components. The first objective of this thesis is to identify the general requirements and constraints of the system. This can only be done rudimentary because of a lack of experimental data. The project which incorporates this investigation is founded on a cooperation with the TU Dresden. Currently, a team at TU Dresden is doing research on aerospike nozzles with SITVC [5, 6]. Their expertise was a vital part of identifying the constraints of the DMTS. Moreover, they delivered data from numerical simulations which are subsequently used to evaluate the performance of the nozzle and its suitability.
Main goal of this work is to analyse the propellant consumption and dry mass impact on the ULPM. Therefore, a reference use-case is set up in which the DMTs replace the TAPUs. To calculate the propellant consumption and dry mass a stage model needs to be developed. It is composed of models based on the system simulation environment EcoSimPro and Microsoft Excel. It is set up in way so that it can be used for follow-up studies and focuses on the development of an easily adaptable model in order to analyse the system performance parametrically. The DMTS uses an aerospike nozzle with the capability of TVC via secondary fluid injection SITVC. This should be a key function to counter disturbances which have otherwise to be countered by the currently installed CGRS responsible for GNC-operations. To evaluate the potential performance gain the propellant consumption for disturbance control within a defined mission scenario is compared between the DMTS and the CGRS. The same is done for the dry mass impact under the assumption that the DMTS can partially replace the CGRS. A comparison of the mass budget of the current configuration and the altered configuration shall then show if one can expect a performance increase or decrease. To answer possible future needs of the ULPM the work has a look into a higher thrust mode of the DMTS. Therefore, a second use-case is defined as an evolution design including an afterburning mode with GOX. Its performance is evaluated with a comparison of the deorbiting time and propellant consumption, but a dry mass impact is excluded from this work.

1.2. Structure of this work

In the following chapter the basic principles of this work are explained. The isentropic equations of state describing nozzle properties are shown here to later explain relations, but are not used specifically for calculating the results. Also the relevant boundaries of the ULPM are explained there. Due to confidentiality reasons the APU system is not quantitatively described. Chapter 3 then delivers the governing equations used in the EcoSimPro models. Furthermore, the basic components for modelling with EcoSimPro are shown.
In the ensuing chapter 4 the general concept of the DMTS is presented and the requirements of the

periphal components such as the valves and the subcomponents such as the nozzle are determined. At the end of this chapter three possible versions of the DMT are derived from the general concept. The first is the reference case and is extensively studied in chapter 6. Here the mass budgets are calculated. The second version is called the evolution design and its feasibility is rudimentary analysed in regards to the foreseen Dual-Mode operation in chapter 7. The third version is not part of this work. Before the reference case can be studied, the stage model needs to be set up. Its elements can be found in the chapter 5 inserted after the general concept definition. The first section deals with the geometric boundaries of the ULPM and gives the estimations used for the dry mass calculation. It also shows the current feed lines and the additional lines needed for the DMTS integration. However, a mass calculation is reserved for the subsequent chapter. The second section of the stage model chapter explains the build-up and validation of the EcoSimPro models employed for the propellant consumption calculation.
Because the aerospike nozzle is in its details defined by the project partners from the TU Dresden, their data entered the analysis at certain points of this work. Sometimes, iterations in the design process were necessary. It is made sure, that their generated data is distinctly labelled in this work.

2. Foundations of this work

2.1. Basic principles of rocket engines

The following principles of the isentropic thermodynamic relations of rocket engines were derived from common literature like Turner [7, p.42ff]. Actual results were not obtained with them in this work, but they will be used in the following chapters to explain certain correlations of flow properties and propulsion system parameters. The Γ function is here a shorter expression of the equation containing the heat capacity ratio κ.
The critical mass flow $\dot{m}$ through a nozzle is given in equation (2.1) and is proportional to the total pressure p_c and the throat area A_t and inversely proportional to the total temperature T_c in the chamber. The thrust F of the engine is principally a function of p_c, A_t and the nozzle expansion ratio ϵ. One of the most important parameters to characterize an engine is the specific impulse I_{sp}. It is independent of p_c and A_t and is only bound to the geometry via ϵ, but it is heavily dependent on the exhaust gas properties like T_c and the specific gas constant R. Other less influencing variables are the nozzle exit pressure p_e and the ambient pressure p_a.

$$\dot{m} = \frac{p_c A_t}{\sqrt{R T_c}} \Gamma(\kappa) \tag{2.1}$$

$$F = p_c A_t \Gamma \sqrt{\frac{2\kappa}{\kappa - 1}} \sqrt{1 - \left(\frac{p_e}{p_c}\right)^{\frac{\kappa-1}{\kappa}}} + \epsilon \frac{p_e - p_a}{p_c} \tag{2.2}$$

$$\epsilon = \frac{A_e}{A_t} = \Gamma \left(\frac{p_e}{p_c}\right)^{-1/\kappa} \left(\frac{2\kappa}{\kappa - 1} \left(1 - \left(\frac{p_e}{p_c}\right)^{\frac{\kappa-1}{\kappa}}\right)\right) \tag{2.3}$$

$$I_{sp} = \frac{F}{\dot{m} g} = \sqrt{R T_c} \sqrt{\frac{2\kappa}{\kappa - 1}} \sqrt{1 - \left(\frac{p_e}{p_c}\right)^{\frac{\kappa-1}{\kappa}}} + \epsilon \frac{p_e - p_a}{p_c} \tag{2.4}$$

Pressure losses in feed lines can be calculated with the common definition to be found in Idelchik [8, p.37]. ζ is the pressure loss coefficient and ρ the density.

$$\Delta p = \frac{1}{2} \zeta \frac{\dot{m}^2}{A^2 \rho} \tag{2.5}$$

2.2. Setup of the A6 ULPM

The Ariane 6 will be the new heavy payload launcher of Europe succeeding the Ariane 5. Its upper stage also called ULPM uses cryogenic hydrogen and oxygen as propellants for the Vinci main engine, a closed-cycle expander engine with 180kN. But this is not the only thrust generating system. A secondary system for low thrust operations is the APU which delivers thrust between 110 and 300N with two nozzles. The APU also the purpose of repressurizing the propellant tanks. The ULPM is equipped with a CGRS controlling altitude and attitude of the vehicle using GH2 from the part of the hydrogen tank that does not contain liquid, the ullage compartment. This tank is located below fairing and payload and has a nearly spherical shape. The oxygen tank is situated between hydrogen tank and Vinci Main engine and has a more flattened spherical shape. All images and explanations in this section originate from internal communication and documents within Arianegroup. [2, 9]
In order to simplify things the coordinate system is redefined here as in comparison to the real definition for the ULPM. The origin of the coordinates is located on the beginning of the Vinci Thrust Frame (ViTF). For this work the TAPUs lie in the here defined x-y-plane (see fig. 2.1). The z-axis rests perpendicular to it forming a left-handed coordinate system. The helium tanks are tilted to the x-y-plane with an angle of 55° (see fig. 2.2).
The CoG varies with the payload, and propellant loading and changes over the course of the mission. Also the dry structure is not final yet. For this work it is assumend that it stays within a range of 50 mm of the x-axis. The variation of its axial position is set to be between 4490 mm and $x_{CoG} = 7990$ mm over the course of the mission.

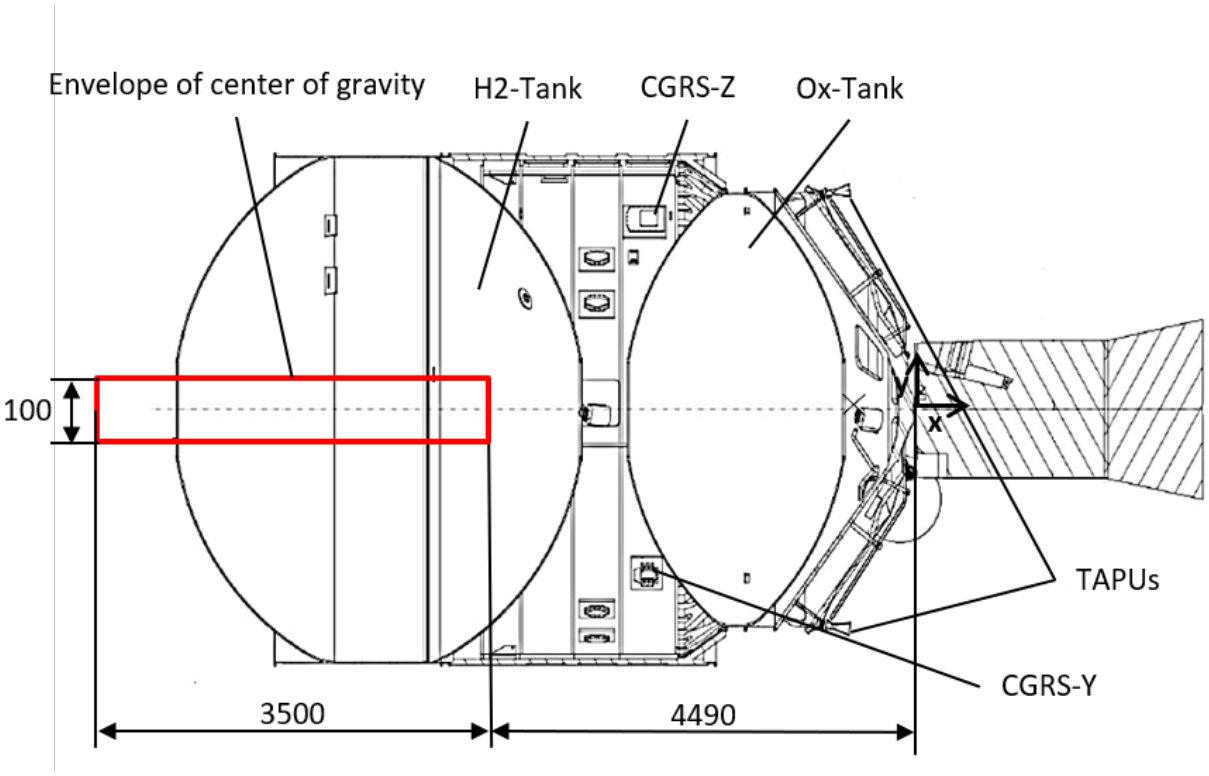

Figure 2.1.: Sectional view of the ULPM with estimated CoG envelope [9]

2.2.1. The APU

In order to follow a IVF design philosophy [1] and reduce the helium mass for pressurization purposes a pressurization and repressurization system working only with hydrogen and oxygen

has been developed. It consists of two pumps, a gas generator, a heat ex-changer, several valves and two exhaust nozzles. The pumps feed liquid hydrogen (LH2) and liquid oxygen (LOX) from the tanks to the heat ex-changer where it evaporates before entering the gas generator. The combustion in the gas generator delivers the heat for the evaporation in the first place. But not all of the evaporated propellant has to be combusted. Depending on the need a part of the GH2 or GOX, respectively is fed back into the ullage compartment of the propellant tanks effectively increasing temperature and pressure in the tank. The hot gas produced in the gas generator is expanded in two nozzles called TAPUs. Depending on the valve position all of the propellants fed to the APU system can be combusted and then only used for generating thrust. Six different Operating Points (OPs) have so far been defined for the APU. Three for (re)pressurization purposes and three for pure thrust generation. For this work only the latter are considered and designated as OP1, OP2 and OP3. They differ in their thrust level.

Hot gas OP	1	2	3
F_{TAPU} [N]	150	75	55

Table 2.1.: Thrust level per nozzle of selected OP of the APU [9]

To realize this the heat exchanger has a complex shape. It contains a circular closed body in the center funneling the hot gas into an annular channel. The heat is exchanged at the walls of several hundred tubes transporting the propellants inside the annular channel. The tubes are segmented into two oxygen and one hydrogen heat exchanger. While the hydrogen heat exchanger is always active, one of the oxygen heat exchangers is not when no tank pressurization is desired.

2.2.2. Cold gas properties

The already mentioned propellant tanks contain liquid and gaseous phases of hydrogen or oxygen, respectively. During boost or thrust mission phases an acceleration exerts a force on the propellants and they settle. Then the gaseous fraction can be extracted from the top of the tanks. This section of the tank filled with the gaseous phase of the propellant is considered ullage compartment. It is therefore not a fixed volume, but heavily depends on the pressure and temperature and the residual propellant mass in the tank. For the scope of this work only the gas fractions of the propellants are of interest. During the mission they experience a range of temperatures and pressures. The lowest and highest possible condition in the tank is used here to define two OP for this work. They are defined in 2.2 and 2.3. The pressure range is estimated to be same for both gases, but the oxygen experiences higher temperatures.

GH2	OP1	OP2
p_{Tank} [bar]	3.1	0.925
T_{Tank} [K]	153	34

Table 2.2.: Properties of GH2 in the ullage compartment

GOX	OP1	OP2
p_{Tank} [bar]	3.1	0.925
T_{Tank} [K]	300	150

Table 2.3.: Properties of GOX in the ullage compartment

2.2.3. The Cold gas reaction control system

The CGRS consists of four clusters. While the CGRS-Y and -Yn consist of a single longitudinal thruster each with the same orientation as the redefined x-axis, the CGRS-Z and -Zn-element carry five thrusters oriented longitudinal, tangential and radial to provide attitude control in each direction. To each other they are oriented with 90° with the CGRS-Y thruster tilted 50° to the x-y-plane. The CGRS and the TAPUs use actually the same nozzle. Only difference is the expansion ratio which is 5.2 for the cold gas thrusters. The pressure loss from tank over feed line and valve to the nozzle is derived from a reference sheet [9].

$$\frac{\Delta p_{CGRS,feed}}{p_{Tank}} = 0.239 \tag{2.6}$$

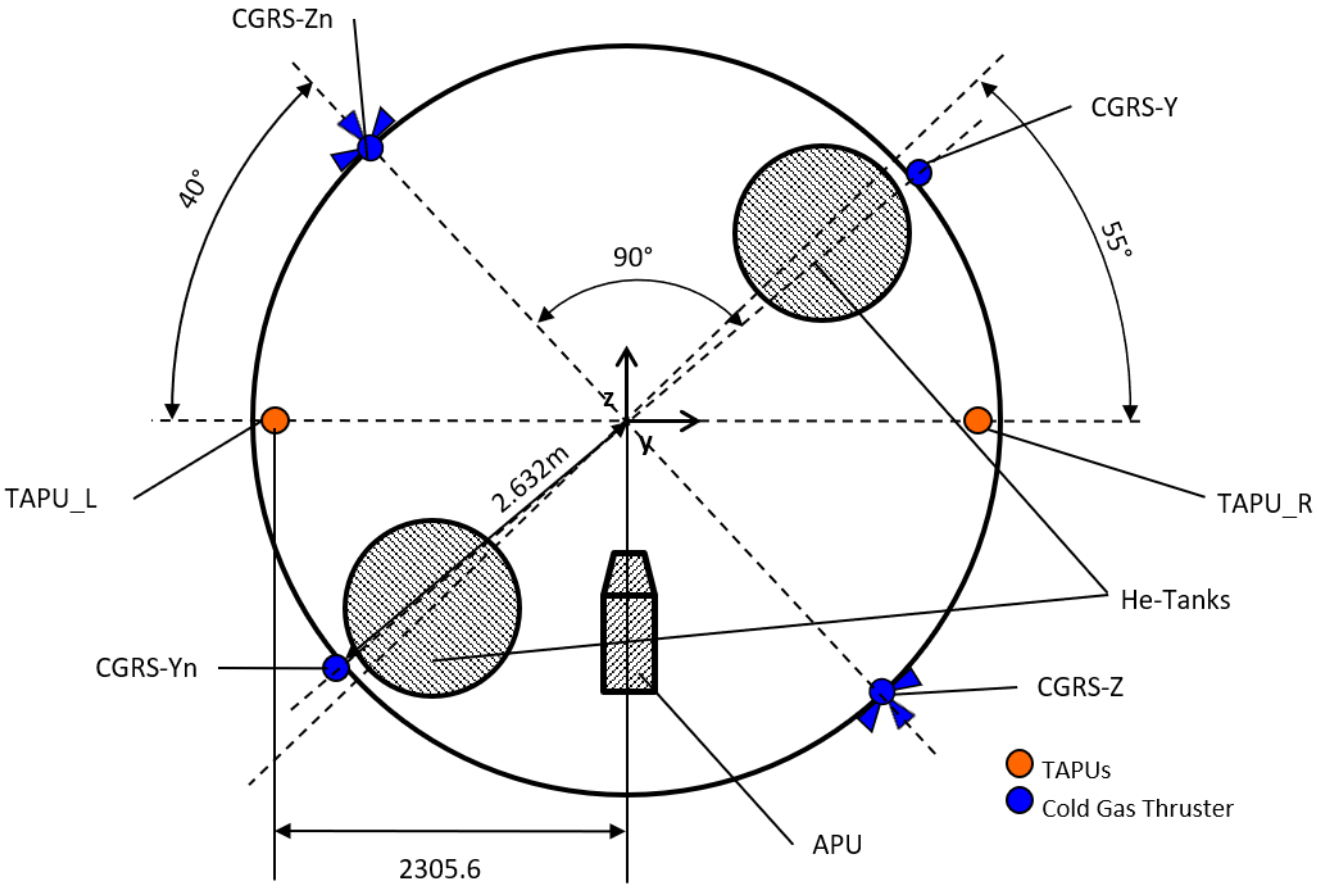

Figure 2.2.: Position of the cold and hot gas thrusters seen from the ULPM bottom

2.3. Thrust Vector Control

TVC sees many applications in air and spacecrafts like fighter planes, missiles and rocket engines. It is necessary whenever the flight path vector needs adjustment by redirecting the ejection of the exhaust flow. If a spacecraft has several nozzles or engines than a TVC can be realized by throttling each nozzle. Methods for single nozzle are gimbals, mechanical deflection of the exhaust gas or side injection of fluid (see fig. 2.3. A good example for a gimballed nozzle are the solid rocket boosters of the Space Shuttle or Ariane 5 where in case of a Liquid Propellant Rocket Engine (LPRE) the whole engine is gimballed [7, p.68]. One option of aerodynamic thrust vectoring is the injection of a liquid or gas downstream from the nozzle throat and has found applications in solid propellant rockets like the Minuteman. Mechanical TVC systems result in a substantial mass gain because they need flexible feed lines and joints while aerodynamic systems can alter the thrust vector only to smaller angles than compared to the mechanical ones.[10, p.613]

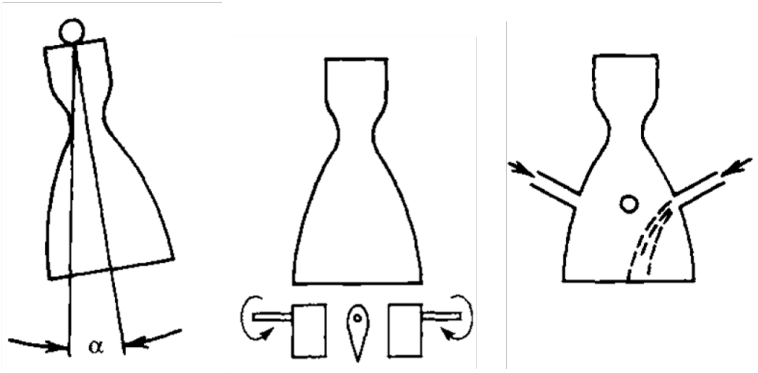

(a) Nozzle gimbal (b) Jet vanes (c) Fluid injection

Figure 2.3.: Methods for single nozzle thrust vector control [10, p.612]

2.3.1. Thrust Vector Control via side injection of fluids or gases

Injecting a fluid in a supersonic flow results in a side force F_s, which is not just composed of the pure injection momentum. A part of the force results from an altered pressure distribution at the wall. This is caused by phenomena as shock formation, boundary layer separation and differences in the injectant pressure and the undisturbed primary flow pressure (see fig. 2.4). In relation to this an amplification factor A_f is defined. Throughout literature the amplification factor appears with different definitions. Huzel [11, p.224] defines it as a ratio of specific impulses of the side injection $I_{sp,s}$ to the primary flow $I_{sp,p}$. For this work the definition of Eilers [12, p.40] is taken, regarding A_f as the ratio of actual generated side force F_s to the pure momentum of the injection F_i (2.7). The injection does not just create a side force, but it also increases minimally the axial thrust. This increase is denoted as ΔF_{ax}.

$$A_f = \frac{F_s}{F_i} \tag{2.7}$$

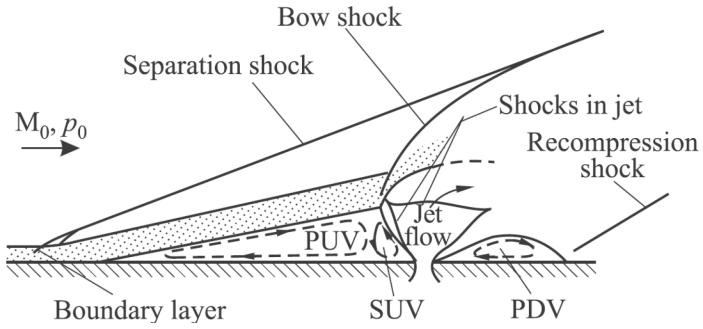

Figure 2.4.: Flow field with side injection on a flat plate [13]

Hot gas has the superior performance as injectant in contrary to liquids (see fig. 2.5). Liquid injection has a lower efficiency because it needs a feed system and pressurized tanks while the injection of hot or cold gas just needs robust valves and pipes. This is the reason liquid injection sees application only in older vehicles. [10, p.608ff]

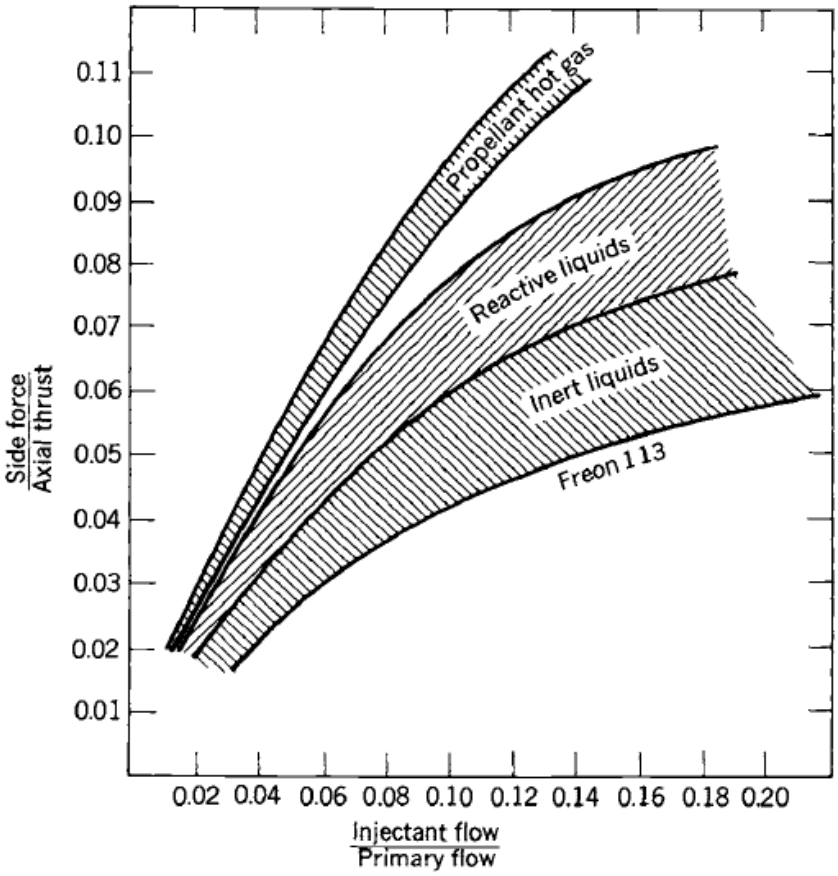

Figure 2.5.: Performance regions of various side injectants in TVC nozzles[10, p.619]

Zukoski et al. [14] conducted several experiments injecting different gases in a supersonic flow over a flat plate. They tried to obtain fundamental information concerning the interaction process of the injectant with the primary flow and determine similarity rules, specifically a scaling law of the side force. Equation (2.8) shows such a law as a ratio between the side force F_s and the thrust of the primary flow F_p. It was determined mainly under the following assumptions:

1. The injection occurs on a flat plate
2. The geometric boundaries of the plate are far enough away from the injector
3. The jet is perpendicularly injected at sonic velocity into an uniform supersonic flow
4. The injectant expands isentropically to the ambient pressure with its velocity vector parallel to the surface downstream of the injector
5. Changes in axial thrust of the primary flow caused by non-optimum expansion and by secondary injection are neglected

$$\frac{F_s}{F_p} = \frac{\dot{m}_i}{\dot{m}_p}\sqrt{\frac{T_{0,i}}{T_{0,p}}\frac{M_p}{M_i}} \tag{2.8}$$

This equation does not rely on the geometry of the orifice, but only on the mass flows, molecular weight and total temperatures. It show that F_s is proportional to the square-root of the total temperature of the injectant and inversely proportional to its molecular weight. [14]

2.4. Aerospike nozzles

For more than half a century, aerospike nozzles have been investigated by governmental institutions and corporations as alternative to conventional bell-shaped nozzles. The interest varied over the decades. Starting with Rocketdyne and the United States Airforce in 1967 first development attempts were made for a future version of the Saturn V propulsion [15]. That never came to be and the subject was not picked up until three decades later. In 1996 National Aeronautics and Space Administration (NASA) planned to propel the successor of the Space Shuttle, the X-33 Venture Star with an aerospike engine, but the project was cancelled shortly after the turn of the millennium [16]. In recent years the interest in aerospike engines has reemerged in academia and the commercial sector. Companies like ARCA Space Corporation try to develop aerospike engines to ultimately use them in Single-Stage-To-Orbit Launchers as main engine [17]. Unfortunately, to this day aerospike engines have never seen actual usage in a spacecraft. The reasons for this are manifold. In case of the X-33 Venture Star the aerospike engines were already developed and verified in various tests. The reasons for the program stop came due to manufacturing problems with the propellant tank[16]. The term plug nozzle and the term aerospike are often used interchangeably in common literature. Turner [7, p.266ff] delivers the following definition: A plug nozzle has a conical shaped plug which is surrounded by exhaust gases and can be understood as an inverted bell nozzle. The aerospike is a variant of the plug nozzle with a truncation of the cone. This leads to a flat surface at the end called base plate. While the plug nozzle is rotationally symmetrical with an annular combustion chamber, the aerospike can come in a linear or even clustered adaptation (see fig. 2.6). From this point on, only the term aerospike will be used to describe those nozzles. The truncation of the cone results in a reduced nozzle mass but also in a reduced performance which has to be weighed against each other for every single design.

(a) Annular aerospike on an experimental rocket [18]

(b) Linear aerospike of the XRS-2200 engine [16]

(c) Clustered aerospike of the Prospector 10 experimental rocket [19]

Figure 2.6.: Variants of aerospikes

The promise of aerospikes as main engines during endo-atmospheric flight was always their altitude adaptive capabilities. But they also seem to have potential advantages for purely vacuum applications which are of interest for this work. They can be smaller and lighter than conventional bell nozzles at the same performance or provide a higher I_{sp} at the same geometrical dimension depending on the degree of truncation of the cone [5]. The Utah State University tries to make use of that within their MUPHyN Thruster project. Their aerospike nozzle is designed for propelling a CubeSat and hot- and cold-fire tests have been conducted successfully [12]. Equations describing the flow in an aerospike nozzle are not outlined here. Further insight can be found in Wisse [20].

2.4.1. Realisation of SITVC on an Aerospike

In section 2.3 the phenomenon of side injection is briefly explained on a flat plate, independent of geometric boundaries set by a nozzle. The important design parameters on which the side force mainly depends are the injection velocity, mass flow and injection pressure. With a side injection in a nozzle to realize an actual SITVC geometric parameters follow: the location of the injector or injection orifice, the cross-sectional area and shape of the orifice and the angle of injection. Important performance coefficient is hereby the specific side impulse $I_{sp;s}$ generated by the side injection as ratio of F_s to the mass flow $\dot{m}_i$ normalized by the gravitational acceleration g to obtain the unit in seconds. For convenience it is defined as being perpendicular to the undisturbed thrust vector or equally the geometric center line of the nozzle not the nozzle wall or cone surface.The size of the injection orifice determines the mass flow and the size of the shock wave. While F_s increases with $\dot{m}_i$ it is influenced by location and angle of the injection. However, within bell-shaped or other nozzles with a closed contour it sees a limit when the shock wave or the injected fluid, respectively, gets reflected on the opposing wall (see fig. 2.8). For this nozzles extensive research with SITVC has been done in the past while there has not been given much attention to it on aerospike nozzles. Because massive gimbals would be necessary for large aerospike engines, SITVC seems to a more favourable method of controlling the thrust vector. That is why Rocketdyne belongs not just to the first ones doing research on aerospikes but also to those who did the first SITVC studies on aerospikes [15]. More recently were the studies by Eilers et al. [21] at the Utah State University and Probst et al. [6] at the TU Dresden. In summary, the studies concluded that highly energetic gases with low molecular weight and specific heat deliver superior performance and that the amplification factor increases with a smaller orifice and a location further downstream of the throat. The investigations done do not indicate that SITVC on aerospike nozzles delivers a higher performance than on classically shaped nozzles. While it is easy to calculate the pure momentum through the injection it is by no means easy to determine the amplification of it through the in 2.3.1 described flow phenomena acting on the surface of an aerospike. Till this day no analytical correlation predicts the amplification

exactly. Therefore only numerical simulations validated by experiments can make a statement of the actual side force. [5]
The main advantage here for aerospikes is that there is the potential to use the injection as stand-alone reaction control system when the primary flow is not active ($A_f = 1$) [22, p.40]. The before mentioned CubeSat obtains such a capability with its MUPHyN thruster [12].

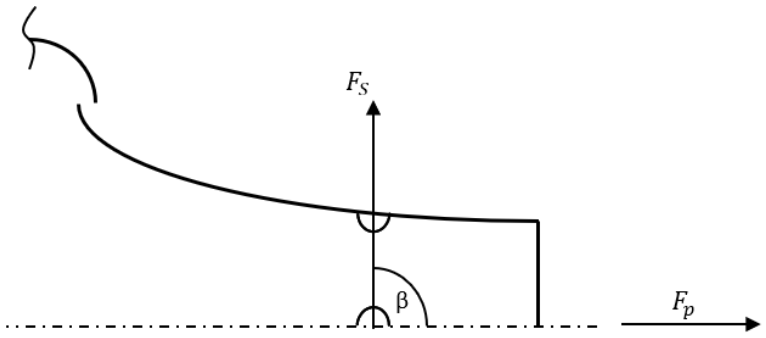

Figure 2.7.: Secondary injection on spike of the nozzle

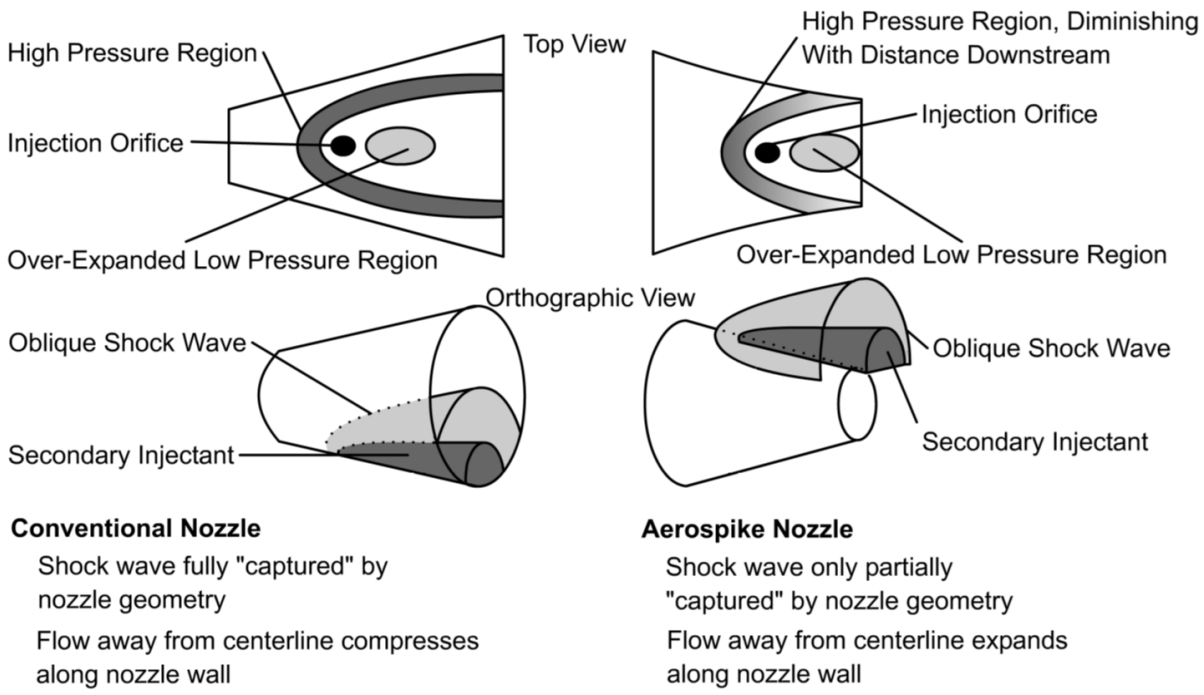

Figure 2.8.: Representative side injection flow patterns on conventional and aerospike nozzles [12, p.138]

3. Modelling with EcoSimPro and the ESPSS library

The analysis and simulation software EcoSimPro in its version 5.6.1 was used for the investigations done in this thesis. EcoSimPro is a simulation tool developed by Empresarius Agrupados Internacional suitable for modelling physical systems of any sort: electrical circuits, mechanical mechanisms, closed-loop-controls, etc. It employs an own object-oriented programming language called EcoSimPro Language (EL) designed to model continuous and discrete behaviours by expressing physical systems with Differential Algebraic Equations (DAEs), Ordinary Differential Equations (ODEs) and discrete events. The software is useful for studying transients or steady states.
In order to create a model, the system is resolved into interconnected components. EcoSimPro delivers sets of predefined components which are grouped into libraries like the thermal, electric or mechanical library coded in EcoSimPro Language (EL). Each component has one or more ports to transport information between components. They define the allowed inputs and outputs and differ with their respective physical domain. Fluid ports can only be connected to fluid ports and transport the fluid properties like temperature, pressure, chemical composition, mass flow, enthalpy etc. Likewise, thermal ports carry temperature, conducted heat etc. Electric ones carry resistance, voltage and current, while signal ports carry ones or zeros. The user can model the system and connect the components either by programming it with EL or set up a schematic with the graphical user interface. There the ports are connected with colourful lines. An example of such a schematic is given in fig. 3.1.

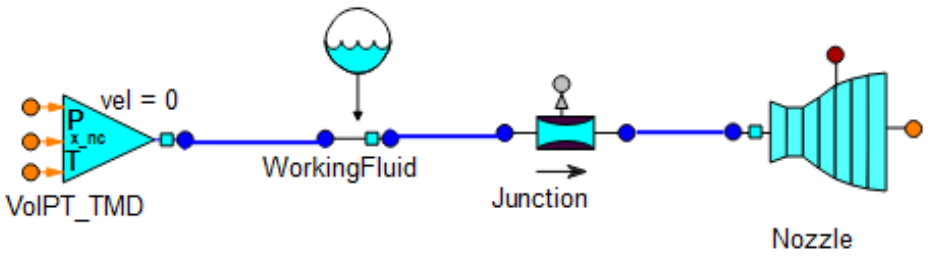

Figure 3.1.: Example of a fluid network in the graphical user interface

After the schematic has been successfully compiled, a partition can be generated. A partition carries the mathematical description of the model containing the boundary and unconstrained variables. Under a certain partition experiment files can be generated. Here the values are assigned to the boundary variables and settings for the numerical calculations can be specified. It is decided here whether the steady or the transient solver will be called, the latter requiring a definition of the integration period and the time step. Fig. 3.2 shows the organisation of partitions under components and experiments under partitions. An example of this can be found in appendix D.3. [23]

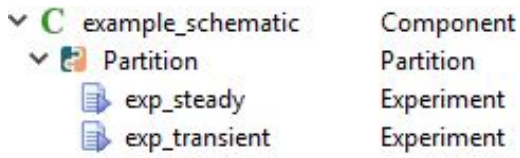

Figure 3.2.: Order of component, partition and experiment in the workspace

3.1. ESPSS - European Space Propulsion System Simulation

European Space Propulsion System Simulation (ESPSS) is a set of libraries developed by European Space Agency and other contributors as a simulation platform for spacecraft and launch vehicle propulsion systems within the EcoSimPro simulation environment. Version 3.2.2 contains nine libraries. The relevant ones used in this work are briefly explained here.

3.1.1. Calculation of fluid properties

The *Fluid_properties* library contains data tables with the properties for most fluids used for space propulsion and functions to calculate additional fluid properties e.g. those of mixtures. There are different categories of fluids referred to as working fluids depending on the type used:

- Perfect gases or Van-der-Waals gas
- Simplified liquids
- Real fluids
- User-defined fluids
- Mixture of perfect gases or Van-der-Waals gas
- Mixture of a real fluid with a perfect gas

The properties of perfect gases are obtained from the CEA database and polynomials [24]. Transport coefficients like viscosity μ and thermal conductivity λ are either calculated with polynomial expressions based on data from the Refprop NIST database [25] or use estimation methods. The latter is only chosen when the NIST database is not extensive enough and additional property data like dipole moments is available. Van-der-Waals gas is calculated with standard adaptations to the prefect gas equations, but the transport coefficients are calculated like for perfect gas. While simplified liquid properties are interpolated from 1D tables, real fluids use 2D tables considering either liquid, superheated, supercritical or two-phase flow which depends on temperature and pressure. Under two-phase conditions the mass fraction, the void fraction and transport properties are calculated simply from the saturation properties of the liquid and steam phase. If extrapolation is needed, data from the NIST and the CEA tables are combined. Properties of mixtures of perfect gases or Van-der-Waals gases are calculated with linear mixing rules assuming the same temperature for all the constituents. Using real fluids only mixtures of a real fluid with gases that do not condense are allowed. The properties are calculated simply. In case of two-phase flow the homogeneous equilibrium model is used to calculate the properties. [26, p.41-72]

3.1.2. The Fluid Flow 1D library

In ESPSS all elements (sub-components) can basically be distinguished into capacitive and resistive elements. In capacitive elements the mass (3.1) and energy conservation (3.2) equations are im-

plemented and calculate state variables like pressure, density, temperature, enthalpy and velocity with flow variables as input. Resistive elements receive state variables and calculate flow variables (inertia terms) like mass and enthalpy flows. Out of this logic follows that a port of a capacitive element can only be connected to a port of a resistive element and vice versa. This distinction was made to allow transient behaviour and avoid algebraic loops. All explanations are taken from [26, p.73-140]. The elements of the library consider:

- phase changes
- flow inversion, high speed phenomena and sonic limitation in pipes, volumes and junctions
- concentrated load losses in valves
- heat transfer between walls and the fluid

Working Fluid

Every fluid network needs this element where the used fluid is defined for the whole network. Usually only one fluid can be defined per network unless there are mixing elements like mixers or combustors where a working fluid element can be placed upstream of each inlet port. It is also the element where a non-condensable gas as second fluid is chosen. ESPSS accesses the fluid database with this element.

Boundary element

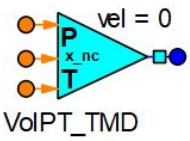

For time-dependent boundaries of fluid networks ESPSS delivers several elements to chose from. They differ in the variables they constrain. There is a variation between velocity, temperature, pressure and non-condensable mass fraction. The graphically represented element here leaves the user to constrain temperature, pressure and the non-condensable mass fraction while the velocity is automatically set to zero. This makes it effectively a boundary with total conditions. Depending on the constraining variables they are either capacitive or resisitive elements indicated by the square in front of the port. The red ports are input ports for analog control signals. If they are not connected the constrained variables have to be eventually defined in the experiment file.

Volume

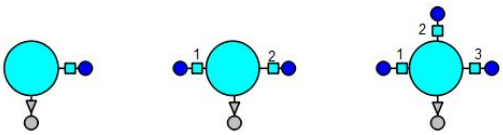

Volume elements are the basic capacitive element including the mass conservation equations for the working fluid and the non-condensable gas (3.1) as well as the energy conservation equations (3.2). Because of the multiple inheritance capability of the programming language other versions of the volume element exist. Other elements such as pipes and nozzle contain variations of the volume element. The basic one is the constant adiabatic volume ($\frac{dV}{dt} = 0, \dot{Q}_{in} = 0$). The number of connected ports range from one to nine. $\dot{m}_j$ and $(\dot{m}h)_j$ are the respective mass and total enthalpy flow calculated at the connected resistive type elements. With it the average velocity in the volume is calculated after (3.4) which is required for the total energy conservation equation and is here presented for a volume with two ports. The mass flows in the ports j can be positive or negative and is defined positive when entering the volume. That is why a subtraction is performed in (3.4). Also it is assumed that a mixture of non-condensable gas and working fluid in two-phase condition has a homogeneous temperature. Assuming thermodynamic equilibrium all state variables can be calculated. If the volume is not adiabatic then the element is equipped with a thermal port. $\dot{Q}_{in}$ is then non-zero and calculated with (3.5). The wall temperature is the temperature delivered to a connected port ($T_{wall} = T_{port}$). h_{film} is the wall film coefficient calculated by a routine based on empirical correlation which can be found in the appendix of [26].

$$\rho \frac{dV}{dt} + V \frac{d\rho}{dt} = \sum_{j \in ports} \dot{m}_j \tag{3.1}$$

$$V \frac{d\rho}{dt} e_0 + \rho \frac{dV}{dt} e_0 + V\rho \frac{de_0}{dt} = \sum_{j \in ports} (\dot{m}h)_j + \dot{Q}_{in} + pdV \tag{3.2}$$

with

$$e_0 = e + v^2/2 \tag{3.3}$$

$$v = \frac{1}{2A} \left(\left(\frac{\dot{m}}{\rho} \right)_{in,j=1} - \left(\frac{\dot{m}}{\rho} \right)_{in,j=2} \right) \tag{3.4}$$

$$\dot{Q}_{in} = h_{film} A \left(T_{wall} - T \right) \tag{3.5}$$

Junction, mass flow law and valve

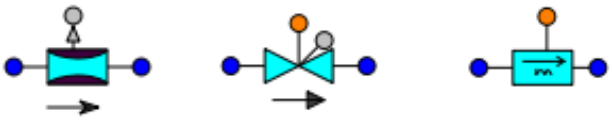

Contrary to the former mentioned element the junction is the basic resistive type. It represents a concentrated pressure loss at constant flow area and can impose a sonic limitation of the mass flow. It is considered that the incoming and outgoing mass and enthalpy flows are equal. By receiving state variables it calculates the mass flow assuming momentum equilibrium. Depending on the user's choice, a formulation with a pressure loss coefficient ζ (3.6) or a valve flow coefficient C_V is used. Only the former one is of interest here because it was the option of choice in this work.

$$(I_1 + I_2)(A\frac{dG}{dt} + G\frac{dA}{dt}) + \sqrt{A_{ref}}\frac{dG}{dt} = (p + \frac{1}{2}\rho v^2)_1 - (p + \frac{1}{2}\rho v^2)_2 - \frac{1}{2}(\zeta + \zeta_{crit})\frac{G\|G\|}{\rho_{up}} \tag{3.6}$$

I_j are the inertias at the ports imposed e.g. through acceleration multiplied by the time derivative of the mass flow

$$\frac{d\dot{m}}{dt} = A\frac{dG}{dt} + G\frac{dA}{dt} \tag{3.7}$$

As for the volume element there are various elements inherited from the junction. One of it is the valve. In order to avoid singularities in the matrices when the valve flow area A is zero at closed condition, derivatives of $G = \dot{m}/A = \rho v$ instead of $\dot{m}$ are used. For the same reason the term $\sqrt{A_{ref}}\frac{dG}{dt}$ is implemented and referred to as valve inertia, but is always very small.
The last term includes the pressure loss with the definition made above in equation (2.5).

$$\Delta p_{loss} = \frac{1}{2}\zeta\frac{G^2}{\rho} \tag{3.8}$$

$G\|G\|$ is chosen here instead of G^2 because the pressure losses are linear to the mass flow for laminar regimes ($G < G_{lam} : \Delta p \sim \dot{m}$). Then $G\|G\| = G_{lam}G$ is considered with $G_{lam} = \eta_{up}Re_{lam}/\sqrt{A}$. η_{up} is the upstream kinematic viscosity. Re_{lam} is the Reynolds-number indicating laminar-turbulent transition and is set to 2000 by default.
While ζ is the pressure loss coefficient entered by the user, ζ_{crit} is a correction factor set by a routine to limit G to be less than or equal G_{crit} to impose sonic flow limitation. G_{crit} is calculated either in the upstream connected capacity element based on empirical correlations or with assumed ideal expansion, depending on the user's choice.
The valve element has an additional signal input port (orange) and a signal measurement port (grey). The orange port allows dynamic change of the valve area which can be opened and closed linearly or with a quick opening. Therefore the variable *pos* in the experiment file describes the percentage of opening. A simplified junction element is the mass flow law or *JunTMD*. Placed in a fluid network it fixes the mass flow as a boundary condition. One has to be careful by utilizing it and it is highly recommended to only place it at the inlet boundaries.

Tube and pipe

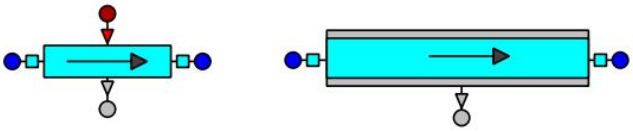

The tube element consists of a interconnection between volume and junctions elements, starting and ending with the former ones. The number of used elements depends on the number of nodes set by the user. Tube elements provide and inlet and outlet fluid port, a thermal port (red) for heat exchange and a signal measurement port (grey). The utilized correlations are more sophisticated than for simple volume and junction elements. They cover heat exchange and pressure loss through friction inside the tube. The governing equation for transient mass (3.9), momentum (3.10) and energy conservation (3.11) are given below. The tube element also contains expressions for the mass

flow correlation of the non-condensable gas and mixtures which are not specifically mentioned here. The mass flow (3.9) and (3.11) contain the wall compressibility k_{wall}. $\Delta\xi$ describes the influence of friction per node. To smooth pressure oscillations and decrease calculation time the momentum equation contains a damping factor or artificial viscosity μa.

$$A\frac{\partial \rho}{\partial t} + \frac{\partial(\rho v A)}{\partial x} = -\rho A k_{wall}\frac{\partial p}{\partial t} \tag{3.9}$$

$$A\frac{\partial(\rho v)}{\partial t} + \frac{\partial}{\partial x}\left(A\left(\rho v^2 + p + \mu_a\right)\right) = -\frac{1}{2}\frac{\Delta\xi_j}{\Delta x}\rho v|v|A + \rho g A + p\frac{dA}{dx} \tag{3.10}$$

$$A\frac{\partial(\rho e)}{\partial t} + \frac{\partial}{\partial x}\left(A\left(\rho v h - \lambda\frac{\partial T}{\partial x}\right)\right) = -\rho e A k_{wall}\left(\frac{\partial p}{\partial t}\right) + \frac{\Delta\dot{Q}_j}{\Delta x} + \rho g v A \tag{3.11}$$

The pipe element is inherited from the tube element and has a wall which can exchange heat with the environment. Therefore, wall roughness and thickness and an ambient temperature have to be given as input.

Tee

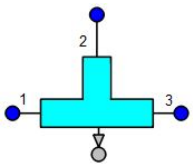

For including a branch in the pipe system this element is used. It contains a volume element in the center connected to three junction elements as three outlets or inlets. Each junction can have a different diameter and pressure drop coefficient.

Nozzle

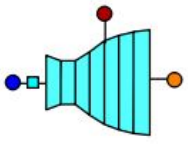

The Nozzle element is basically a volume at the inlet, a 1D-mesh cylindrical area-varying tube and a junction at the outlet connected to a boundary. Within the tube a sonic transition can occur at its narrowest point, the throat. For the contour a 1D table is entered with dimensionless diameter over normalized length. This profile is then warped with the throat diameter. Important parameter is here the expansion ratio ϵ which performs a rotation of the divergent part of the contour so that contour and ϵ fit. The standard profile employed by EcoSimPro is depicted in the appendix in fig. D.1b.
The ambient pressure and temperature are set by the user. The junction at the end allows shock waves under non-adapted conditions. The performance of the nozzle is that of the last node where F and I_{sp} are calculated.

3.1.3. The Combustion Chamber library

This library includes various components dealing with combustion processes. Fluids are here called chemicals. Properties of an arbitrary mixture of chemicals like λ and c_p are obtained from CEA coefficients. The equilibrium molar fractions of an arbitrary mixture of reactants are derived from the Minimum Gibbs Energy Method. Advantageous is that the combustion model includes transient phenomena, wall heat exchange and pressure drops. The transient formulation includes vaporization and non-equilibrium phenomena based on transient conservation equations. On the other hand numerical instabilities can arise during the calculation and the integration time step is very low which increases calculation time. During the calculation the total pressure loss is not completely conserved leading to typical errors between 0.5 % and 1 %. The 1D Combustor element is the basic element of this library. It cannot be included in the graphic user interface but other components inherit it. It produces a new mixture of chemicals which becomes the working fluid of all other components connected downstream. For the sake of stability, valve opening-closing sequences are critical for the ignition and must be treated with care.

Mixer element

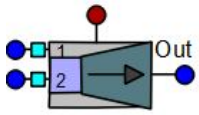

To simulate a mixture of two pure fluids or of a fluid with combustion gas, one can use the mixer element. With it a combustion chamber with more than two injectors can then be modeled by placing this element upstream of one of the injectors. It uses similar formulations as the volume element, but has to account for differences or shifts in the enthalpy of chemicals defined by CEA and pure fluids defined about the Refprop routines. Friction pressure drop is computed using the same formulation as for tube elements by means of the average velocity, the equivalent hydraulic diameter and the evaluation of the friction coefficient.

Preburner

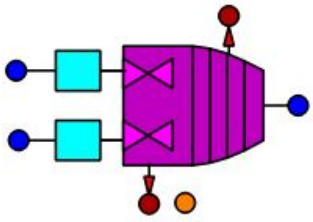

A preburner element is modelled with a 1D discretization featuring the combustion process for liquid and gas propellants with two injectors and two cavities. Cavities are volume elements with a thermal port and resemble the inlets for the fuel and oxidizer. Both ports are merged into one forming a thermal port for the injector head. The other thermal port stems from the nozzle and chamber. The injectors are junctions and so their pressure loss will be calculated by entering a pressure loss coefficient. Geometric parameters like chamber diameter, length and contour have to defined. The latter is entered as a 1D table with diameter over length. The mixture ratio MR is defined in (3.12).

$$MR = \frac{\dot{m}_{oxy}}{\dot{m}_{red}} \tag{3.12}$$

When initializing the element, one can choose the equilibrium or the non-equilibrium reaction delay model for the combustion process. It covers ignited and non-ignited conditions. To start ignition an ignition flag needs to be set by the user. If the fluid is a liquid it will be vaporized within a delay time. The heat for the vaporization is taken from the combustion heat. For each volume j of the chamber the molar fraction y_k, heat and transport properties are calculated using the Minimum Gibbs energy method. It is an implicit function of the mixture molar fractions (see (3.13)), pressure and specific enthalpy of the reactants k. Under equilibrium condition it is exemplary given in (3.15). It depends on the number of moles N_k depending itself on the mass fraction x_k. For the propellants these are calculated in the cavities. Temperature must be determined iteratively, enthalpy by the known transient equilibrium conditions. However, the pressure is calculated with the perfect gas state equation $p = \rho RT\eta_{comb}$. This way the combustion efficiency η_{comb} finds its way into the calculation as an user-given parameter. The last volume transports the properties to the next downstream connected element e.g a nozzle.

$$MW_{mix} = \sum_{k=1,Nchem} y_k MW_k \tag{3.13}$$

$$N_{k,j} = \frac{x_{k,j} MW_{mix}}{MW_{k,j}} \tag{3.14}$$

$$\left(y_{k,eq}, T_{eq}\right)_j = f_{MinGibbs}\left(N_{k,j-1}, h_j - v_j^2/2, p_j\right) \tag{3.15}$$

Combustion Chamber Nozzle

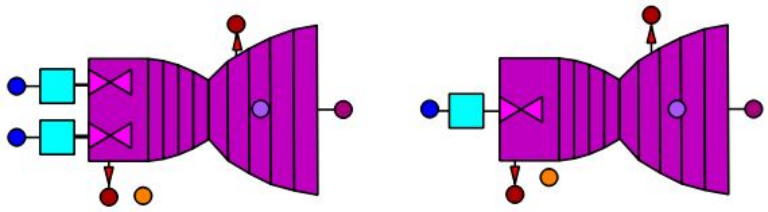

The combustion chamber nozzle is simply the connection of a preburner and a nozzle. A thermal port at the nozzle wall allows a connection to a cooling jacket. The user can decide if the gas composition in the supersonic nozzles is in equilibrium or frozen. When in equilibrium the nozzle can be chosen as non-isentropic otherwise it is isentropic. A mono-propellant thruster is a derivation with only one injector and can be seen as a convergent-divergent nozzle.

3.1.4. Steady-state simulations with the Steady library

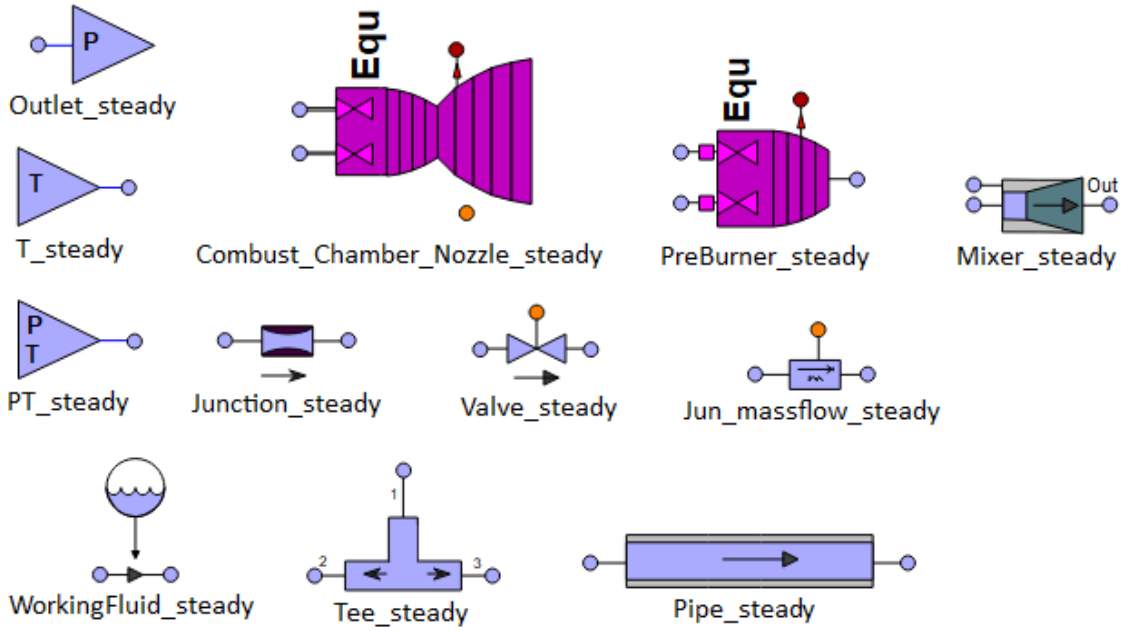

Figure 3.3.: Standard components coded in the steady library relevant for this work

EcoSimPro allows steady simulations by switching the solver. Usually this could be done with the same components described until this point. Under steady-state calculations the time-dependent derivatives are dropped. Unfortunately it is not trivial to use this components designed for transient calculation also for steady-state calculations because of the complexity of the transient equations. This makes parametric studies and design of engine cycles time-intensive and difficult. If one wants to obtain quick results this is not necessarily the best option. Therefore, the here presented library was specifically developed as a tool for pre-design phases and parametric studies. With it, it is possible to design whole engine cycles and obtain geometric quantities like throat diameters with short calculation times. The library contains the common components of every rocket engine cycle: pumps, heat ex-changers, pipes, valves, combustion chambers etc. The relevant components used for the models in this work are shown in 3.3. Unfortunately, a simple nozzle component does not exist. Instead, a combustion chamber nozzle was used and its second inlet port foreseen with a negligible mass influx. The steady components have two substantial differences from the transient counter-parts apart from the neglected time-derivatives: There is no separation anymore in capacitive and resistive elements and fluid ports can now have more than one connection to another port. Most components inherit a setting for Off-Design or Design. This modes decide which variables will become input parameters and which will become outputs of the calculation.

- Design Mode: With this mode enabled for a junction, geometric variables become an output. The mass flow is fixed then and the cross-sectional area is an output. Mass flows and pressure losses can be fixed for certain components. The combustion chamber allows different Design modes. Either chamber temperature, pressure and mixture ratio or just the mixture ratio can be fixed with throat diameter as a necessary input.
- Off-Design Mode: This mode is designed for making steady-state calculations of an already existing cycle where the geometry and other parameters like the pressure loss coefficient is fixed. Mass flows and pressure losses are calculated.

Usually an entire Off-Design or Design condition is modelled with all components in the same mode. But the user is not bound to this. Even though it is not trivial the user can define bound-

ary and unconstrained variables in the partition and leave components in different modes. This needs a fundamental understanding of the governing equations. Otherwise strange boundary conditions can appear or the successful calculation is very sensitive to the initial conditions. Governing equations for stationary flow calculation expressed for a node in a component are:

Mass conservation

$$\dot{m}_j = \rho_j v_j A_j \tag{3.16}$$

Momentum conservation

$$p_{j+1} = p_j - \frac{1}{2}\xi_j \frac{\dot{m}^2}{\rho_j A_j} \tag{3.17}$$

For pipes is considered $\xi_j = fr_j \Delta L / d_j$ with fr as the friction factor as function of wall roughness and Reynolds-number. The last term is the ratio of length increment to diameter.

Energy conservation

$$q_j = \dot{m} \left(h_{j+1} - h_j \right) \tag{3.18}$$

4. Development of a general Dual-Mode Thruster concept

The idea of the DMT was brought up prior to this thesis and serves as starting point. This chapter introduces the concept and makes a first assessment of requirements and constraints. Main objective of this investigation is to cover up potential for performance and flexibility increase of the ULPM through modification of the secondary thrust system. Thereby the current TAPUs nozzles shall be replaced with DMTs. DMTS refers to the whole system composed of the thrusters, valves and other peripheral elements. Section 4.2 defines possible use-cases for the DMTS. These use-cases deliver the frame for evaluating the potential of the system.

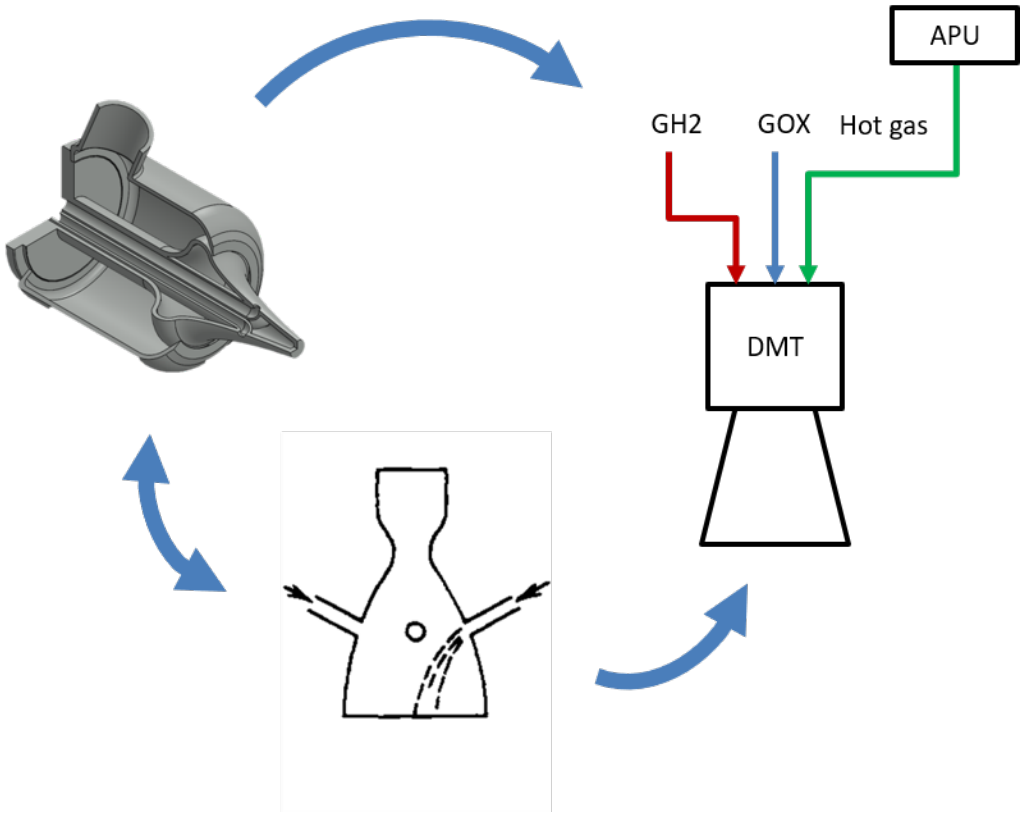

Figure 4.1.: Technologies merged for the Dual-Mode Thruster with aerospike nozzle and SITVC (images from [27, 10])

Fig. 4.1 shows the combinations of the technologies merged for this concept. The merging results in an increased complexity of the system. Also the depth of the investigation is limited by a time frame and so each part of the system can only be studied to a certain extent in this work. The justification of analysing the whole system at once and not each technology on its own in several studies lies in the specific objective of this work.
Currently the CGRS is composed of several clusters of thrusters using GH2 to perform general attitude and orbit control operations, countering disturbances among them. The reduction of structural mass shall be achieved by removing a part of the clusters and use the GH2 mode of the DMTS for

axial thrust generation instead. The hope is that the use of one nozzle reduces the amount of nozzles, pipes and valves on the ULPM
Disturbances arise from the hot gas operation of the APU. Instead of using the CGRS for it, a dedicated TVC should counter the disturbances. The secondary thrust system of the ULPM has two nozzles. Therefore the thrust vector could be altered by regulating each nozzle, but only within the plane of the nozzles. A list of advantages and disadvantages of different TVC methods applied on the secondary thrust system of the ULPM can be found in table 4.1. Nevertheless, it is decided for this work to use the method with secondary injection. A quantitative study comparing different TVC methods for the secondary thrust system is not part of this investigation.

TVC method	Regulating each nozzle	Gimbal each nozzle	Secondary injection at each nozzle
Advantages	+ simple	+ large thrust vector angles covered	+ same control routines as CGRS
Disadvantages	- only TVC in nozzle plane	- large mass impact	- only small thrust vector angles covered

Table 4.1.: Advantages & Disadvantages of TVC applied on the hot gas APU system of the ULPM

Critical for the reducing the non-propulsive resource need is then that the SITVC needs less propellant resources as the CGRS to create the same torque around the CoG. Part of this investigation is therefore a comparison of both systems. Foundation of this comparison is that the maximum disturbance would be of 20 N m. As SITVC can also be realized with a standard bell nozzle and the dual-mode operation is independent of the nozzle shape, there is no actual need for an aerospike. As mentioned in section 2.4, that even though it is still unclear if an aerospike is also superior in performance, it potentially offers an higher thrust-to-weight ratio. But the most significant reason is that with the SITVC on an aerospike GNC operations are possible because the side injection orifices point outwards and could be used without the primary flow active.
The cold gas mode with GOX is an option to increase flexibility at a cost of a higher structural mass. Like the A5 ESC-A upper stage had it before, the A6 ULPM would then have a possibility of using expendable oxygen for axial thrust generation.
A preliminary design of the DMT would look like fig. 4.2. It is pointed out that this graphic does not represent the actual proportions to each other.

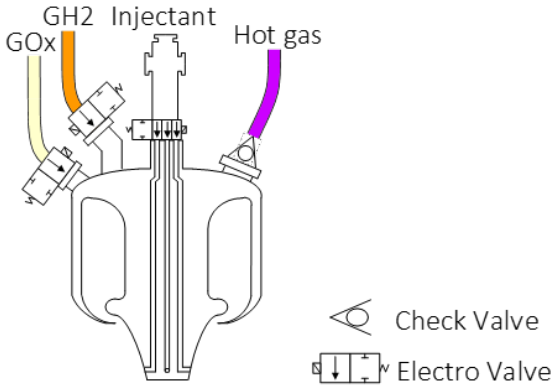

Figure 4.2.: Concept of a DMT with first peripheral elements

4.1. Identifying requirements and constraints

The process of determining a feasible design is not straight forward. The use case for the DMTS is the application on the ULPM. That means it will be integrated into an existing system. Specifically, the connection to the APU means that its gas generator becomes a boundary with valves, pumps and ultimately the propellant tanks behind it. When in the process of evaluating all constraints and system impacts more and more inter-dependencies between the DMTS and the boundaries appear so do new constraints. Then the former set requirements have to be checked again and perhaps re-evaluated. One goal of this work is to identify the major implications of the design on the surrounding systems and vice versa. The process of doing so is illustrated in fig. 4.3. It is derived from a more extensive approach for liquid rocket propulsion systems analysis described by Humble [28, p.192ff].

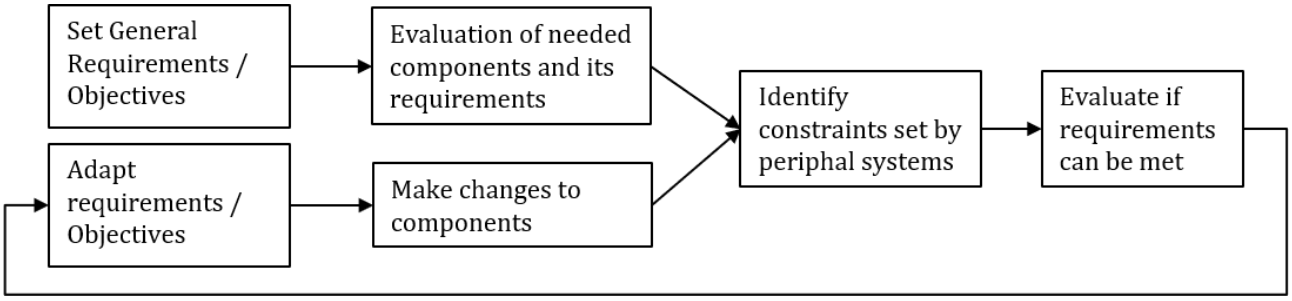

Figure 4.3.: Sketch of strategy towards identifying system constraints

4.1.1. Functional requirements

The first functional requirements follow from the statements made at the beginning of this chapter.

- Capability of TVC countering a max. disturbance of 20N m
- Capability of stand-alone GNC operations with injection orifice
- Cold gas mode with GH2 and optional GOX
- Hot gas mode with the APU hot gas
- After-burning mode with hot gas
- Stand-alone combustion mode as GOX/GH2 burner

4.1.2. Geometric requirements

The geometric extension of the nozzle must allow a placement on the current thrust frame of the TAPUs. The TAPUs are currently installed with an angle of $\delta = 8°$ between the stage's center axis and the nozzle's center line. This has to be retained so that the exhaust plume of the thrusters do not impose a force on or contaminate the subjacent ViTF.
The design must allow the attachment of valves to the entry ports of the nozzle and the attachment of the feed lines to the valves. The diameters of the thruster inlets are assumed here as to be the same as for the components the DMT seeks to replace. This means the hot gas inlet has 25 mm like the hot gas feed lines. The GH2 feed lines to the thruster have a diameter of 40 mm [9]. The injectant feed line has no reference to any existing parts so its diameter is set to be 10 mm for this work. If these geometric requirements can be uphold can only be answered with a complete CAD model of the thruster and not within this work.

4.1.3. SITVC requirements

Because of a lack of experimental data about the amplification it is not easy to determine which of the three available fluids should be used as injectant. A discussion about this follows in section 5.1.6. The TVC realized has to be capable of

- generating a force sufficient enough to counter a defined perturbing torque of 20N m
- steering possibilities in all four directions of horizontal and vertical axis.

4.1.4. Nozzle requirements

For simplification reasons the injection angle is defined as angle between nozzle center line and injection direction and is set to $\beta = 90°$. The canals for SITVC will reach through the whole nozzle cone. The requirement that steering needs to be possible in all axis directions requires four orifices and four canals. In section 5.1 it is shown that only three orifices are necessary. Still the nozzle cone has to be capable of accommodating all canals while keeping its structural integrity. This limits the orifice effective cross-sectional area $A_{Orifice}$. Equation (2.1) shows that this constraint limits F_s. Larger orifices means placing them more upstream where the cone is wider but studies described in section 2.4.1 suggest a placement of the orifice further downstream of the throat for maximum side force amplification. This will be a design issue for a possible future design. A trade-off to obtain a feasible solution has to be made after analysis of experimental results. Moreover, larger orifices will probably disturb the primary flow more drastically when there is no side injection active, reducing the nozzle's performance.

4.1.5. Material and structural requirements

The nozzle has an additional manufacturing requirement. It is foreseen to be 3D-printed with Silicon nitride (SI3N4). The unique shape of the aerospike leaves the throat designed as a ring slot. The 3D-printing technique constrains the minimum width of this ring slot to be 1 mm due to manufacturing tolerances. This has an influence on the design of the cone which results in constraining the expansion ratio.
The material has to withstand the gas temperatures because a cooling architecture can either not be realized due to the small size of the thruster or should not be necessary to not increase the system's complexity. In communication with the project partners from the TU Dresden a maximum limit was set to $T_{max} = 1200\,\mathrm{K}$ even though the material can probably withstand higher temperatures. [27]

4.1.6. Valve requirements

In order to realize the different modes, the first peripheral components to be installed are the valves. They are necessary so that the hot gas cannot enter the cold gas feed lines during the hot gas mode and that cold gas cannot enter the APU from the subjacent DMTs. The cold gas operation requires a mono-stable valve. Response time and leakage and other typical requirements for valves are not quantitatively determined for them, but should be comparable to those of the CGRS. On the hot gas side only a check valve is necessary because the APU already disposes of mono-stable valves above the gas generator.
In order to fulfill the requirement of TVC on every axis each orifice needs to be actuated separately. As mentioned before three orifices per thruster are sufficient for the application on the ULPM. This requires a 3-way-valve placed between the canal inlets and the injectant feed line.

All valves have to handle the gas temperatures. The lower temperature limit is set by the hydrogen, the upper limit is set by the hot gas. The detailed requirements have to be discussed with the specific use case (see 6.1.3). A cost requirement is that there is no need for developing a new valve. Possible solution from existing valves are shown in 5.1.4.

4.2. Deriving use-cases for evaluating the potential of the DMTS

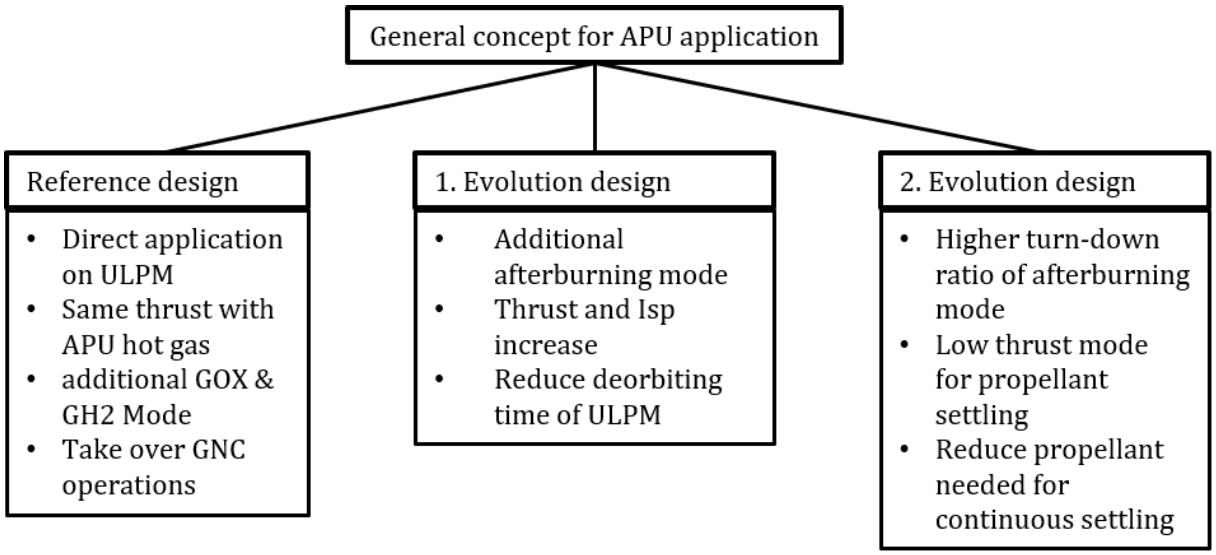

Figure 4.4.: Derivation of possible use-cases for different designs of the DMTS

The general concept of the DMTS allows for different use-cases. The reference design is foreseen for a direct application on the ULPM with GNC operations. In chapter 6 its potential propellant mass saving is weight against the dry mass impact it has. This design aims for an increase in flexibility in propellant handling and mass saving. This design is investigated extensively in this study.
In general, there is a desire of thrust augmentation of the secondary thrust system between 400 N and 800 N for boost or deorbiting phases of the ULPM. One aspect of this investigation is to find out if one version of the DMTS is capable of a higher thrust mode than currently possible with the APU system. Because the APU has to serve the purpose of tank pressurization and thrust generation, it is a very complex system with a lot of constraints. Redesigning it with a doubling of the thrust is therefore a costly and time-intensive endeavour. Here the DMTS could use GOX and combust it with the fuel-rich hot gas from the APU. This is considered as the after-burning mode. Requirement is that the APU does not need to be redesigned. Also the DMT has a higher temperature limit with potentially higher I_{sp} making the deorbiting maneuver less costly. The higher thrust reduces the deorbiting time which gives flexibility to the mission phase design. This design was rudimentary analysed in chapter 7, but a complete dry mass impact is not additionally calculated.
Another desire on the ULPM goes into the opposite direction: A secondary thrust system with a higher turn-down ratio for a thrust mode at ca. 30 N total thrust. This would make continuous settling of the propellant possible with a lower mass consumption. This is inspired by the Saturn V 3rd stage which used an ullage burner to settle the propellant [29, p.6-11ff.]. To answer this need a possible second evolution design could use the afterburning mode at a low thrust. However, this idea has to be investigated in a follow-up study and does not lie in the scope of this work anymore. It is merely mentioned here to present possible solutions with the DMTS for all needs future upper stages address to a secondary thrust system.

5. Stage model

The results later presented in this work were generated with a stage model described in this chapter. It was a necessary part of this work to develop a model because this is the first investigation made on a system like this. In order to support possible follow-up studies the results need to be comprehensible, reproducible and easily extendable. Because of the different aspects and system domains which needed to be analysed the stage model is not a cohesive model comprising of a program with a graphic user interface or a single model in EcoSimPro. It is rather a conglomeration of different models embedded in EcoSimPro and Microsoft Excel. The EcoSimPro models are divided in those who were used for the design process to obtain geometries and those who were designed to deliver performance data like thrust and mass flow. The Excel sheets contain mass budget calculation and parametric studies combining geometric constraints of the ULPM with the thruster performance evaluated with the EcoSimPro models.

5.1. Integration of the DMTS on the A6 upper stage

With the current application foreseen the DMTs will be placed on the thrust frame of the TAPUs. A Visio schematic of the integration into the line routing can be found in appendix A.

5.1.1. Connection to the hot gas feed lines

The check valve will be connected directly to the nozzle and the hot gas feed line to the check valve. There is no need for redesigning the hot gas feed lines but in order to make space for the valve they need to be shortened. Currently the hot gas feed line consists of two rigid lines and a flex line in between them. These flex lines are necessary to compensate thermal expansion or contraction of the structure under influence of different temperatures. However, their mass is higher than that of normal rigid lines.

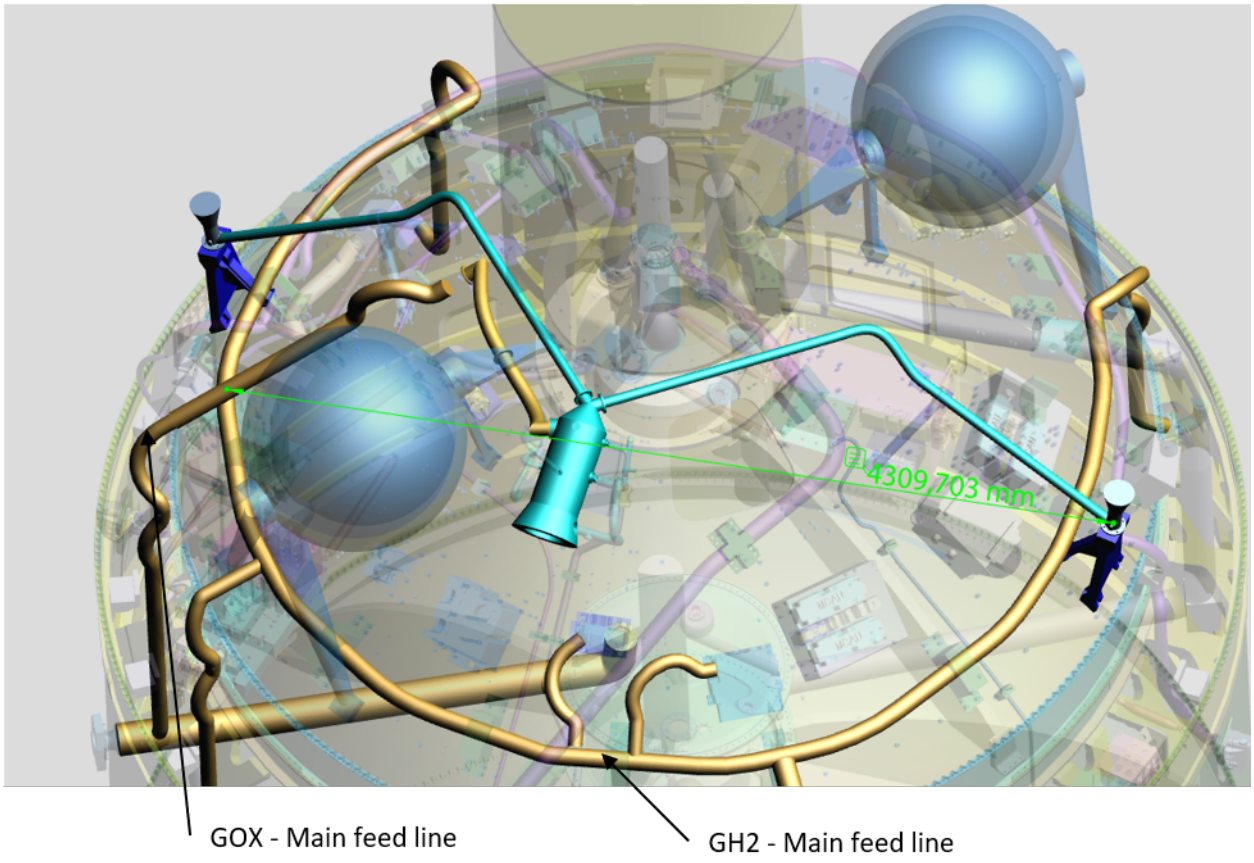

Figure 5.1.: Considered feed lines on the ULPM [9]

5.1.2. Connection to the GH2 gas feed lines

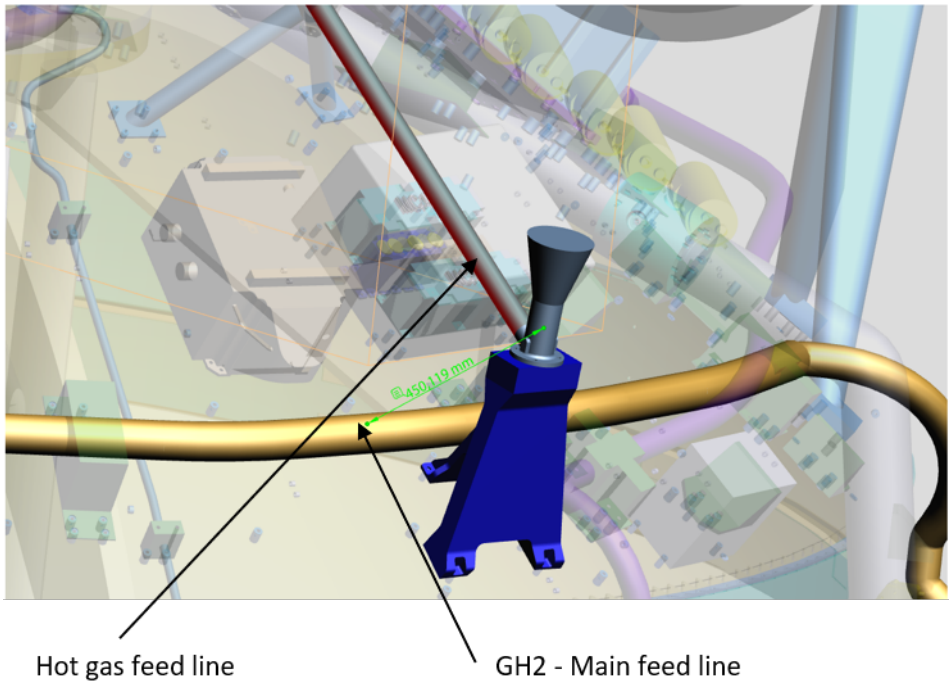

Figure 5.2.: GH2 main feed line near the TAPU [9]

The main feed line of the GH2 is arranged in a ring supplying the four the CGRS cluster. This ring has a connection to the upper part of the hydrogen tank and other peripheral components e.g. for tank filling or flushing. Fortunately, the main feed line is situated close to the TAPU. Because of thermal expansion during the thruster's hot gas operation a flex line has to be part of the connection. Due to the small distance the entire feed line can be a flex line. Both lines have the same length out of symmetric reasons.

Thruster	1	2
Flex line length	0.45	0.45

Table 5.1.: GH2 feed line element lengths in $[m]$ for DMTS CGH mode

5.1.3. Connection to the GOX gas feed lines

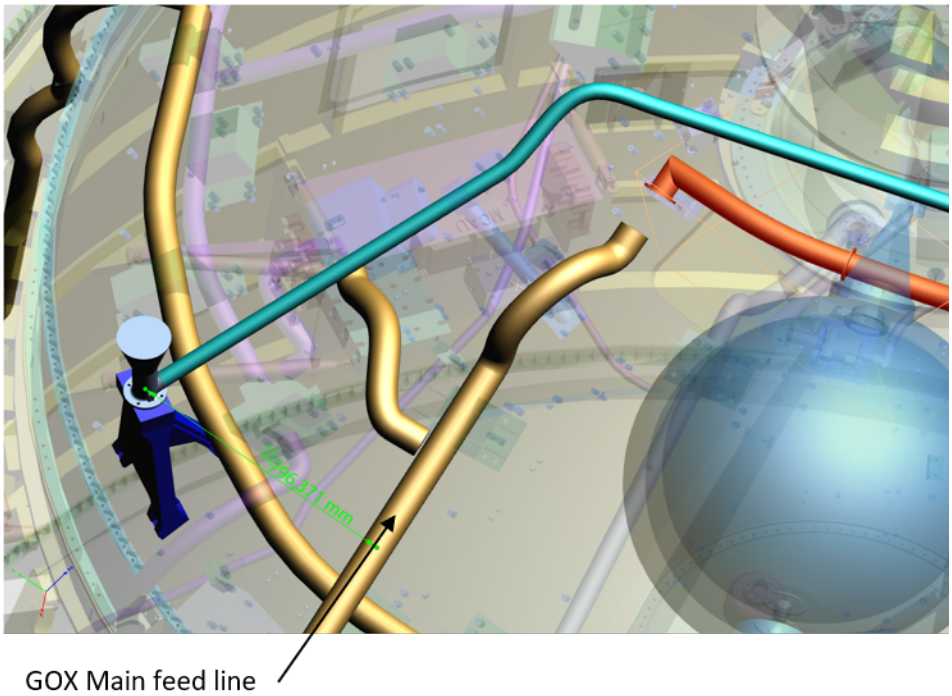

Figure 5.3.: GOX main feed line near the TAPU [9]

The realization of the GOX-mode is more expensive in piping mass. The closest GOX line is the one coming from the APU supplying the oxygen tank with re-pressurization gas. Here no symmetry exists for the thrusters. While the distance to the closer situated TAPU is relatively short with roughly 0.8 m, the distance to the opposite thruster is not. Also it is not possible to connect it with a straight pipe, but rather it will be curved. A straight connection would be roughly 4.3 m, but to account for its curving it is estimated to be $4.3\,\mathrm{m} * PI * 0.5 \approx 6.8\,\mathrm{m}$. Due to the small length the first feed line is assumed to be completely a flex line. The longer feed line will have a flex line integrated with the same length as the flex line for the GH2 side. The different length lead to different pressure losses. This is countered by placing a calibrating orifice in the shorter feed line to equalize the pressure losses.

Thruster	1	2
Rigid line length	0	6.4
Flex line length	0.8	0.45

Table 5.2.: GOX feed line element lengths in [m] for DMTS CGO mode

5.1.4. Possible valve solutions

A new development of a valve has to be avoided. Therefore, the model inputs (mass m and pressure loss coefficient ζ_{valve}) are oriented on existing valves already in use on the ULPM which can be used with minor adaptions. For the cold gas feed lines a mono-stable electro-valve used for the CGRS could be used if it can be qualified for higher temperatures. If not, the electro-magnets need to be thermally decoupled from the surrounding structure. Problematic is their low maximum temperature under which they can guarantee correct opening and closing of the valve. A fitting solution for the hot gas check valve could not be obtained within this work, but a check valve used for nitrogen flushing could come close to it. Because of a lack of data the given ζ_{valve} of the CGRS valve is used for the check valve as well.

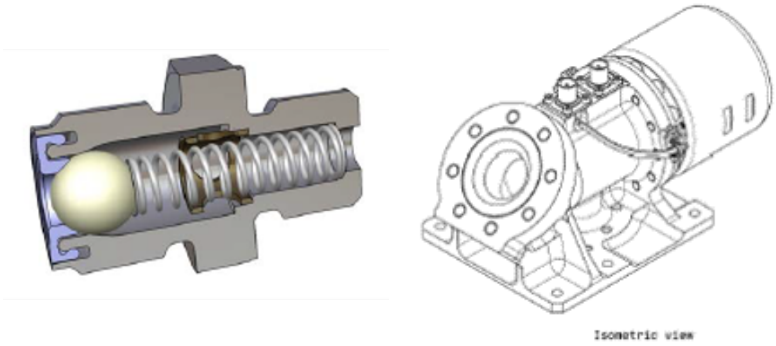

(a) Check valve of the nitrogen flushing circuit [9]

(b) Mono-stable valve used for the CGRS thruster and the APU feed system [9]

Figure 5.4.: Realistic valve solutions for the DMTS

Valve solution	m [kg]	ζ_{Valve} [-]
CGRS valve	4.3	10
Check valve	1.3	(10)

Table 5.3.: Mass of different valves used on the ULPM

5.1.5. Formulations for the mass estimation of the additional dry mass

For the mass calculation of rigid lines a wall thickness t of 1mm was assumed made out of standard steel with inner diameter d_{in}, length L and a density ρ of 7850 kg/m^3 [30, p.64]. The mass results is equal the one of a straight hollow tube.

$$m_{rigid} = \rho L \pi \left(A_o - A_{in}\right) = \rho L \pi t \left(t + d_{in}\right) \tag{5.1}$$

The mass of flex was calculated similar, but with an additional multiplying factor. This was evaluated from the already known weight of the existing flexible line of the hot gas side which was compared to a rigid line made out of steel with the same L, d_{in} and t. The resulting factor has a value of 2.66. Flexible lines are heavier because the tube is composed of several layers of metal stripes which makes them much thicker.

$$m_{flex} = 2.66 * m_{rigid} \tag{5.2}$$

Longer pipes will need screws, brackets and clamps to be mounted on the ULPM. It is here estimated to be 20 % of the total pipe mass.

$$m_{pipe} = 0.2 * \left(m_{flex} + m_{rigid}\right) \tag{5.3}$$

Masses of the flanges belonging to each pipe end were estimated with a factor derived from existing parts scaling with d_{in}.

$$m_{Flange} = 10 \, \frac{\mathrm{kg}}{\mathrm{m}} \, d_{in} \tag{5.4}$$

Tee components also called distributors or terminals were estimated in a similar way.

$$m_{Distributor} = 110 \, \frac{\mathrm{kg}}{\mathrm{m}} \, d_{in} \tag{5.5}$$

Calibrating orifices are estimated with $m_{CalOri} = 0.5\,\mathrm{kg}$.

5.1.6. Realization of SITVC

Both DMT will be equipped with the capability of SITVC. If this would be done for a thrust system with just one nozzle, this nozzle would need at least four orifices to ensure TVC in every direction. Because the current secondary thrust system comprises two nozzles in the horizontal plane it has in total four orifices in this plane. Shown in fig. 5.5a the logical choice is to spare the orifices pointing inwards. The before-mentioned requirement of not contaminating the ViTF and the helium tanks prohibits a redirection of the flow towards the subjacent structure. In conclusion, each thruster is equipped with three orifices distributed in 90° - 90° - 180° (see fig. 5.5b).

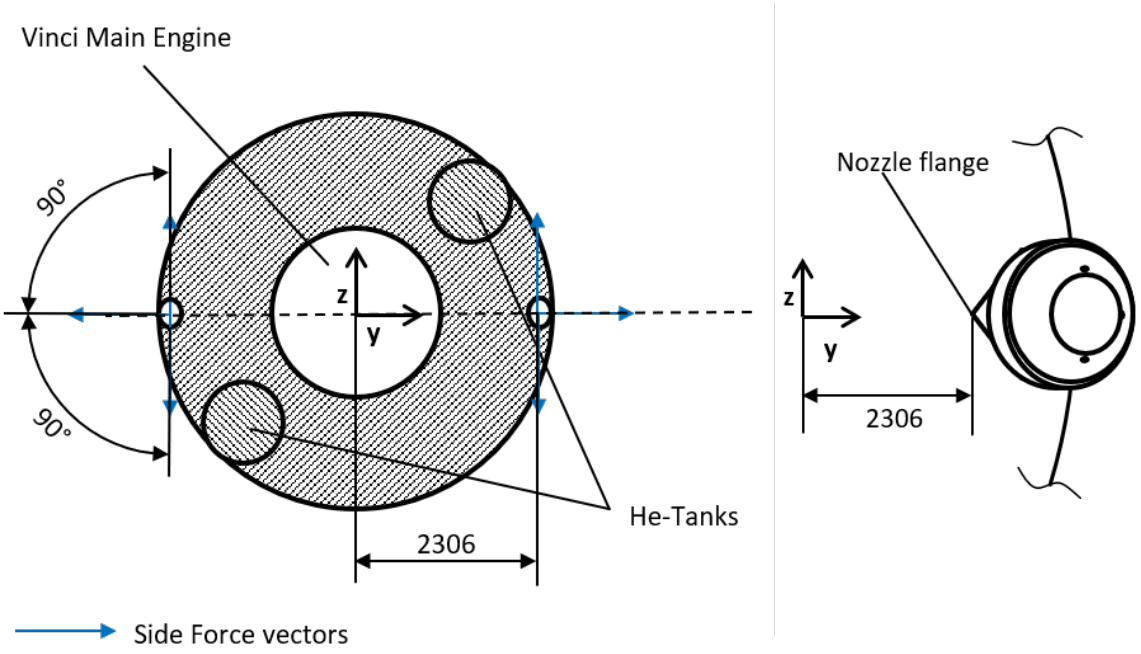

(a) Rear view of ULPM with aerospike nozzle installement

(b) Orifice distribution seen from the y-z-plane

Figure 5.5.: Rear view of ULPM with aerospike nozzle installment and side force vectors

Choice of injectant

For the application of SITVC on the current ULPM only three types of gases are to be considered available: Actual hot gas produced by the APU, GH2 or GOX. Having the relation (2.8) in mind, the first two gas options seem favourable because of their low molecular weight and the expected higher temperatures of the hot gas. The SITVC should be active during the use of the APU. So hot gas will always be the primary flow. For the sake of completeness all possible combinations are listed in table 5.4. F_s is proportional to F_p. Cold gas has a lower thrust and I_{sp} than hot gas (see tables 6.5 and 6.7). Injecting cold gas into a cold gas main flow will have significantly lower F_s. Also the injection of GOX into the hot gas primary flow is to be expected to produce the lowest side force. Therefore this investigation only focuses on the injection of hot gas into hot gas and GH2 into hot gas. A future study has to reveal if the A_f of oxygen is higher when combustion at the injection port occurs for hot gas with higher temperatures that allow self-ignition.
The great advantage of using hot gas is the stationary flow from the gas generator. The amplification and the thrust decrease have only to be determined experimentally for one hot gas OP. Using GH2 makes the system dependent on p_{Tank} and T_{Tank} which are a function of $\dot{m}_i$ and the other way around. The attitude control algorithm then requires specific data of A_f and F_s for a whole range of p_{Tank} and T_{Tank}.
One issue has to be mentioned here regarding the amplification: As described in section 2.3.1 the injection also causes an amplification ΔF_{ax} of the axial thrust. This is not a problem for a stand-alone thruster. But the application on the upper stage foresees two thrusters. When it is used on both simultaneously, which is the case for injection in the x-z-plane, also no problem arises. On the other hand, in the x-y-plane only one thruster will use its SITVC function at that moment to allow a rotation or countering a rotation around the z-axis. Increasing the axial thrust for that thruster while the other maintains its thrust level will create a second torque around the z-axis. Depending on the orientation of the thruster which is here 8°, this torque can potentially neutralize the first torque compromising the TVC. This is a problem when the injectant comes from a different source like in the case of GH2. Still, ΔF_{ax} is as hard to determine as A_f and relies on experiments. A different issue emerges when injectant and primary flow have the same source: An inter-dependency is created

because the tap-off of gas and than reinjection in the nozzle will affect F_p negatively due to losses and shocks despite the amplification of the axial thrust. In that case it leads to a lower thrust on one side and the second torque is added to the first. The effect is positive and the actual necessary F_s does not have to be that high, but it has to be taken into account by the GNC algorithm.
This issue with ΔF_{ax} is not investigated specifically in this work. However, it has to be analyzed experimentally.

Main flow / Injectant	Hot gas	GH2	GOx
Hot gas	High side force	Moderate side force, dependence on tank pressure	Low side force, dependence on tank pressure
GH2	unfeasible on ULPM	low side force, dependence on tank pressure	very low side force, dependence on tank pressure
GOX	unfeasible on ULPM	very low side force, dependence on tank pressure	very low side force, dependence on tank pressure

Table 5.4.: Evaluation of possible combinations of primary flow and injectant for SITVC

Determining the force needed to counter the disturbance

The torque the SITVC creates depends on the axial position of the CoG. The further away, the longer the lever and the higher the torque. Evaluating the maximum force needed is then done at the shortest distance for a defined torque. As frame of reference the coordinate system lies at the connection between upper stage structure and ViTF. Following assumptions are made for determining of the necessary maximum force induced by the secondary injection $F_{s,max}$ to counter $M_P = 20\,\mathrm{N\,m}$ and comparing it to the CGRS.

1. The disturbance induces a torque around the CoG of $M_P = 20\,\mathrm{N\,m}$ normal to the regarded plane
2. The side injection and F_s is perpendicular to the nozzle center axis
3. F_s attacks at the injection orifice, its position is estimated to be 80 mm away from the nozzle flange
4. The upper stage's spin around its center axis is neglected

According to the relation between torque and force $M = FL$ $F_{s,max}$ has to be calculated at the closest possible position of the CoG. Fig. 5.6 shows this principle for both regarded planes. Under assumption two $\gamma = \delta$ is valid. Then for the x-y-plane $F_{s,max,xy}$ is calculated as following

$$F_{s,max,xy} = \frac{M}{L_x cos(\gamma) + L_y sin(\gamma)} = 5.2\,\mathrm{N} \tag{5.6}$$

In a similar way for $F_{s,max,xz}$ the x-z-plane is

$$F_{s,max,xz} = \frac{M}{2L} = 2.8\,\mathrm{N} \tag{5.7}$$

The division by two is made because the orifices on both sides need to be activated.

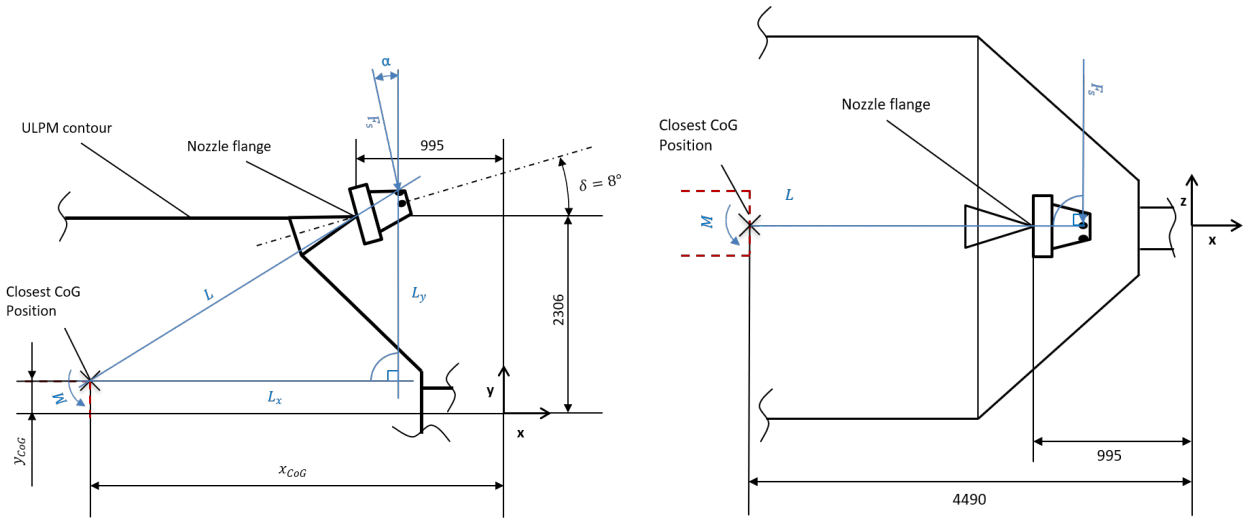

(a) Lever of side force in x-y-plane

(b) Lever of side force in x-z-plane

Figure 5.6.: Visualisation of the angle of attack of the side force creating a torque

5.2. Developing a transient EcoSimPro Model of the DMTS

For the evaluation of the performance an EcoSimPro model of the DMTS has been developed. It is a model of two thrusters with three inlet ports. Each thruster has a inlet port for the hot gas. The hot gas is hereby just a boundary. Yet, the available data about the gas properties at the nozzle inlet are not sufficient enough to take them directly as input. To obtain the desired hot gas properties a model including a gas generator, heat exchanger and hot gas feed lines is necessary. In this work the DMTS has the APU as boundary. The model is therefore a simplified model of it and has to be capable of reproducing the hot gas properties of the three selected APU OP. Because geometric variables were a needed output, Steady models in design mode were used for their determination. A Steady model is hereby a EcoSimPro model created with the components of the Steady library. If certain parameters of the geometry were needed, a Design model was employed. If a performance calculation is needed than a transient model was set up. Usually first geometric parameters are searched for and then given as input to a transient model. The goal is to obtain a transient model for the DMTS to be used for follow-up studies.

5.2.1. Modelling the hot gas boundary condition under steady-state conditions

Developing and validating a complete APU model in EcoSimPro with heat ex-changer and pumps would have been outside of the scope of this work and therefore not the objective. The model subsequently described simply has to deliver the hot gas properties at the nozzle inlet. Therefore, it only needs to be valid for the three selected operating point of the APU. It does not make a claim to be capable of simulating the complete transient behaviour of the APU apart from the defined operating points. Therefore, it was sufficient to set the boundaries of the model at the inlets of the gas generator and use results from numerical simulations as input and a means to validate the EcoSimPro model. The simulations were done at the Arianegroup site in Ottobrunn with the 2D solver Rocflam prior to this work simulating heat ex-changer, gas generator, hot gas feed lines and

nozzles but also excluding the pumps. OP1 is used to design the model while OP2 and OP3 are taken for its validation.

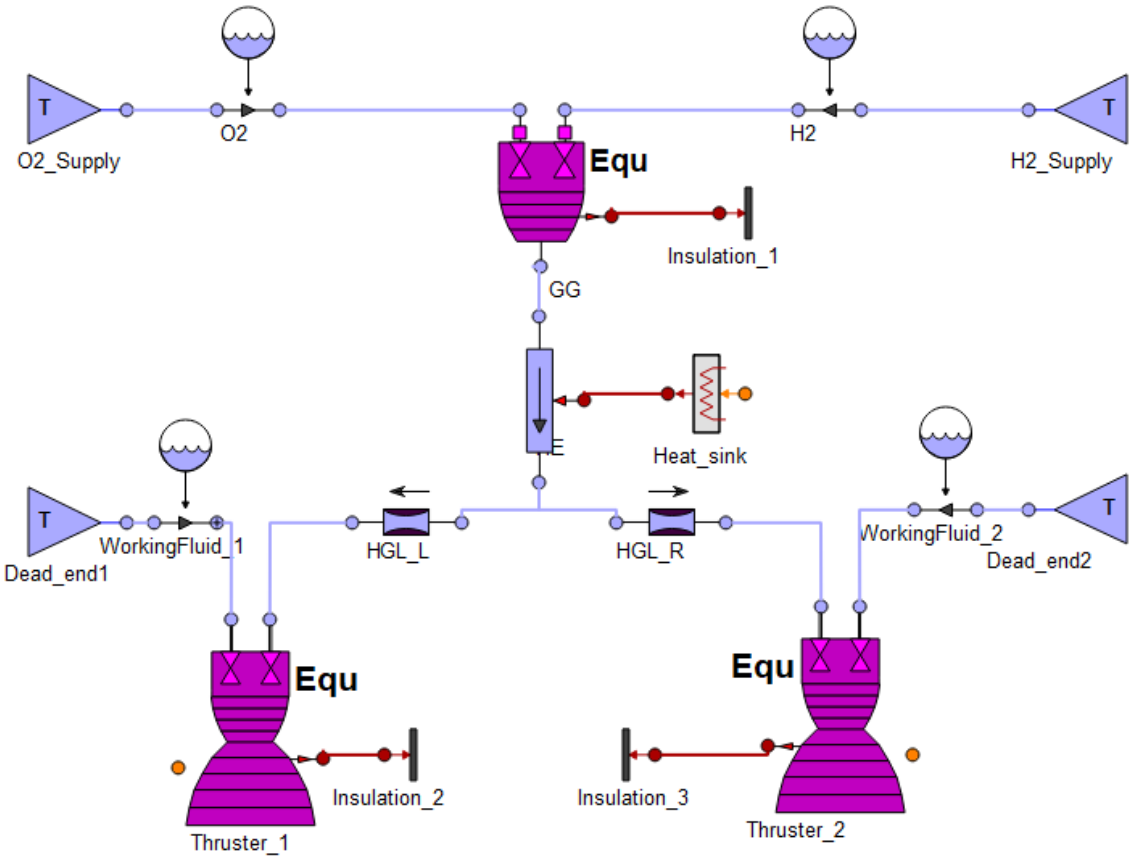

Figure 5.7.: Steady design model to obtain geometric parameters

The model seen in fig. 5.7 is a design model. It was created to obtain missing geometric variables resulting from either a lack of data or because simplifications of the model made it necessary. Two major simplifications had to be done for the model:

1. The heat ex-changer on the gas generator side is modelled as a heat sink
2. The hot gas feed lines are modelled as a concentrated pressure loss with junctions

Modelling the gas generator

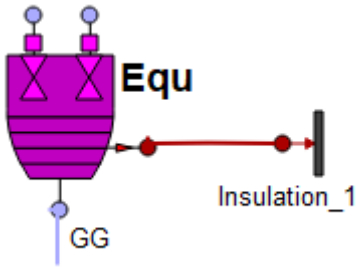

Figure 5.8.: The Steady gas generator component

The gas generator component has here an adiabatic wall with its thermal port connected to a insulation component. It is assumed that heat only is lost in the heat exchanger downstream of the gas generator. For the design mode the pressure loss for the injector was given. Instead of fixing the injector cross-sectional area A_{Inj} it was decided to use the known pressure loss coefficients of the injectors ζ_{Inj} and leave A_{Inj} as output. This was done under consideration of calculation stability. In design mode the standard is a fixed ζ with A as output. Changing this requires a manipulation of the set boundaries in the partition definition and leaves the algorithm to iterate the result. The injectors in EcoSimPro are two simple junctions while in reality the injector head is composed of several injector elements with a more complex geometry to improve propellants mixing.
The geometry of the chamber is simplified to a cylinder with a conical end. The set parameters and obtained output for the gas generator are normalized in 5.5. A_{Inj} is put into relation with the total A_t of both nozzles while the normalized profile is expressed over respective chamber diameter to chamber length.

$\zeta_{Inj,oxy}$	0.9911
$\zeta_{Inj,red}$	1.021
$A_{Inj,oxy}/(2\,A_t)$	$7.53 \cdot 10^{-2}$
$A_{Inj,red}/(2\,A_t)$	$30.72 \cdot 10^{-2}$
$d_c\ /\ L_c$	0.433
$d_{c,out}\ /\ L_c$	0.153

Table 5.5.: Normalized geometry of the gas generator model

Modelling the heat exchanger

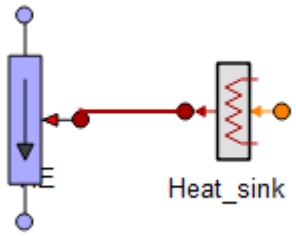

Figure 5.9.: The hot gas heat ex-changer component comprised of a tube and a heat source element

The heat exchanger leads to a cooling of the gas generator and a vaporizing of the liquid oxygen (LOX) and liquid hydrogen (LH2) coming from the respective pumps. Because the boundary is drawn here directly above the gas generator inlet, the cold gas side of the heat ex-changer is not taken into account. Therefore, heat is extracted from the gas generator via a heat sink. This is modelled with a tube element and connection of a heater element to the thermal port. The tube element represents the hot gas side of the heat ex-changer. The heater element can extract heat when it gets a negative value on its signal port.
The actual heat exchanger is not a single straight tube but has a very complex geometrical shape. The tube element in the EcoSimPro model is therefore not a comparable geometry. The length compared to the gas generator is set to 1.22 L_c. The tube component allows a parameter called *number of parallel tubes*. This was set to 30 with the diameter set to 10mm and shows to be a working solution for the model. It is necessary to do that so that the cross-sectional area is large enough to not choke the flow, but also allows enough surface area compared to volume for the heat to be

extracted from the flow. The amount of heat $\dot{Q}_{HE}$ to be extracted needs to be determined separately for each of the three operating points. The data shows that the pressure loss in the heat exchanger is relatively small compared to the hot gas feed lines. Therefore it was not modelled exactly but it is ensured that the pressure loss in the model is of same magnitude.

Modelling the hot gas lines

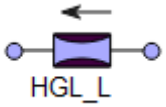

Figure 5.10.: Junction representing the hot gas line with a concentrated pressure loss

The second major simplification of the model is the replacement of the entire hot gas line with a single junction. This had to be done because of a lack of data. Resembling the hot gas line with a tube would have required input parameters such as wall roughness and wall heat conductivity. A negligible decrease in temperature between the hot gas line ends is expected [2]. An adiabatic tube element would have caused an temperature increase because of the friction taken into account. A junction resembles here an iso-thermal element combining all pressure losses of the hot gas line within one pressure loss coefficient ζ_{HGL}. Unlike for the injectors of the gas generator ζ_{HGL} is hereby an output variable after the boundary conditions have been manipulated just for this cause. A_{HGL} is set equal to the cross-sectional area of the actual hot gas line of 490.9 mm^2.

Modelling the nozzles

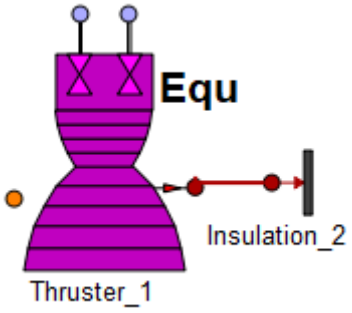

Figure 5.11.: Nozzle represented by a combustion chamber nozzle component

As explained in section 3.1.4 no nozzle component exists for the Steady library. So a combustion chamber nozzle component was used instead. In order for a successful compilation the oxidizer port was connected to a temperature boundary. In design mode the pressure and mixture ratio is fixed. The pressure in the boundary is therefore a negligible output. The mixture ratio can not be zero because then the simulation fails due to singularities. It is therefore set to 0.0001, so that the oxidizer mass flow is quasi non-existent. The geometry with nozzle throat diameter d_t, nozzle subsonic length L_{sub} and supersonic length L_{sup} is equivalent to the real nozzle. For the nozzle inlet a $\zeta_{nozzle,in} = 1$ as a discharge from a straight tube into an infinite volume [8, p.640] is assumed. The influence of the installation angle between nozzle and hot gas line on the pressure loss by diverting the flow was disregarded. The geometry was adapted to the real nozzle with simplifications in the

convergent part similar to those of the gas generator (see appendix D.1a) and the standard profile (see appendix fig.D.1b). The component requires a nozzle efficiency as input which is calculated with the known data and the simulated data from EcoSimPro for the OP1.

$$\eta_{Nozzle} = \frac{F_{real}}{F_{EcoSimPro}} = 0.939 \tag{5.8}$$

5.2.2. Transient model of the hot gas boundary

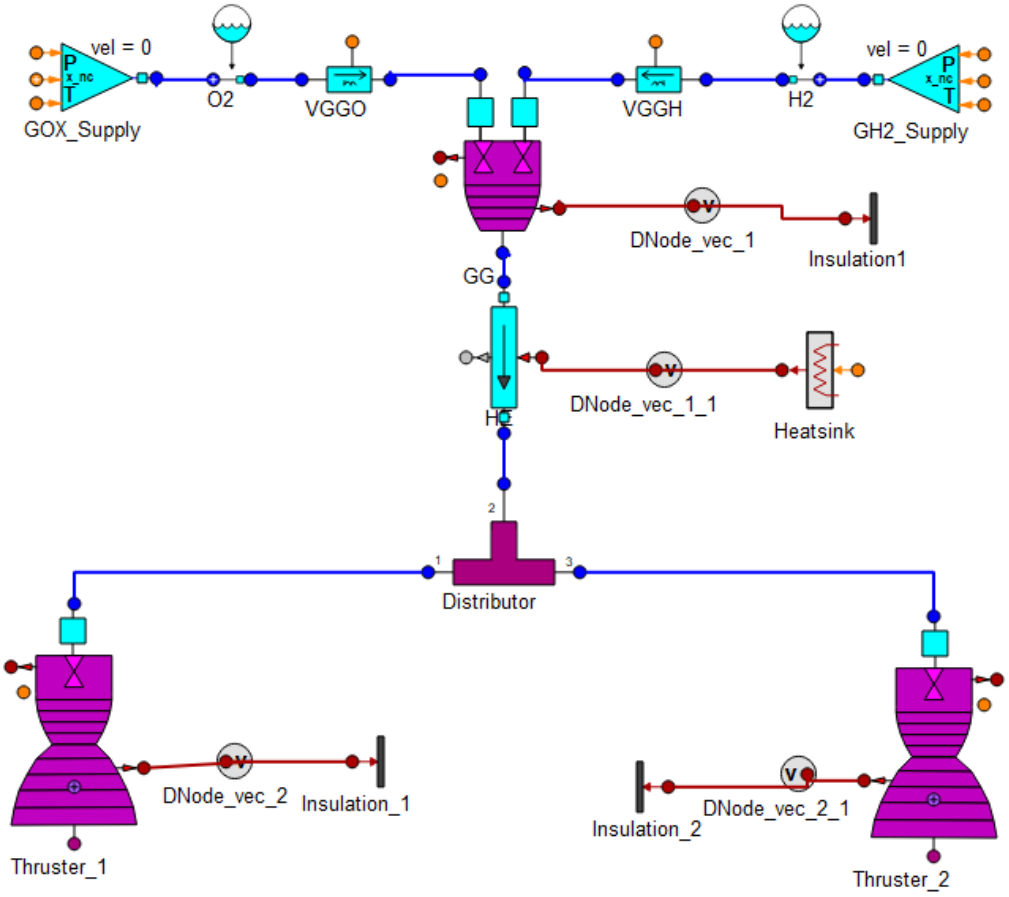

Figure 5.12.: Transient model of the hot gas boundary

Instead of using a standard nozzle component, a Combustion Chamber Nozzle with one blocked inlet was taken. That makes the transfer from the steady model to the transient model easier because the components are more similar. The tee component resembling the distributor is essentially made up of junctions, so ζ_{HGL} is included in the component. The geometry definition of the transient components includes the same parameters as the steady ones. Difference is here, that the components need common initialization values for pressure and temperature.
The extraction of heat via a heat sink leaves a serious constraint. For the transient model the inlet mass flows must be fixed. This is necessary in order to guarantee a the validity of the model. When in following models components which create pressure-losses are added downstream for example to represent valves, then this will have an impact on the mass flow. If one observes equation (2.1) one can see that it depends upon the upstream pressure in the nozzle. So adding a valve or altering the injector pressure drop in the nozzle will influence the mass flow. Then this model would become invalid because after equation (3.18) the heat flux depends upon temperature and mass flow and

the constant heat extraction would no longer represent the APU OPs. Therefore those have to be kept constant at the boundary. The result is that the pressure, even though it is an input parameter for EcoSimPro, cannot be fixed. Making downstream changes will increase the gas generator's inlet pressures at the boundary of the model. This point will be later picked up once a model for the DMTS is presented.

5.2.3. Validation of the model with APU OPs

It is repeated here that the model cannot make statements about the APU outside the defined operating points. The validation is here a proof that the model shows no great deviations from the numerical simulations for OP2 and OP3 with a geometry that was designed with OP1. This is done for the Off-design and transient model. OP1 is included here as well showing as expected, the smallest deviations. Before the actual validation can be done a design model has to determine the $\dot{Q}_{HE}$. The following steps were taken.

1. Setup the design model with all known geometric parameters and fix pressures and temperatures in gas generator and nozzle
2. Determine $\dot{Q}_{HE}$ for OP1, OP2 and OP3
3. Determine ζ_{HGL}, $A_{GG,inj,oxy}$ and $A_{GG,inj,red}$ for OP3 with the design model
4. Setup the off-design and transient model with all known and new geometric parameters
5. Compare pressures, temperatures and thrust calculated with off-design and transient model with the real data

Obtaining $\dot{Q}_{HE}$ for each operating point

It is not possible to manipulate the boundary conditions of the partition of the steady design model in a way that $\dot{Q}_{HE}$ becomes a output variable. Presumably because of the governing implicit equations in the tube element. Instead an iterative routine implemented in the experiment file figures out $\dot{Q}_{HE}$. This is possible in two ways: Either the exit temperature or the mass flow is target value. The iteration routine sets values for the input signal for the heat sink and compares it with the target value until the actual value from the numerical simulation is reached. It was decided to use the mass flow as target value because for later studies the mass flow becomes the important quantity. The mass flow is determined by the nozzle throat. Recalling equation (2.1) one can see that a full model with already implemented nozzles is necessary for the iteration of $\dot{Q}_{HE}$. The iteration routine is included in an experiment file to be found in appendix D.4.

$$\dot{m} \sim \frac{A_t p_{0,nozzle}}{\sqrt{T_{0,nozzle}}} \tag{5.9}$$

The complete input data depending on each OP for the model is as follows:

OP	1	2	3
$\dot{Q}_{HE}$ in [W]	-67136	-77829	-118083

Table 5.6.: Definition of $\dot{Q}_{HE}$ serving as input of future models

Obtaining ζ_{HGL}

Regarding (2.5) ζ_{HGL} depends on mass flow and density so it cannot be determined independently of $\dot{Q}_{HE}$. So it has to be determined with the same model. This is not complicated and the model can deliver ζ_{HGL} as output when the junction area is given as input which requires a manipulation of the boundary conditions of the mathematical model. The simulation delivered for OP1 $\zeta_{HGL} = 1.7522$. This value was set as geometric parameter for all following simulations.

Comparing model data against numerical data

Feeding this data into the the transient model delivers a complete set of output variables. A selection of them is compared against the numerically available data.

Deviation [%]	1	2	3
p_{GG}	-0.17	0.04	0.09
p_{Dis}	-0.48	-0.21	0.12
p_{Nozzle}	-0.38	-0.35	-0.39
T_{GG}	0.05	0.04	-0.04
T_{Nozzle}	13.97	14.08	13.9
$\dot{m}_{Tot}$	0	0	0
F_{tot}	-0.34	-0.23	0
I_{sp}	-0.34	-0.23	0

Table 5.7.: Deviations of temperature, pressure and thrust from the given numerical data

While the remaining values showed very small deviations, the temperatures in the nozzles however, did show a roughly 14 % higher temperature. It could not be resolved where this error is coming from. A first attempt was to look at the iteration routine, but adding more or less heat would just increase or decrease the temperature in the nozzle. Having the above mentioned relation in mind a lower temperature would just lead to an increased mass flow. Then the deviation would appear in the mass flow. It is not possible to obtain the same mass flow and the same temperature with the given throat area. There are two possible explanations.

1. The given data was calculated with a smaller nozzle diameter. Also the low η_{Nozzle} calculated for the model seems to indicate that.
2. The worse capability of EcoSimPro of calculating two-phase two-gas flows in transsonic regimes leads to an error in the calculation of the critical mass flow [2].

5.2.4. Complete transient model of the DMTS

Goal of the modelling with EcoSimPro is to obtain a model of the DMTS which can be used for first evaluations and in future studies can be connected to more sophisticated models for example a propellant tank model or a full APU model. Excluding the heat exchanger and the pumps of the APU is a serious constraint because it limits the statements which can be made about the impact

of the DMTS on the adjacent APU system. However, this limitation proves to be a great advantage, too. Without the heat exchanger and the pumps the gas generator can produce any desired gas properties only to be adjusted by a defined pressure loss and temperature. The combination of gas generator, heat sink and junction fulfils therefore the very requirement of a parametrically analysable model which can be applied to not just the APU but any hot gas system on any possible future upper stage. The graphical representation of the complete model can be found in the appendix D.2.

Implementing three inlet ports

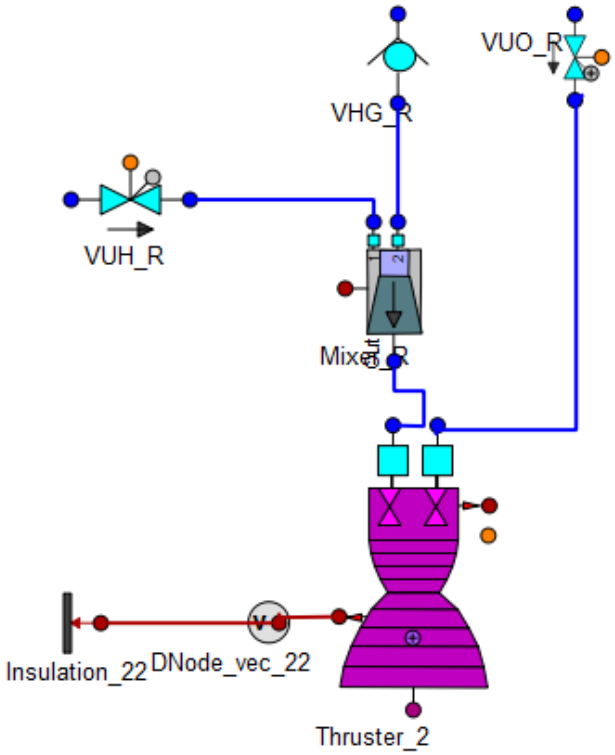

Figure 5.13.: Dual-Mode operation in a transient model of the DMTS

The three inlets are here realized with a Mixer element. VUH is the GH2-valve and VUO the GOX-valve. For the hot gas side a check valve component is used, which is just a variation of the valve suppressing any back flow.

Implementing the aerospike nozzle

In the ESPSS library an aerospike component can not be found. It simply includes only a standard-bell nozzle. Coding and validating an aerospike nozzle in EcoSimPro would have exceeded the given time frame. So a simpler approach is undertaken here. As done before for the TAPU the aerospike nozzle finds its way into the model over η_{nozzle} as the ratio of actual thrust to calculated thrust. Because there is a lack of experimental data for aerospike nozzles in this thrust class, the values from the numerical simulation from the TU Dresden were taken and put into proportion to results for a nozzle component in EcoSimPro with the same A_t and ϵ [27]. The in section 6.2 later presented comparison shows a negligible difference between an 1D bell nozzle simulated in

EcoSimPro and a 2D aerospike nozzle simulated in a internally-used code of the TU Dresden. For all models the η_{Nozzle} could then set to 1.

Implementing the SITVC function

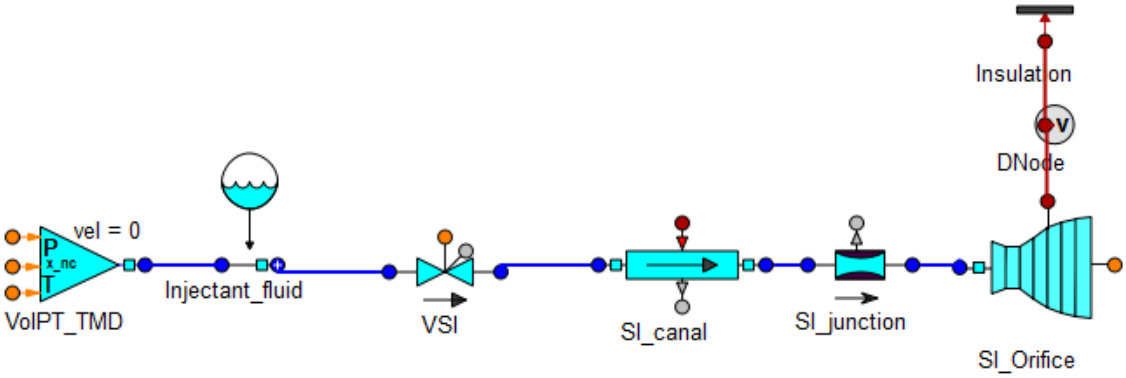

Figure 5.14.: Exemplary schematic of the SITVC canal

Fig. 5.14 shows the SITVC model before it is implemented in the larger model of the DMTS. The outlet orifice is here modelled with a nozzle instead of a junction, because the nozzle component already calculates F and I_{sp} which is of interest here. The ϵ is set to 1.0001 avoiding singularities but create results similar as an orifice. Considering a heat exchange between the primary flow and the side injection is outside of the scope of this work. Nevertheless, a tube element with a thermal port is implemented in advance for future investigations. The canal is a tube component covering the distance from the 3-way-valve to the orifice. It can be connected to the one of the combustion chamber nozzle. Usually the tube can calculate a pressure loss and serves as capacitive component between valve and junction. Its parameters for the friction calculation were lowered to make the pressure loss in the tube component negligible, because it showed to be more practical to enter a pressure loss coefficient from experimental data into the model via the *SI_junction*. The 3-way-valve *VSI* has a pressure loss coefficient of $\zeta_{VSI} = 10$ estimated from existing valves.

Complete model of the DMT with SITVC functionality

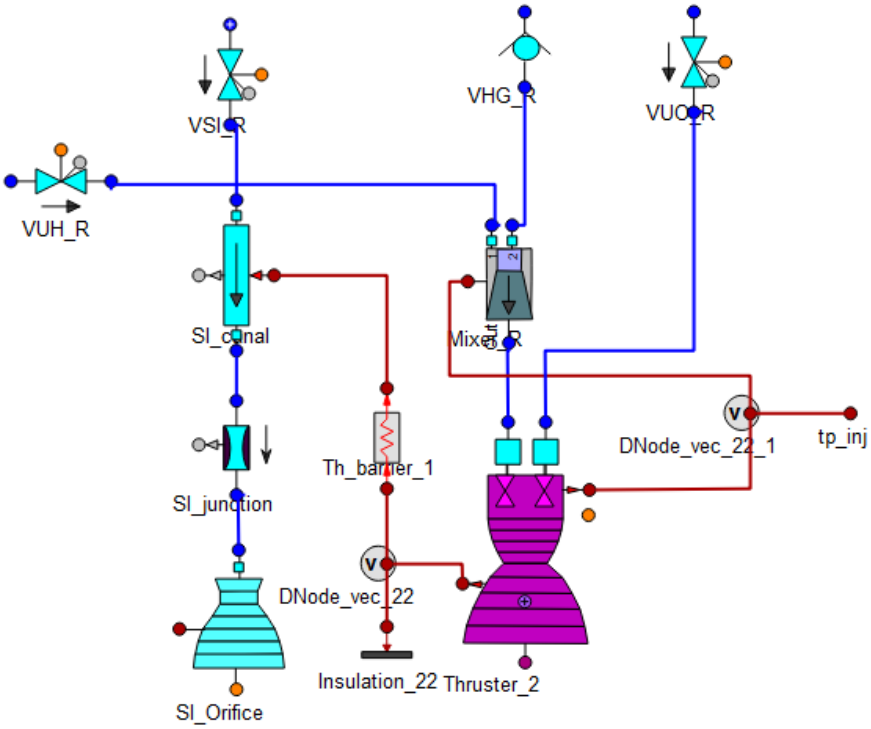

Figure 5.15.: Complete model of the DMT with SITVC implemented with full functionality

The above schematic can be represented by a new created component, coded for the purpose of use in future works. Fig. 5.16 shows this component symbolically. For the representation of the SITVC functionality one canal is sufficient. All inter-connected components can be represented by a single user-defined component. It was coded in EL. The code of the new component can be found in appendix D.5.

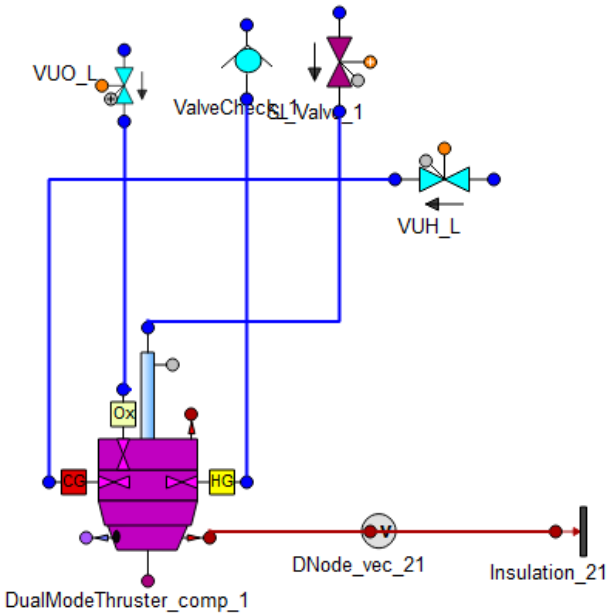

Figure 5.16.: Graphical representation of the user-defined DMT component written in EL

5.3. Simplified model of a CGRS thruster

The model presented here is a single thruster from the CGRS. The inlet conditions are those directly in front of the nozzle. p_{Tank} is hereby multiplied with the pressure loss ratio from (2.6). Values of the tank conditions for GH2 can be found in table 2.2. η_{nozzle} is set to 1. The model was validated with the existing reference point for the thruster $p_{Nozzle,inlet} = 236\,\text{kPa}$ and $T_{Nozzle,inlet} = 150\,\text{K}$. The reference calculation was done prior to this work with the 2D solver Rocflam.

	EcoSimPro Model
$(\%F)_{error}$	-1.65
$(\%\dot{m})_{error}$	1.54

Table 5.8.: Deviation of the model from the 2D numerical simulation

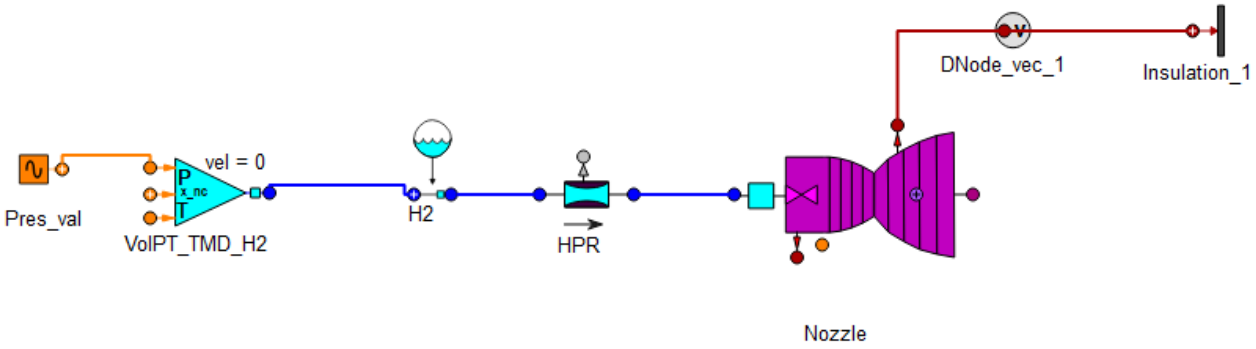

Figure 5.17.: Simplified transient model of a CGRS thruster

6. Preliminary Design of a reference case with the DMTS

So far the general requirements were defined and a description of the stage model was given. This chapter focuses on a specific use-case on the ULPM. This use-case is here designated as reference case. Reference because it just stands for the basic replacement of the TAPUs with an aerospike nozzle with the same A_t. It shall realize the following modes. The underline _ stands here for the respective OP.

Designation	Description
HG:OP_	Hot gas from three APU OP
CGH:OP_	GH2 as cold gas with two OP
CGO:OP_	GOX as cold gas with two OP

Table 6.1.: Operating modes of the DMTS in reference use-case

6.1. Requirement specification

6.1.1. Suitability of an aerospike nozzle for the DMTS project

Alongside this study the TU Dresden designed a preliminary 2D-model of the aerospike. Within the frame of the reference use-case it should be comparable to the TAPU. There are following parameters on which the comparison can be based: Throat area A_t, thrust F, mass flow $\dot{m}$ or the I_{sp} as well as the nozzle mass. One parameter has to be fixed for both nozzles, the others are used for the performance evaluation. For example, one can fix F at a specific OP for both nozzles and then compare the I_{sp}. To make a reference case for this investigation, it was decided to set the throat area A_t of the aerospike to the same as the TAPU nozzle. For the comparison the OP of the APU was taken with the highest thrust of $F = 300\,\mathrm{N}$. To make the comparison valid the TAPU was simulated with the same numerical routine as the aerospike. The results from TU Dresden are presented here to show that an aerospike is suited for the foreseen applications. It shows that the aerospike does not have superior performance, but also no negative impact. The increase in I_{sp} in terms of percent is around 1.3 %. Remarkable is just that the expansion ratio for the aerospike is lower by a factor of 7.8, but still the aerospike achieves the same thrust. The expansion ratio had to be lowered down to 10 to not violate the manufacturing requirement of a slot width of 1 mm. In order to fulfil the required throat area the shape of the cone had to be adapted. Also the cone was truncated to 60 % of its potential length in order to exchange performance for mass reduction. Both decision were made on the recommendation of the TU Dresden. Furthermore, in order to accommodate all three canals and keep the structural integrity of the cone, the maximum diameter of the injection orifices was set to 6 mm and the canal diameter to 8 mm. A first design of the TU Dresden evaluated a pressure loss coefficient in the canal of $\zeta_{SI-Canal} = 2.28$. This simulation was done with the OP1 and the side injection canal was designed with the same hot gas properties as existing in the nozzle. Fig. 6.1

shows the first 3D model of the aerospike designed by the project partners. [27]

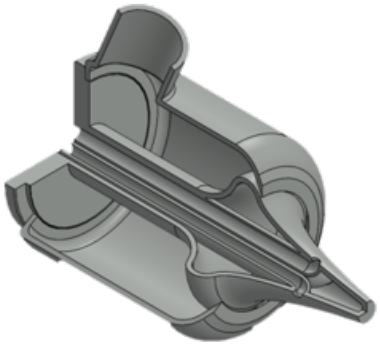

Figure 6.1.: 3/4 sectional view of first design of an aerospike for the reference case [27]

Deviation from TAPU	Aerospike
ϵ $[-]$	10
$(\%F)_{error}$ [N]	0
$(\%\dot{m})_{error}$ [kg/s]	-1.32
$(\%I_{sp})_{error}$ $[s]$	1.3

Table 6.2.: Deviation of the Aerospike nozzle from the TAPU calculated by the 2D solver of TU Dresden [27]

6.1.2. Constraints set by the APU

The additional check valve should not significantly change the OP of the APU. The influence of the DMTS on the APU should be as minimal as possible. A redesign of the system or the hot gas feed lines has to be avoided. Due to the limitations of the used EcoSimPro model this cannot be evaluated. See section 6.3.1

6.1.3. Specific valve requirements

The valve's needed operational range is defined by the gas properties the fluid has during different modes. The operational ranges can be found in the table below. They are derived from the minimum and maximum temperatures of the GH2, GOX and hot gas. The range cover the closed and open condition of the valves. The cold gas valves will only experience such high temperatures through heat conduction from the nozzle. Still, this is a necessary requirement. The magnets need to release the opening mechanism. A model of the heat conduction has to evaluate at a later design stage if the magnets need a thermal decoupling or not [2]. A geometric requirement is that they have a higher nominal area A_{nom} than the nozzle in order to not limit the mass flow. For the reference case it means $A_{Valve,nom} \geq A_t$. The 3-way-valves temperature range depends on the chosen injectant.

Valve	T_{range} [K]
Hot gas check valve (VHG)	35 - 600
GH2 cold gas valve (VUH)	35 - 600
GOX cold gas valve (VUO)	35 - 600
3-way-valve (VSI)	35 - 600

Table 6.3.: Temperature requirements of the valves set by the flow properties

6.2. Determining aerospike nozzle performance for the stage model

As explained before, the aerospike nozzle performance is carried into the EcoSimPro models over η_{nozzle}. Specifically, this is done with the thrust of the hot gas OP1 mode. It is assumed here, that the determined $\eta_{Aerospike}$ then stays constant for all other operating points as well as the cold gas modes. For the comparison the transient model of the DMTS is used with η_{nozzle} first set to 1. Then the obtained thrust is compared to the results given as input from TU Dresden [27]. A comparison shows that the values from 2D simulations from Dresden for the thrust are actually higher, but only by 0.4%. Due to this low result and out of lack of experimental data $\eta_{Aerospike}$ was set to 1 for all calculations in EcoSimPro.

$$\eta_{Aerospike} = \frac{F_{Numerical,TUDresden}}{F_{EcoSimPro}} \approx 1 \tag{6.1}$$

6.3. Performance of the hot and cold gas mode

The calculation of the performance can be done with the fully integrated transient DMTS model or the submodels of it. Basically there are three adaptions to it in comparison to the APU model. The valve is added between hot gas feed line and the expansion ratio and nozzle efficiency is changed.

6.3.1. Hot gas operation

Because in the model the mass flow is fixed at the inlet of the gas generator, we obtain the performance at all three APU OPs at the same nozzle inlet conditions as the original TAPU. To reach the same mass flow and the same temperature the pressure is adapted at the gas generator inlets. Therefore, the implementation of an additional pressure loss has an upstream effect, but not a downstream one. The deviations from the original operating points are shown below and show a negligible performance increase with the aerospike.

HG:	OP1	OP2	OP3
$(\%I_{sp})_{error}$ & $(\%F)_{error}$	0.7	0.73	0.81

Table 6.4.: Hot gas mode performance deviation of the DMT from the TAPU in the reference case

Analyzing the impact on the APU system

In reality, the check valve placed between the APU and the nozzle causes an additional pressure loss. This will alter the pressure in the nozzle which alters the mass flow. If the APU system wants to maintain its thrust level, the pumps upstream of the gas generator have to compensate this. The pump behaviour follows a characteristic curve depending on the pump power P and the pump efficiency η_{nozzle} and regulate mass flow and pressure rise (see [10, p.379]). To account for additional pressure losses the pumps will shift the OP. Without integrating the pumps into the model no statement can be made about that shift. In the current model the mass flows at the gas generator inlets are kept constant, so the pressure is adapted by the routine. The pressure rise can be used to make a rudimentary statement about the magnitude of the shift. With $A_{Valve} = 491\,\text{mm}^2$ and $\zeta_{Valve} = 10$ the valve causes a pressure loss of 17.5 %. This leads to a pressure increase in the gas generator of 16.3 % for OP1 and 15.8 % for OP3.

6.3.2. Cold gas mode with GH2

The calculation was done here with the 5.3. To use it for the DMTS only the expansion ratio needs to be changed. One could also use the fully integrated DMTS model, but this is more time consuming. The CGH-Mode was evaluated at two different OP derived from table 2.2. The pressure is reduced by 23.87 % to account for pressure losses before entering the nozzle. The value was not specifically determined for the DMTS. Actually this is the value of the CGRS-Y thruster. Essential for this work is a comparison between the CGRS thruster and the DMT. It is assumed here that both experience the same pressure drop from tank to nozzle making this effectively a direct comparison between the nozzles. They only differ in their expansion ratios. This assumption turns out to be more in favor of the CGRS because the feed line is shorter having a lower pressure loss for the DMT which means the DMT could deliver higher thrusts. The temperature is assumed to remain constant between tank and nozzle.

CGH	OP1	OP2
p_{Nozzle} $[kPa]$	236	70.419
T_{Nozzle} $[K]$	153	35.6
F $[N]$	57.01	17
$\dot{m}$ [kg/s]	0.0243	0.0324
I_{sp}[s]	179.3	71.3

Table 6.5.: CGH-Mode performance in the reference use-case

Comparison with CGRS Thruster

In table 6.6 one can find the deviation of the CGRS thruster from the aerospike. The aerospike delivers here a 3.3 % higher I_{sp} for the same tank properties. Considering calculation errors this does not indicate significant propellant mass savings by using the CGH mode of the DMT.

CGRS	OP1	OP2
F $[N]$	55.2	16.5
I_{sp} $[s]$	185.7	88.9
Deviation $(\%F)$	3.26	3.29

Table 6.6.: Comparison of the performance of CGRS and DMT

6.3.3. Cold gas mode with GOX

The same model as employed for the CGH mode can also be used for the CGO mode with a different experiment file. From the properties of the table in 2.3 two OPs for the CGH mode are derived. A pressure loss for the lines was not estimated yet so $p_{Tank} = p_{Nozzle}$. This is so far acceptable because the actual pressure in the oxygen tank was not determined specifically. The performance of the CGO mode can be found in 6.7. It is significantly lower than the CGH mode because of the higher molecular weight of oxygen.

	OP1	OP2
p_{Tank} [kPa]	310	92.5
T_{Tank} [K]	300	150
F $[N]$	75.5	22.5
$\dot{m}$ [kg/s]	0.1121	0.0474
I_{sp} $[s]$	68.7	48.4

Table 6.7.: GOX mode performance in the reference design

6.4. Comparing SITVC and CGRS propellant mass consumption for disturbance control

Main goal of this investigation is to cover up potential for propellant mass reduction. In section 6.3.2 the results show that there is no great increase in I_{sp} which could have made maneuvers with the CGH mode of the DMT more lucrative. Another level on which a comparison can be made is the mass consumption of the SITVC function and a CGRS thruster. The comparison is hereby not based on the thrust, but on the propellant mass needed to counter the same disturbance over a period of time. As already defined the perturbation causes a maximum torque around the CoG of $M_P = 20\,\mathrm{N\,m}$. Advantageous for the SITVC is the longer lever it has to the CoG which should bring about the hoped performance increase. The different thrusters are not situated in the same plane. So this exemplary comparison has to be simplified and is made for each thruster in its own plane. That means they both see the same perturbation in their respective plane with the torque vector normal to the plane. This is illustrated in fig. 6.2.

Fig. 6.3 shows a comparison of the force a CGRS thruster or a side injection orifice has to bring up when it encounters a perturbation. The longitudinal thruster is oriented in parallel to the ULPM's center axis. Therefore the lever is constant. This is not the case for the side injection into the x-y-plane which is illustrated in fig. 5.6a. At $x_{CoG} = 5600\,\mathrm{mm}$ the CGRS would switch from a longitudinal thruster of the Y-cluster to the two tangential thrusters of the Z- and Zn-cluster.

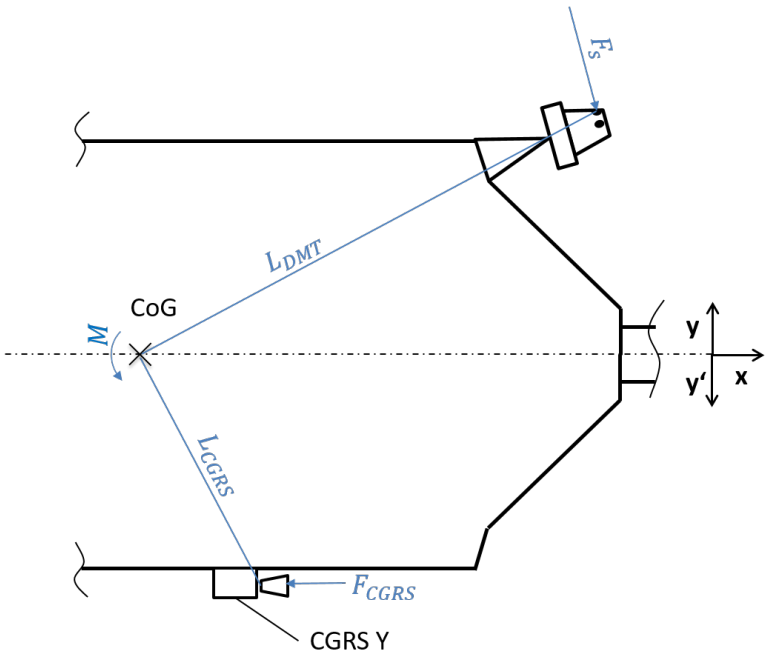

Figure 6.2.: Illustration of simplified comparison between CGRS and SITVC function

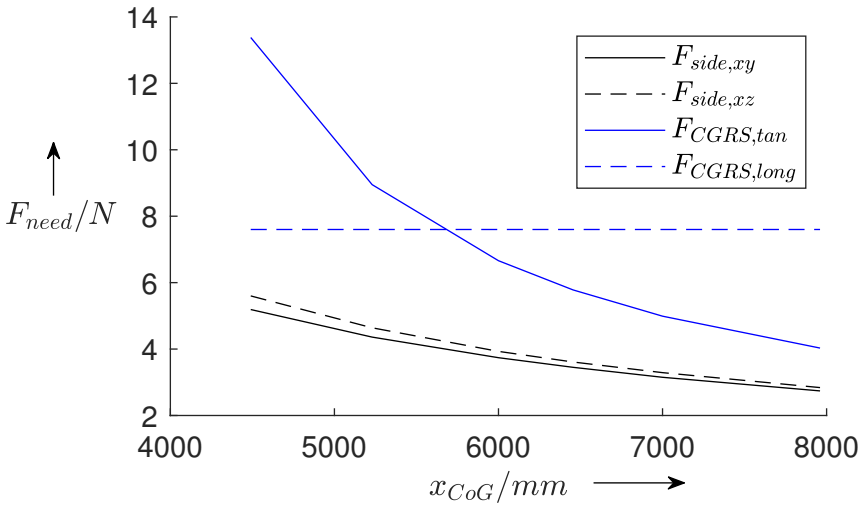

Figure 6.3.: Forces needed for side injection and longitudinal and tangential CGRS thruster to counter 20 N m at different axial positions of CoG.

The analysis done in fig. 6.3 serves as mere justification for a more detailed study. Needing a lower force means a lower mass consumption. But the above graph is calculated purely over geometric preconditions of the upper stage. The actual feasibility depends on the requirements set by the nozzle. With the limitation of the injection orifice diameter $d_{orifice}$ also the side force generated out of pure momentum is limited. The only advantageous thing is the amplification by the primary flow which will lead to a higher side force. But this amplification cannot yet be done analytical and experimental data is missing. On the other side, the CGRS-thruster is a nozzle with more than twice in throat diameter and can expand the gas.
Therefore, to make a statement about performance increase or decrease a qualitative comparison of the impulse need of each system is done. The impulse necessary to counter a torque caused by a disturbance is as follows [31, p.276]

$$\Delta I = \frac{1}{L}\int_0^{t_M} M_P dt = \frac{M_P t_M}{L} \tag{6.2}$$

Because of the numerous variables possible a mission scenario is defined and the comparison is first made between the side injection in the x-y-plane as depicted in fig. 5.6a and the CGRS-Y-thruster. The mission time t_M is set to 18 000 s. During that time M_P appears constantly. The impulse need ΔI of both systems depends on their distance to the CoG. Initially it is assumed that this is at the closest possible distance to the DMT solely on the x-axis ($y_{CoG} = 0\,\text{mm}$, $z_{Cog} = 0\,\text{mm}$). In the subsequent section the dependence of the propellant mass is shown over the entire range of the axial CoG-position.

M_P [N m]	20
t_M [s]	18000
x_{CoG} [mm]	4490
SI canal	adiabatic

Table 6.8.: Mission profile exemplary for a long ballistic phase

	CGRS-Y	Side injection of DMT
L [mm]	2632	4232
ΔI [N s]	136778	93394

Table 6.9.: Impulse need for a defined mission for side injection and CGRS

To deliver that impulse the thruster or side injection has to be used a certain amount of time. The thrust depends on the pressure. For the CGRS this is p_{Tank}. On a real mission p_{Tank} and T_{Tank} would slowly decrease during the use of the thruster because of the GH2 mass slowly leaving the tank. At a certain point when the saturation pressure is reached the liquid phase would reboil and the pressure would rise again. Furthermore, the tank is not perfectly isolated and will receive different heat influxes during this mission. [2]
For a simple qualitative comparison those effects are neglected. For the GH2 two OP of interest are used. The one where p_{Tank} and T_{Tank} are at its highest and lowest value during a mission. The CGRS can only operate between those two points. It is assumed that they stay constant over the time. The real mass consumption of the CGRS will not lie at one of those points, but between those two. This is a major simplification, but it delivers a range in which the actual mass consumption lies. The performance of the thruster at those two points are already given in table 6.6. The total mass consumption is then $m_{prop} = \dot{m} * \Delta I / F_s$.

	m_{prop} in [kg]
OP1	75.1
OP2	157

Table 6.10.: Performance of a CGRS thruster at two different OP

6.4.1. Mass consumption of SITVC with GH2 in x-y-plane

One of the two possible injectants for the side injection is GH2. This case delivers a direct comparison to the CGRS because it depends on the same GH2 source. The same pressure loss from the tank to the DMT is assumed with addition of a pressure loss in the injection canal. The assumption that the pressure loss from tank to thruster is the same for CGRS and DMT is made further on. The evaluation is done with the model from section 5.2.4. Because an analytical solution of A_f is not possible a different approach was taken. It was tried to analyze the performance for different A_f with a reasonable magnitude. As maximum is set here 3.5 which seems to be possible and is based on experience from TU Dresden [27]. The definition of A_f in this work (see equation (2.7)) is very convenient because it is independent of the primary flow. $A_f = 1$ is only the pure momentum of the injection and can be seen as the stand-alone application without active primary flow when GH2 is used. Every other A_f is just the multiplication of that force at the same $\dot{m}_i$. The performance evaluation allows an indication for future experimental studies which A_f actually have to be reached to get a substantial mass saving. Another important assumption made for this scenario is an adiabatic SITVC canal. Under this condition the calculation is independent of the primary flow and simplifies the investigation of the SITVC performance.

A_f	OP	F_s [N]	$\dot{m}_{i=GH2}$ [kg/s]	m_{prop} [kg]
1	OP1	8.65	0.00568	63.7
	OP2	2.60	0.00362	138.1
2	OP1	17.31	0.00568	31.9
	OP2	5.20	0.00362	69.1
3.5	OP1	30.29	0.00568	18.2
	OP2	9.09	0.00362	39.5

Table 6.11.: Performance of SITVC with GH2 at the same OP

At $A_f = 1$ the $I_{sp,i}$ for the stand-alone application is between 155.4 s and 73.3 s. In the table above the value for OP2 at $A_f = 1$ shows $F_s = 2.6$ N which is half of $F_{s,min}$. That means that an operational limit is reached when the a constant disturbance exceeds 10 N m. $A_f = 2$ marks therefore the minimum amplification that has to be reached. Nevertheless, this cannot be seen as a definite limitation because the assumption of constant pressure and temperature leads just to the outer limits which will never be reached. With $F_s \sim p_{Tank}$ it can only be estimated that in a stand-alone application ($A_f = 1$) the disturbance can not be countered when $p_{Tank} \leq 185$ kPa.
Fig. 6.4 shows the potential mass saving if the SITVC is used with GH2 instead of the CGRS compared for each OP. The lines in the graph show the range where the actual mass saving can be expected. The problem with using GH2 is the dependence of the decreasing tank pressure and temperature. Equation (2.8) shows that the A_f depends on $\dot{m}_i$ which decreases over longer use of the SITVC functionality. In that case the range is circumscribed by the black and red line or to put it into specific terms: The absolute mass saving for this mission scenario will lie between 14 kg and 120 kg. In relative terms this is 17 % to 77 % of the propellant mass the CGRS needs.

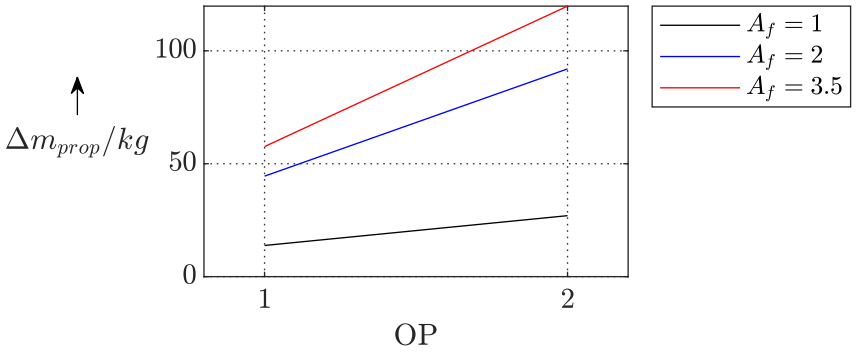

Figure 6.4.: Propellant mass saving of GH2 resources with GH2 as injectant compared to the CGRS

6.4.2. Mass consumption of SITVC with hot gas in x-y-plane

Using hot gas as injectant has other preconditions than GH2. The latter depends on variable gas properties due to the tank. The former is a gas tap-off of the primary flow. Under this condition the injection has constant properties, but an inter-dependency is created between primary flow and injection flow (see section 5.1.6). SITVC functionality is only of interest for the APU OP1 because it is used for such long missions as described in the mission profile above. Therefore only it finds consideration.
A first evaluation of F_i with the maximum $d_{Orifice} = 6\,\text{mm}$ showed a side force of 20.5 N at $\dot{m}_i = 9.26\,\text{g/s}$. This is nearly 19 % of the original mass flow and 13 % of the original axial thrust. To keep the influence of the tap-off as minimal as possible, the design criteria for the injection was set to meet the $F_{s,min}$ with a 25 % margin ($F_s = 1.25F_{s,min}$). To make a first design of the nozzle the project partners of the TU Dresden used hot gas to evaluate the geometry of the SITVC canal. That is where the $\zeta_{SI-canal} = 2.28$ originates from. Instead of reproducing their results, their obtained values are used directly for the following investigation. They evaluated that $d_{Orifice}$ had to be 3.385 mm with $F_i = 6.54\,\text{N}$. [27]
One important fact is that there is no stand-alone application possible with the hot gas because the APU system can not be throttled down that far. This is the reason why there is just a check valve. With the main flow always active there will always be an amplification. Therefore, $A_f = 1$ marks the lower performance limit of the system which will never really be reached.

F_i [N]	$\dot{m}_i$ [kg/s]	A_f [-]	m_{Prop} [kg]
6.54	0.00294	1	42
		2	21
		3.5	12

Table 6.12.: Performance of SITVC with hot gas [27]

Based on this a comparison can be made between the CGRS and the hot gas injection. It is done twice for each A_f of the hot gas injection with both OPs of the CGRS and presented in fig. 6.5. The absolute mass saving lies between 33 kg and 145 kg.

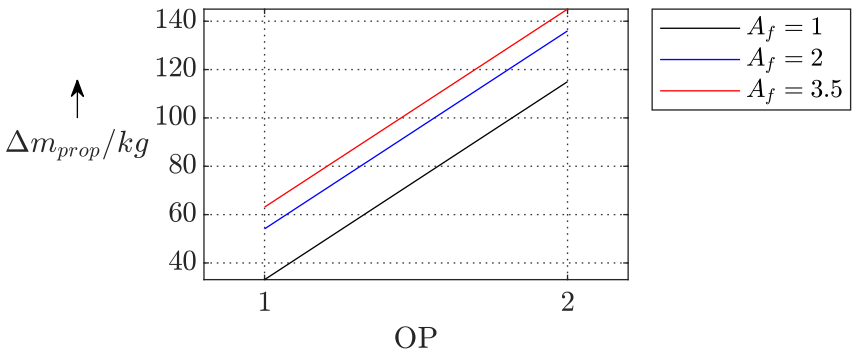

Figure 6.5.: Propellant mass saving of using hot gas injection instead GH2 with the CGRS

6.4.3. Propellant consumption at higher CoG in x-y-plane

Fig. 6.3 already showed that the F_s needed decreases when the CoG lies further away. At 7990 mm it reaches it farthest distance when the ULPM is fully loaded. The figure below shows the propellant mass consumption for several cases. The above extensively described case can be seen as the worst-case with the lowest propellant mass saving potential. The graph includes the CGRS showing that it always consumes more propellant. Here only the lowest and highest A_f is given with the best results for the hot gas as injectant at expectedly highest A_f. One exception has to be made for the case with GH2 as injectant at OP2 and $A_f = 1$. Here F_s is too low and cannot act against the defined perturbing torque. In table 6.13 the CGRS thruster consumption is set off to the SITVC consumption yielding the absolute mass savings for the worst and best outcome. It sums up all results for the side injection performance. With no amplification at the highest tank pressure and temperature the lowest mass saving are attained compared to the CGRS. At the highest amplification and the lowest pressure and temperature of the GH2 the upper limit is 150 kg. At this point it is repeated that the assumption of constant pressure and temperature only show the lower and upper limits which will never be reached. The actual value will lie in between those limits.

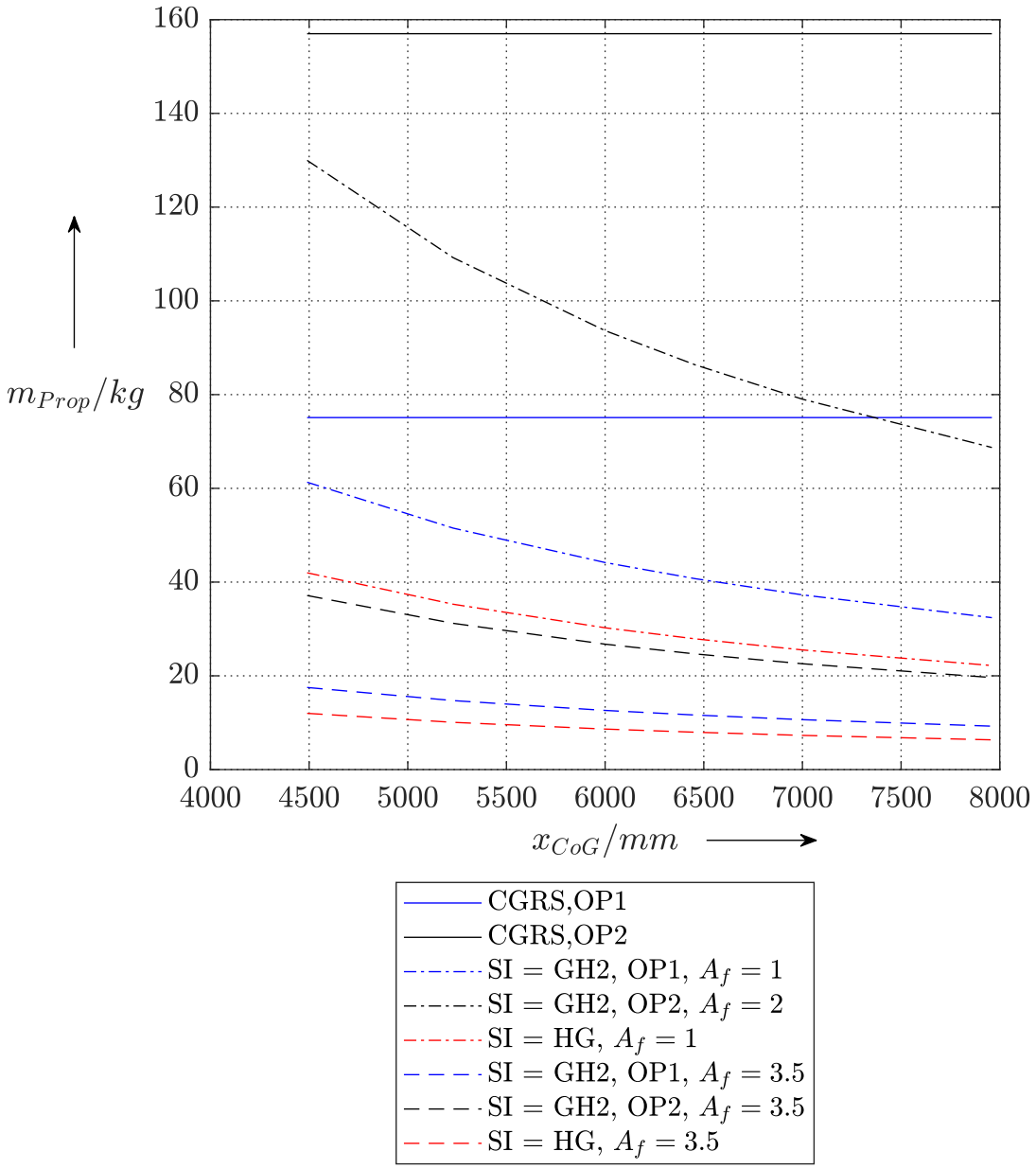

Figure 6.6.: Propellant mass needed over the axial range of the CoG for SITVC and GH2 as injectant

Abs. propellant mass saving [kg]	
SITVC with GH2	13.8 ... 137.3
SITVC with Hot gas	33.5 ...150

Table 6.13.: Range of propellant mass saving for different injectants

6.4.4. Mass consumption of SITVC in x-z-plane

Making a comparison for the x-z-plane is more complicated than for the x-y-plane. If a perturbing torque appears the side injection orifices on both nozzles have to be used. For a comparison the assumption has to be made that the CGRS-cluster are repositioned so that between the CGRS-Z and -Zn cluster and the DMTs a 90° angular distance exists. This effectively places them in the x-z-plane. Then the longitudinal Z thruster or the tangential Zn thruster are used depending on the distance to the CoG. Fig. 6.7 illustrates this. In fig. 6.3 one can see that the switch between longitudinal and tangential thruster comes at ca. 5600 mm. There is the greatest distance between the necessary forces and the highest potential mass saving. The lowest is at the outer end of $x_{CoG} = 7990\,\text{mm}$. Furthermore, just as for the x-y-plane the mass saving potential depends on p_{Tank} and T_{Tank} of the GH2 where the lowest difference in mass consumption is at the highest tank values. Depending on the A_f the mass saving potentials are summarized over x_{Cog} and tank properties in the table below. It also shows that the distribution is smaller than for the x-y-plane injection, but always has a positive impact. Also the two orifices can always counter the required M_P and do not reach an operational limit.

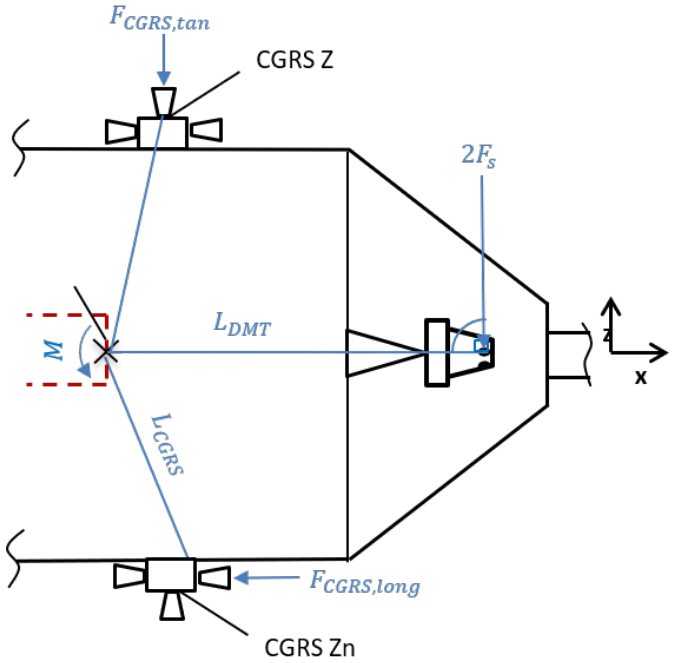

Figure 6.7.: Simplified comparison between CGRS and SITVC function in x-z-plane

Abs. propellant mass saving [kg]		$A_f = 1$	$A_f = 3.5$
SITVC with GH2	$x_{CoG} = 7990\,\text{mm}$ & OP1	6.2	30
	$x_{CoG} = 5600\,\text{mm}$ & OP2	50.5	126.4
SITVC with Hot gas	$x_{CoG} = 7990\,\text{mm}$ & OP1	16.7	33
	$x_{CoG} = 5600\,\text{mm}$ & OP2	122.5	147

Table 6.14.: Range of propellant mass saving for different injectants in x-z-plane

6.5. Evaluating the dry mass impact

The other half of the mass budget calculation is the estimation of the dry mass impact added to the ULPM. The mass formulations for different parts are taken from section 5.1.5. The dry mass was segregated into the architectures necessary for each function of the DMTS. The nozzle will be 3D-printed and its mass was estimated by the TU Dresden to 1 kg. The detailed calculations are not to be found here, but in the appendix B. Here merely the dry mass outcome is presented.

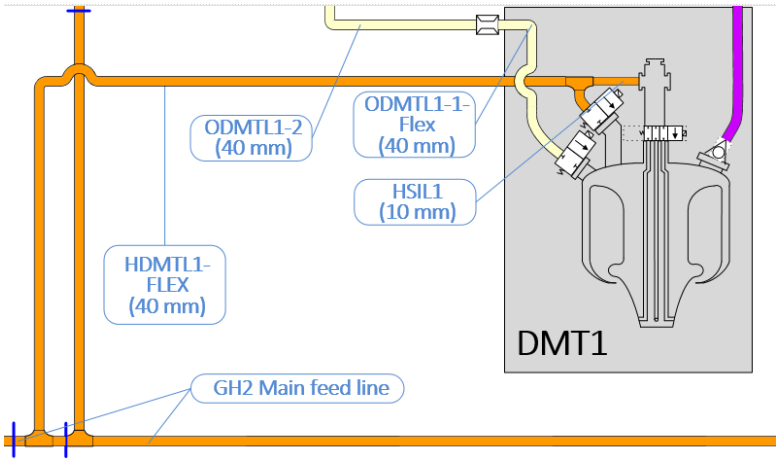

Figure 6.8.: Schematic of the DMT1 connected to the fluid lines

6.5.1. Additional dry mass for hot gas side

The hot gas side just needs an additional check valve at each thruster.

Part	$m[kg]$
Check-Valve	2.6
Total	2.6

Table 6.15.: Additional dry mass for the hot gas mode

6.5.2. GH2 side dry mass impact

Attaching the feed lines of the DMT to the main GH2 feed line needs a terminal with flanges to split the tube in two. Under the condition that the CGRS-Y cluster can be spared no additional terminal is needed for the second DMT because it already marks the end of the GH2 feed line. This explained more detailed in section 6.5.5. The length for the flex line to the thruster was estimated in section 5.1.2.

Mass [kg]	DMT1	DMT2
Terminals with flanges	5.2	-
Flex-Lines with flanges	2.01	2.01
Valves	4.3	4.3
Total	17.82	

Table 6.16.: Additional dry mass for the cold gas mode with GH2

6.5.3. GOX side dry mass impact

The GOX side mass is different for each thruster due to the asymmetry of the pipe length.

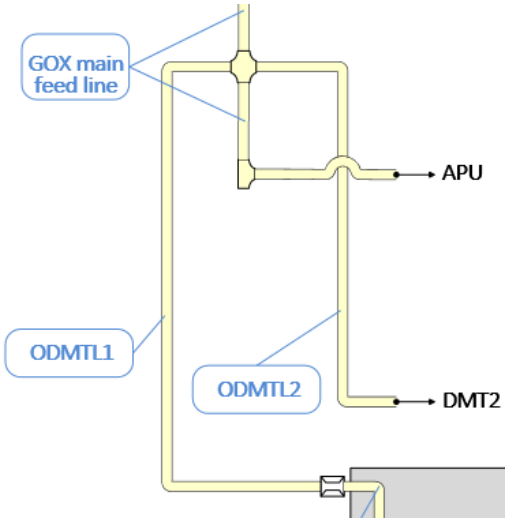

Figure 6.9.: Schematic of the addtional architecture on the GOX side

Mass [kg]	DMT1	DMT2
Terminals with flanges	5.2	
Rigid lines with flanges	-	7.22
Flex-Lines with flanges	2.95	2.01
Calibrating Orifice	0.5	-
Valves	4.3	4.3
Brackets & Mounts	1.53	
Total	28.01	

Table 6.17.: Additional dry mass for the cold gas mode with GOX

6.5.4. SITVC dry mass impact

The dry mass for the SITVC functionality does not depend on the chosen injectant because lines, valve and distributor would be identical. The terminal is directly attached to the thruster and allows

a distribution of the injectant and primary flow.

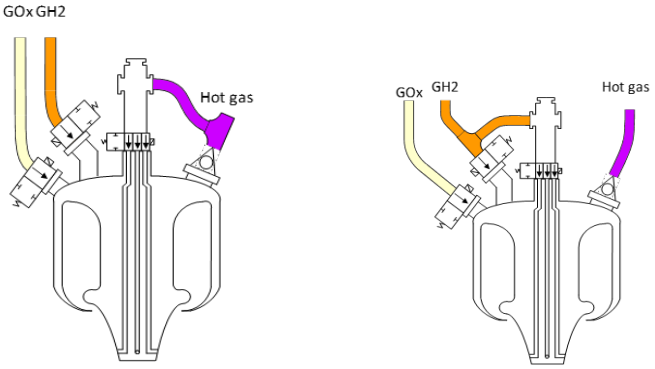

(a) DMT with hot gas side injection

(b) DMT with GH2 side injection

Figure 6.10.: DMT with possible side injectants

Mass [kg]	
Terminal	4.4
Rigid Line with flanges	0.227
3-Way-Valve	4.3
Total (single DMT)	8.93
Total	17.9

Table 6.18.: Dry mass of SITVC for both thrusters

6.5.5. Estimation of CGRS-Y and -Yn thruster dry mass

Under the assumption that the DMTS can replace two CGRS thruster the dry mass of those thrusters can be saved. This is then weighed against the dry mass of the DMTs. In the following the dry mass of the two CGRS thruster is evaluated with the same formulations. Reason for this is that the pipe length could be acquired but not its mass from the provided data. The feed lines to the CGRS have a $d_i = 40\,\text{mm}$. The nozzle mass is combined with the valve mass and is about 4.6kg. Between the connection to the GH2 main feed line and the thruster is an additional flex line and ridid line.
Special of the CGRS-Y thruster is it is situated at the end of the main feed line and not on a side arm. So a part of the main feed line can be removed all together. The length was estimated to be 1.5 m and is the length from the DMT2 to the attachment of the flex line. This is illustrated in fig. 6.11. The terminal for the DMT2 is just added for the understanding. In table 6.16 it is already excluded. After the installation the DMT2 it will be situated at the end of the GH2 main feed line.

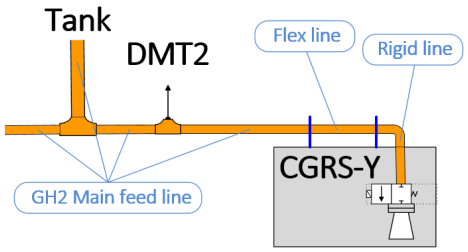

Figure 6.11.: Illustration of the expandable mass of the CGRS-Y-Thruster

In contrary, the CGRS-Yn thruster sits at a side arm of the main feed line. A terminal is therefore necessary. The feed line from there to the thruster consists of the flex and rigid line.
Table 6.19 shows a total replaceable dry mass of 29 kg.

m_{dry} $[kg]$	CGRS-Y	CGRS-Yn
Part of main feed line	1.52	-
Terminal with flanges	-	5.2
Flex line with flanges	3.97	3.98
Rigid line with flanges	1.63	1.63
Thruster and valve	4.6	4.6
Brackets	1.1	0.8
Total	29.04	

Table 6.19.: Total estimated dry mass of the possibly replaceable CGRS-Y and CGRS-Yn thruster

6.6. Total mass impact of the reference model

The DMTS is foreseen to take over certain GNC operations which currently the CGRS is responsible for. By over-taking these operations or functions a part of the CGRS could be removed. In the section before it was already mentioned that this should be the Y- and Yn-thruster. Due to the limited time frame of this investigation it cannot be stated definitely that this does not lead to a limitation of the upper stage's GNC capabilities. Not all aspects and possible disturbances were covered which might arise. Only a deeper investigation on the side of the GNC development can do this. The idea is that with the use of the CGH mode all operations are possible that are currently possible with the Y- and Yn-thruster. Table 6.20 compares the additional dry mass for the CGH mode of the DMTS with the dry mass of the CGRS-Y and -Yn thrusters which can potentially be removed. It shows a potential dry mass saving of 12.9 kg. The calculation also rudimentary regards the dry mass impact due to a repositioning of the remaining CGRS-Z and -Zn clusters. If one observes fig. 2.2 the axis between the TAPUs is tilted 50° to the CGRS-Z- and Zn-thruster. The repositioning alters this angle to 90° so that all cold gas using thrusters have the same angular distance again. With a closer look one can see that this mass is estimated to be 1.52 kg. This is the mass subtracted from the main feed line at Y-end and is then added on the other end where the the Zn-thruster is situated.

Mass change [kg]	Added	Removed
Expendable mass of CGRS Y- and Yn-cluster		29.04
Additional mass for repositioning of Z- & Zn-cluster	1.52	
Nozzle replacement	2	5.2
CGH-mode functionality	17.82	
Saving potential for GH2 operations		12.9

Table 6.20.: Potential dry mass saving by using CGH mode of DMT instead of CGRS

In table 6.21 the complete dry mass impact is listed. Two trade-offs are made for the reference case. A design with reduced functionality and one with full functionality. They only differ in the incorporation of the CGO mode because it increases the launchers flexibility, but also its dry mass.

Mass change [kg]	Added	Removed
Expendable mass of CGRS Y- and Yn-cluster		29.04
Additional mass for repositioning of Z- & Zn-cluster	1.52	
Nozzle replacement	2	5.2
CGH-mode functionality	17.82	
HG-mode functionality	2.6	
SITVC functionality	17.9	
Design with reduced functionality	7.6	
CGO-mode functionality	28.01	
Design with full functionality	35.61	

Table 6.21.: Total dry mass impact of the DMTS system on the upper stage

The SITVC is added to save propellant mass instead of using the CGRS or the CGH mode of the DMTS. Its propellant mass saving potential can therefore be set off to the dry mass impact of the DMTS of 17.9 kg. Updating table 6.13 yields:

Abs. potential mass saving [kg]	
SITVC with GH2	-4.1 ... 119.4
SITVC with Hot gas	15.6 ... 132.1

Table 6.22.: Absolute mass saving potential by adding the SITVC functionality on the ULPM

It shows that for $A_f = 1$ at lowest p_{Tank} and T_{Tank} and closest CoG position the impact is negative when GH2 is used as injectant. But this is the worst-case scenario which will not be seen in reality because the those tank conditions are to be expected at the end of the mission. Also a heat flux between the injection canal and the cone wall is not considered which will heat the GH2 increasing the $I_{sp,i}$ of the injection. If hot gas is used a positive performance impact is to be expected.
For the reduced design the dry mass impact can also be set off to the SITVC propellant mass saving potential (see table 6.23).

Abs. potential mass saving [kg]	Reduced design	Full design (with GOX)
SITVC with GH2	6.2 ... 129.7	-21.8...101.7
SITVC with Hot gas	25.9 ... 142.4	-2.1...144.4

Table 6.23.: Total mass saving potential of the DMTS system on the ULPM

7. Preliminary Design of a higher thrust evolution of the DMTS

Currently, the APU is capable of a maximum thrust of 300 N. For future missions even higher thrust levels between 400 N to 800 N should be possible so the deorbiting maneuver can be accomplished faster giving the upper stage a larger deorbiting window. The APU is a complex system because it has two aims. The first is to provide pressurization gas, the other is to provide thrust. This puts numerous constraints on the system and makes it difficult and expensive to redesign it for thrust increase. An evolution design of the DMTS could provide such an additional function. This is envisioned with an afterburning mode using GOX and mix and combust it with the GH2-rich hot gas from the APU. This would mean an opportunity to use GOX from the ullage and avoid a change of the APU. The idea is basically an ullage-burner like it was used for the Saturn V third stage to repressurize the tanks [29, p.6-11]. In this chapter it is tried make a concept for an evolution case of the DMTS and to identify the major constraints and requirements for such a system. A detailed mass budget like for the reference use-case is not done and the SITVC capability is not investigated here. The former made studies on it were independent of the primary flow, so a higher thrust does not influence the results. Reviewing equation (2.8) one can see that a higher I_{sp} leads to a higher amplifications, but without experimental data it will not be specifically investigated for this case.
The evolution design should realize the following modes. Only the first mode is described here.

HGB:OP_	Afterburning with GOX, GH2 and hot gas from APU
HG:OP_	Hot gas from APU
CGH:OP_	GH2 as cold gas
CGO:OP_	GOX as cold gas

Table 7.1.: Operating modes of the DMTS in evolution design

Developing the concept is difficult because numerous variables have to be taken into account. As starting point it was chosen to set following requirements for the HGB mode:

1. Design OP is again the OP1 from the APU
2. The thrust of the DMT should be doubled: $F_{design} = 300\,\mathrm{N}$
3. Operating temperature is $T = 1200\,\mathrm{K}$

The last boundary is chosen because the highest possible I_{sp} is desired. So the design temperature of the aerospike combustion chamber T_{ACC} is set to the for this work defined maximum temperature of the silicon nitrite. In reality, higher limits are to be expected on side of the TU Dresden [27]. That is the reason why no margin is left here. To reach both aims it is here foreseen to not just insert GOX into the chamber, but also GH2 out of fear constraining the system too much. Especially for the EcoSimPro model described later this is important. The temperature depends on the Mixture ratio (MR). Fixing the temperature means fixing the MR. This fixes $\dot{m}_{GOX}$ because the mass flow of the hot gas is already fixed. Then the A_t is an output depending on the design pressure p_{ACC}. The latter can also not be chosen independently from the APU and the GOX feed system. If p_{ACC} and A_t are fixed then so is the thrust which becomes an output. So allowing the system to also use GH2

lifts constrains and makes the above mentioned design point possible. From that point on a first concept loop was initiated.

7.1. Architecture of the evolution design

When evaluating the concept idea it becomes clear that just opening the GOX and GH2 valves and starting the APU will not lead to a feasible design. First problem is that p_{Tank} of the GOX decreases over operation time. Furthermore, $p_{Tank,GOX}$ is much lower than the APU pressure. So not just has to be there a way of keeping $p_{Tank,GOX}$ constant, but also a throttle device must reduce the pressure of the hot gas. This throttling would then also occur on the HG mode decreasing the APU performance.
Solving this problem is possible, but requires adaptions of the ULPM. A solution would be a buffer tank architecture which stores the GOX and releases it at constant pressure. This idea is inspired by the currently installed IGFS which is responsible for reigniting the Vinci Main Engine. It stores GOX and GH2 to feed it to the chamber. In a future upper stage this reignition system could be designed in a way that it also carries enough resources for the afterburning mode of the evolution design. As a new component added to the ULPM this architecture would have a great mass impact on the upper stage which would probably compromise all efforts of mass reduction. On the other hand the United Launch Alliance (ULA) has concepts of buffer or accumulation tanks foreseen for their Aces upper stage [1]. Fig. 7.1 shows this concept. In order to continue the investigation it is assumed that such a buffer tank structure can be used.

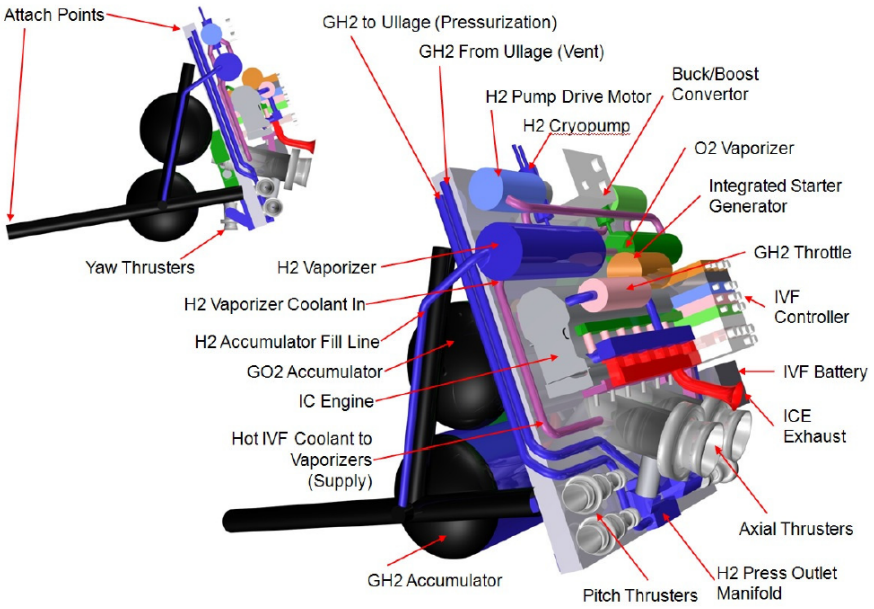

Figure 7.1.: Accumulator tank of ULA's Aces upper stage [1]

7.1.1. The buffer tank architecture

The architecture itself is not designed in this work. The evolution design merely dictates the outputs which it has to deliver. A schematic of such a buffer tank is depicted in fig. 7.2. For the use-case on the ULPM such a structure is not worthwhile for just using it for the DMTS. For a realistic use-case a buffer tank structure should already be installed for other purposes. The DMTS can then profit from it by being connected to it. In that case a potential performance gain is possible. A buffer tank

structure is thereby not a new concept and for other use-cases a viable solution for performance and flexibility increase of modern upper stages. The temperatures in the buffer are here the upper limits of the previous use-case set to $T_{GH2,0} = 150\,\mathrm{K}$ and $T_{GOX,0} = 300\,\mathrm{K}$.

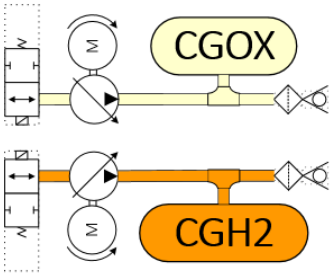

Figure 7.2.: Schematic of a possible buffer tank architecture

7.1.2. The injector

Just igniting the mixture in the thruster after opening the valves is not a viable solution considering flame holding and combustion instabilities. Right from the start it is clear that the evolution design needs a propellant injector. A concept of how the interior could look like is given in 7.3. Using three inlet ports is rather exotic. The GH2 and the hot gas can be collected in the same manifold because the hot gas is already fuel-rich. So just more GH2 is added to it. This is also advantageous for the EcoSimPro model which only can define two injectors in the combustion chamber nozzle component. The GOX needs its own manifold and injector head. Without a CAD model the exact geometry in the aerospike can not be determined within this work. Also the number of injectors is not estimated here. But it is vital for the concept to calculate the total injector area $A_{Tot,Inj}$. The other modes have to work, too and they require that A_t remains the smallest cross-sectional area in order to allow the critical mass flow to be defined there (see equation (2.1)). So a major requirement can be derived from this point on:

$$A_t < \begin{cases} A_{Inj,red} \\ A_{Inj,oxy} \\ A_{Inlet} \\ A_{Valve} \end{cases} \tag{7.1}$$

This is the essential requirement when a Dual-Mode should be realized on a thruster, which has an injector. $A_{Inj,oxy}$ is the GOX oxidizer. $A_{Inj,red}$ is the combined total injector area after the hot gas-GH2 manifold. General literature like Humble [28, p.232] suggests a design pressure drop Δp between 10% and 25%. For the injectors in this concept $\Delta(p\%) = 15\,\%$ is chosen. Future experiments have to prove if this feasible or if combustion instabilities in the aerospike nozzle require higher pressure losses. A standard injector has a $\zeta_{Inj} = 1.7$ [28, p.233].

7.1.3. Ignitor element

Before starting the concept phase there was the idea to use the APU hot gas as an autogenous ignition method to ignite the mixture in the thruster. But a quick evaluation showed that this is not possible. The APU hot gas has a maximum temperature of ca. 600°, which is to low for a hydrogen-oxygen mixture to self-ignite. For this the temperatures must initially reach at least 675 K [32, 65ff.].

Therefore, a ignition method has to be selected, which is outside of the scope of this work. Possible methods could be a spark plug from the APU or catalytic or laser ignition [2].

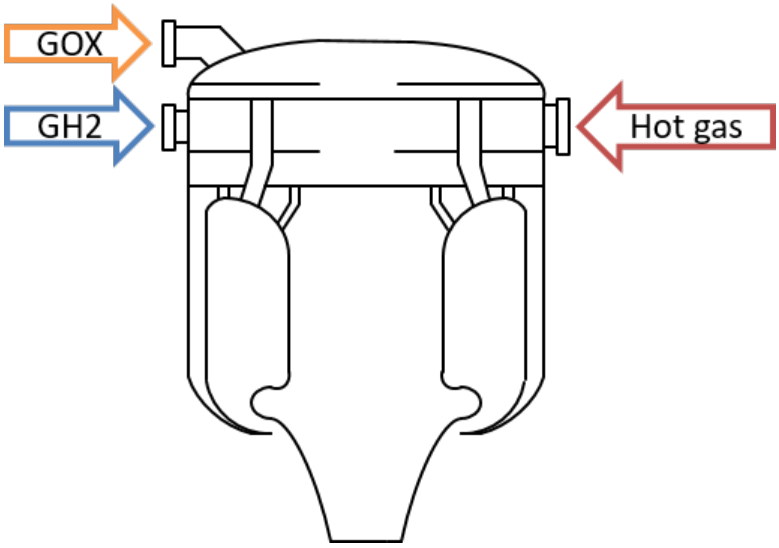

Figure 7.3.: Concept of the evolution design thruster (shown w/o SITVC)

7.2. EcoSimPro model

A special EcoSimPro model had to be developed for this analysis. It is a Steady Design model. The desired output of the model would be $\dot{m}_{GOX}$, $\dot{m}_{GH2}$, p_{ACC} and A_t and setting F_{design} and T_{ACC} as boundary conditions. Also necessary outputs are the $A_{Tot,Inj}$ to prove if the above set requirement is fulfilled. Unfortunately, such a manipulation of the boundary conditions does not seem to be feasible. First attempts ran into problems with missing constraints or unstable simulation with untrustworthy results. With a trial and error approach a feasible model could be obtained. Apart from the standard inputs for the APU component to deliver the hot gas properties, the major inputs and outputs are:

Inputs	Outputs
p_{ACC}	T_{ACC}
$T_{GOX,0}$	$p_{GOX,0}$
$T_{GH2,0}$	$p_{GH2,0}$
A_t	
$\dot{m}_{GOX}$	$\dot{m}_{GH2}$
ϵ	F_{design}
ζ_{Inj}	$A_{Tot,Inj}$

Table 7.2.: Major inputs & outputs of the steady design model of the evolution DMT concept

It shows that some of the desired outputs became inputs. This leads to an unavoidable iterative approach. For p_{ACC} a first estimation is made based on previous simulation results. The transient model of the APU calculated the pressure before the nozzle inlet after the junction representing the hot gas line. The evolution model would now place a valve and an injector between the nozzle and

the hot gas line. Based on the simulation of the DMTS for the previous use-case a $\Delta(p\%)_{Valve} \approx 15\,\%$ of the downstream pressure is used. Together with the set injector pressure loss follows:

$$p_{ACC} = \frac{p_{HGL,out}}{(1+\Delta(p\%)_{Valve})(1+\Delta(p\%)_{Inj}} \approx 480\,\text{kPa} \tag{7.2}$$

With the same input for the GOX and GH2 sides the needed pressure from the buffer is obtained. The T_{ACC} can not be fixed in the model, but with the input of $\dot{m}_{GOX}$ MR is adapted and sets T_{ACC}. With the equation for the critical mass flow (2.1) the simulation delivers $\dot{m}_{GH2} = \dot{m}_{Total} - \dot{m}_{HG} - \dot{m}_{GOX}$. This can be seen as the inner iteration process. Before that is initiated A_t has to be set. Together with p_{ACC} and ϵ the thrust equation (2.2) results in F_design. ϵ is evaluated on the side of the project partners to check the manufacturing requirement and can only be done after an A_t was given. This can be seen as a third iteration process. $A_{Tot,Inj}$ is calculated by EcoSimPro with (2.5). Rearranging it yields:

$$A_{Tot,Inj} = \dot{m}\sqrt{\frac{\zeta_{Inj}}{2\,\rho_{up}\,\Delta(p\%)_{Inj}\,p_{ACC}}} \tag{7.3}$$

7.3. Definition of the design operating point of the afterburning mode

For the first design loop $A_{t,evol}$ is set to 2.571 $A_{t,ref}$ to be smaller then the inlet and the valve. The expansion ratio was first maintained with $\epsilon = 10$, but is set to 30, after a second iteration on the side of the project partners showed that this is feasible [27].

Output		
	1. Iteration	2. Iteration
p_{ACC} $[Pa]$	480000	
T_{ACC} $[K]$	1200	
$\dot{m}_{Tot}$ [kg/per/second]	0.0059	
ϵ [-]	10	30
F_{design} $[N]$	302	314
I_{sp} $[s]$	380	396

Table 7.3.: Geometry and performance of the design operating point

Buffer tank output	
$p_{GH2,0}$ $[KPa]$	638.4
$T_{GH2,0}$ $[K]$	150
$p_{GOX,0}$ $[KPa]$	638.4
$T_{GOX,0}$ $[K]$	300

Table 7.4.: Necessary output of the buffer tank for maintaining the design operating point

7.3.1. Analyzing the injector area requirement

Putting the $A_{Tot,Inj}$ into relation to A_t yields:

$$\frac{A_{Tot,Inj,oxy}}{A_t} = 0.11 \tag{7.4}$$

$$\frac{A_{Tot,Inj,red}}{A_t} = 1.04 \tag{7.5}$$

One can see that the requirement of A_t being the critical flow area is no longer fulfilled. Therefore, the CGO mode does not work. The GH2 mode does work, but just with a tight margin. Observing equation (7.3) from last section, one can see that this is caused by the higher upstream density of the oxygen. This leaves not much space for improvement. Decreasing A_t will decrease $\dot{m}_{total}$ and with it also $A_{Inj,oxy}$ will decrease. Another possibility could be the reduction of $\Delta p\%$, but then the flow becomes sensitive to combustion chamber instabilities. Or ζ_{Inj} is increased. But significant values would be around $\zeta_{inj} \approx 140$, which is an unfeasible option.
The GH2 seems possible so far, but increasing $\Delta p\%$ will make it unfeasible, too.

7.3.2. Evaluating the mass consumption for deorbiting

The initial reason for the evolution was reducing propellant mass and operation time for deorbiting. The current systems creates a total impulse of 473 200 N s. With $t_M = \Delta I / F_{tot}$ and $m_{prop} = \Delta I / I_{sp} / g$ following performance can be achieved with the evolution design.

Impulse need: ΔI [Ns]	473200
Thrust increase $F_{Evol} / F_{APU,max}$	2.1
Mission time reduction $\Delta t_M / t_{M,APU}$ [%]	52.2
m_{Prop} saving [kg]	34

Table 7.5.: Performance increase of the deorbiting maneuver with the DMTS evolution design

8. Conclusion

Modern upper stages like the A6 ULPM demand performance augmentations due to the increasing competition on the launch market. For that reason innovation projects get funded analysing the feasibility of new concept. This thesis made investigations to such a concept: A Dual Mode Thruster System. The starting point was the idea of a thruster system using either the ULPM hot gas or GH2 with the same nozzle. The current nozzle of the APU system and the CGRS use a nozzle with different expansion ratios, but same nozzle throat area. Moreover, a TVC capability via secondary injection is selected for the DMTS because the current ULPM has a need for countering certain thrust vector deviations more effectively than with its Cold gas reaction control system. A special property of the side injection is an amplification of the pure momentum force of the injection due to fluid phenomena. Instead of using a conventional nozzle an aerospike is foreseen for the concept because then the injection orifices of the side injection point outwards giving extra GNC-capabilities without the primary flow active. Aerospikes also potentially offer a higher thrust-to-weight ratio. This investigation was accompanied by studies from the TU Dresden. Their data and expertise about the detailled nozzle design served as input to the system analysis done in this thesis.
Performance increase is translated into mass savings of propellant and dry mass. Main objective of this thesis was to study if the Dual-Mode operation with GH2 and the SITVC can partially overtake functions of the CGRS with the goal to reduce the CGRS dry mass and lower the overall propellant consumption. First, the DMT was presented as a general concept. Two major requirements come with the aerospike: A throat slot width of minimum 1 mm and an orifice location at the end of the cone. The first limits the realizable expansion ratio, the second is limited by the structural integrity of the spike. In a future trade-off the amplification has to be weighed against the orifice position. For evaluating the potential in mass saving two use-cases were derived and studied. The first is a reference case for the adaptation of the current secondary thrust system called the APU. It delivers the hot gas. The DMTS shall replace the TAPUs. The suitability of an aerospike could only be evaluated with a comparison of data from the project partners which showed that even though its expansion ratio had to be reduced by a factor of 8 the aerospike still had a slightly higher I_{sp} of 1.3 %.
To investigate the reference case a stage model was set up with Excel based models for geometry and mass calculations and EcoSimPro models calculating the performance of each mode of the DMT. The EcoSimPro model for the DMTS relies on a model of the APU to calculate the hot gas properties at the nozzle inlet. This model had to be simplified due to the limited time frame and the available data and does not contain the pumps and the heat exchanger element of the APU system. Therefore, the inlet mass flows had to be fixed. Statements about the impact of the DMTS on the APU system are only possible to minor extent and the model is only valid at the entered OP, but cannot describe a full transient behaviour of the APU system. A validation showed a deviation under 1 % for thrusts, pressures and temperatures in the gas generator and the TAPUs. However, it showed a significant error of ca. 15 % with T_{Nozzle}. Till the end of this investigation the exact reason could not be determined but is supposed to come from the inferior two-phase mixture flow calculation of EcoSimPro. In the CGH mode the DMT has an I_{sp} between 179 s and 71 s. The simulation also revealed that this is just 3.3 % higher than the current CGRS. So an actual propellant mass saving by using the CGH mode is not to be expected, but a dry mass evaluation showed a saving potential of 12.9 kg just for using GH2 and hot gas with the same nozzle and if the CGRS-Y and -Yn thrusters can be removed. A qualitative consideration left two combinations for the side injection: Either hot gas or GH2 as injected into a hot gas primary flow. All other combinations were excluded for being unfeasible or inefficient. The amplification can not be determined analytical. Instead, A_f

between 1 and 3.5 were estimated. For the comparison between CGRS and SITVC capability a mission scenario was defined with a constant perturbing torque of 20 N m appearing for a mission time of 18 000 s over the whole axial range of the CoG of the ULPM. The evaluation concluded that with GH2 a propellant mass saving potential between 14 kg and 137 kg and for hot gas a saving potential between 35 kg and 150 kg is probable. The dry mass impact of the whole DMTS includes valves, feed lines, flanges and clamps is estimated to be 7.6 kg plus 28 kg for the CGO mode functionality under the assumption that the CGRS-Y and -Yn thrusters can be removed. In total, the mass saving potential without the CGO mode lies between 6.2 kg and 130 kg for the GH2 as injectant and 26 kg and 142 kg for the hot gas as injectant. Hot gas has the higher mass saving potential as GH2. Also it is fed to the orifice with constant properties coming from the gas generator. However, with hot gas there is not stand-alone GNC-capability possible. Contrary, the GH2 is as dependent on p_{Tank} and T_{Tank} as the CGRS. Also there is a potential compromising effect because not only the side force is amplified but also the primary flow.
This concludes the reference case. The second use-case is a higher thrust evolution of the DMTS which uses all three propellants at once to produce more as twice of the thrust as the current system and an $I_{sp} = 400$ s. The afterburning mode shows a potential mass saving of 34 kg for the deorbitation maneuver. Problematic is that the evolution design comes forcibly with a buffer tank architecture to feed GOX and GH2 at constant pressure to the DMTS. An even major implication is the necessary injector. $A_{inj} > A_t$ is a necessary criterion so that the other modes also can work, not just the afterburning. But in order to realize a necessary pressure loss for instability precautions this cannot be fulfilled with the GOX and barely with the hot gas and hydrogen.

Outlook

The reference design of the DMTS shows the potential for performance increase. The evaluation showed a dependence of the mass savings on the amplification factor. A future study should focus on the experimental evaluation of the amplification factor for the hot gas and GH2 injection. The former seems to be easier to realize and should be started with. If GH2 is chosen, the model for the SITVC should be equipped with a tank model to calculate the dependence of the mass flow on the tank properties and vice versa. Only then a detailed performance gain can be stated and the operational limits defined. By using it on two nozzles it is also critical also to evaluate the amplification of the axial thrust because of its potential compromising effect. The GH2 performance as injectant will possibly be higher due to a heat flux from the primary flow which increases $I_{sp,s}$. In this work it has been considered adiabatic, but when choosing GH2 this should be analyzed to predict its mass saving potential more accurate. For the Dual-Mode operation it is necessary to investigate the impact on the APU system. Therefore, the pumps and the heat exchanger have to be integrated into the DMTS model. The third version of the DMTS with throttling capability should be investigated in a follow-up study. If it comes with an own combustor, the considerations made for the evolution design need to be respected for the follow-up study as well. The assumption of removing parts of the CGRS is made as starting point to this work. A deeper study with a 3D model of the ULPM has to reveal if the CGH mode and the SITVC can cover all GNC-operations of the CGRS-Y and -Yn thrusters.
Future investigations could show potential use-cases for example on a kick-stage, reusable vehicles and on-orbit vehicles.

9. Zusammenfassung (German conclusion)

Moderne Oberstufen wie die A6 ULPM erfordern Leistungssteigerungen aufgrund zunehmenden Konkurrenzdrucks auf dem Markt für Trägersysteme. Deshalb werden Innovationsprojekte finanziert, die die Machbarkeit von potentiellen neuen Technologien oder Konzepten untersuchen sollen. Eines dieser Konzepte wurde in dieser Arbeit untersucht: Ein Dual-Mode-Thruster-System, kurz DMTS. Ausgangspunkt war die Idee die Heißgasdüsen des APU Systems und die Kaltgasdüsen des CGRS zusammen zulegen. Darüber hinaus ist für das DMTS eine Schubvektorsteuerung mittels Seiteninjektion (SITVC) vorgesehen. Der Grund liegt bei dem Bedarf des ULPM's bestimmten Abweichungen des Schubvektors beim Betrieb des APU Systems entgegenzuwirken, was mit einer Schubvektorsteuerung effizienter sein soll als mit dem CGRS. Eine besondere Eigenschaft der Seiteninjektion ist eine Verstärkung der reinen Impulskraft der Injektion durch Strömungsphänomene durch die Interaktion mit dem Hauptabgasstrahl. Statt einer konventionellen Düse ist ein Aerospike für das Konzept vorgesehen, weil dann die Injektionsöffnung rechtwinkelig nach außen zeigt. Dies bietet zusätzliche Lageregelungsmöglichkeiten selbst bei ausgeschaltetem Hauptstrahl. Außerdem bieten Aerospikes potenziell ein höheres Schub-Gewichts-Verhältnis. Diese Untersuchung wurde begleitet durch Studien von Projektpartnern der TU Dresden. Ihre Daten und Expertise über das detaillierte Düsendesign dienten als Input für diese Systemanalyse.
Leistungssteigerung ist hier übersetzt in Reduktion von Trocken- und Treibstoffmasse. Hauptziel dieser Arbeit war es zu untersuchen, ob der Dual-Modusbetrieb mit GH2 und der Einsatz der SITVC teilweise die Funktionen des CGRS übernehmen kann und dabei Trockenmasse vom CGRS einzusparen und Gesamttreibstoffverbrauch zu senken. Zuerst wurden das allgemeine Konzept des DMTS vorgestellt. Die Aerospike kommt mit zwei grundsätzlichen Anforderungen: Eine Ringspaltbreite von 1 mm und einer Position des Injektionsöffnung möglichst am Ende des Konus. Die erste begrenzt dass realisierbare Expansionsverhältnis, die zweite wird durch die strukturelle Integrität des Spike begrenzt. In einem zukünftigen Trade-off müssen diese beiden gegeneinander abgewogen werden.
Zur Bewertung des potentiellen Massenreduktion wurden zwei Anwendungsfälle abgeleitet und untersucht. Der erste ist ein Referenzfall für die Anpassung des aktuellen APU Systems. Der DMTS ersetzt die Heißgasdüsen (TAPUs). Die Eignung einer Aerospike für den Anwendungsfall konnte nur durch einen Vergleich von Simulationsdaten der Projektpartner gemacht werden, die zeigten, dass, obwohl die Expansionsverhältnis um den Faktor 8 reduziert werden musste, die Aerospike immer noch einen etwas höheren Isp von 1,3 % aufweist. Zur Untersuchung des Referenzfalls wurde ein Stufenmodell erstellt, dass aus Excel-basierten Modellen für die Geometrie und die Trockenmassen sowie EcoSimPro-Modelle, die Schub und Massenstrom der einzelnen Modi kalkulieren besteht. Das EcoSimPro-Modell für den DMTS stützt sich auf ein Modell der APU zur Berechnung der Heißgaseigenschaften am Düseneintritt. Dieses Modell musste aufgrund des begrenzten Zeitrahmens und der verfügbaren Daten vereinfacht werden und enthält nicht die Pumpen und den Wärmetauscher. Daher mussten die Massenströme festgelegt werden, was Aussagen über die Auswirkungen des DMTS auf das APU-System nur in geringem Umfang möglich macht. Das Modell ist nur für die betrachteten Betriebspunkte gültig und kann keine transiente Veränderung derer beschreiben. Eine Validierung zeigte eine Abweichung von weniger als 1 % der Schübe und Drücke. Allerdings wichen die Temperaturen in der Düse um ca. 15 % ab. Bis zum Ende dieser Untersuchung konnte der genaue Grund nicht ermittelt werden, aber wird vermutet bei der schlechteren Berechnung von Zwei-Phasen-Mischungen von EcoSimPro. Im CGH-Modus hat der DMT einen I_{sp} zwischen 179 s und 71 s. Die Simulation ergab auch, dass dieser Wert nur 3,3 % höher ist als der einer CGRS Düse. Eine tatsächliche Treibstoffmasseneinsparung durch die Verwendung des

GH2-Modus ist also nicht zu erwarten, aber eine Bewertung der Trockenmasse ergab ein Einsparpotenzial von 12,9 kg, wenn der GH2-Modus des DMT die CGRS-Y und -Yn Cluster ersetzen kann. Eine qualitative Betrachtung ließ zwei Kombinationen für die Seiteninjektion übrig: Entweder Heißgas oder GH2, das in einen Heißgasstrahl eingespritzt wird. Alle anderen Kombinationen wurden ausgeschlossen, weil sie nicht durchführbar oder ineffizient waren. Die Verstärkung der Seitenkraft kann nicht analytisch bestimmt werden. Stattdessen wurden Verstärkungsfaktoren zwischen 1 und 3,5 geschätzt. Für den Vergleich zwischen CGRS- und SITVC-Fähigkeit wurde ein Missionsszenario definiert, in dem ein konstantes Störmoment von 20 N m für eine Dauer von 18 000 s auftritt. Die Bewertung kam zu dem Schluss, dass mit GH2 als Injektant ein Treibstoffmasseneinsparungspotenzial zwischen 14 kg und 137 kg und bei Heißgas ein Einsparungspotential zwischen 35 kg und 150 kg wahrscheinlich ist. Die zusätzliche Trockenmasse des gesamten DMTS, einschließlich der Ventile, Treibstoffleitungen, Flansche und Klemmen wird auf 7,6 kg ohne den GOX Modus und 35,6 kg mit dem GOX Modus geschätzt, sofern die Annahme gilt, dass Teile des CGRS ersetzt werden können. Verrechnet mit der Treibstoffmasse, liegt das absolute Masseneinsparungspotenzial ohne den GOX-Modus zwischen 6,2 kg und 130 kg für GH2 als Injektant und 26 kg und 142 kg für Heißgas als Injektant. Heißgas hat das höhere Masseneinsparungspotential als GH2. Es wird ebenfalls mit konstanten Eigenschaften aus dem Gasgenerator in den Injektionskanal eingespeist. Allerdings ist keine alleinstehende Lageregelungsoperation möglich. Im Gegensatz dazu ist das GH2 ist von den variablen Gaseigenschaften im Tank abhängig ebenso wie das CGRS. Außerdem gibt es einen potenziellen kompromittierenden Effekt, weil nicht nur die Seitenkraft, sondern auch der Primärstrom verstärkt wird. Damit ist der Referenzfall abgeschlossen. Der zweite Anwendungsfall ist eine Weiterentwicklung des DMTS für eine höhere Schubklasse, die alle drei Gasresourcen gleichzeitig verwendet und eine Nachverbrennung durchführt, um mehr als doppelt so viel Schub zu erzeugen wie das derzeitige System mit einem I_{sp} von ca. 400 s. Der Nachverbrennungsmodus zeigt eine potenzielle Masseneinsparung von 34 kg für das Wiedereintrittsmanöver. Problematisch ist, dass die Weiterentwicklung zwangsweise eine Zwischenspeicherarchitektur benötigt um GOX und GH2 mit konstantem Druck an das DMTS zu liefern. Eine weitere Einschränkung tritt durch den Injektor auf. Dessen Fläche muss größer sein als die des Düsenhalses, damit auch die anderen Modi funktionieren können, abseits der Nachverbrennung. Aber um einen notwendigen Druckverlust zur Vorbeugung von Brennkammerinstabilitäten zu realisieren kann dieses Kriterium nicht für den GOX- und nur kanpp für den GH2- und Heißgas-Modus erfüllt werden.

Ausblick

Das Referenzdesign des DMTS zeigt das Potential für Leistungssteigerung. Die Auswertung zeigte eine Abhängigkeit der Masseneinsparung vom Verstärkungsfaktor. Eine zukünftige Studie sollte sich auf die experimentelle Auswertung dieses für die Heißgas- und GH2-Injektion konzentrieren. Ersteres scheint leichter zu realisieren. Wenn GH2 gewählt wird, sollte das Modell für das SITVC mit einem Tankmodell ausgestattet werden, um die Abhängigkeit des Massenflusses von den Tankeigenschaften zu berechnen und umgekehrt. Erst dann kann ein detaillierter Leistungsgewinn angegeben und die Betriebsgrenzen definiert werden. Bei der Anwendung bei zwei Düsden gleichzeitig ist es auch notwendig die Verstärkung des Axialschubs wegen seiner potentiell kompromittierenden Wirkung zu analysieren. Der $I_{sp,s}$ des GH2 wird möglicherweise aufgrund eines Wärmestroms aus der Primärströmung höher sein. In dieser Arbeit wurde der Injektionskanal als adiabat betrachtet, aber bei der Wahl von GH2 sollte dies analysiert werden, um sein Masseneinsparungspotenzial genauer vorherzusagen. Für den Dual-Mode-Betrieb ist es notwendig, die Auswirkungen auf das APU-System zu untersuchen. Daher müssen die Pumpen und der Wärmeaustauscher in das DMTS-Modell integriert werden. Die dritte Version des DMTS mit Drosselfähigkeit sollte in einer Folgestudie untersucht werden. Wenn diese Version des DMTS mit einer eigenen Brennkammer ausgestattet ist, müssen die für das zweite Design angestellten Überlegungen auch für die Folgestudie berücksichtigt werden. Die Annahme, Teile des CGRS zu entfernen,

wird als Ausgangspunkt für diese Arbeit betrachtet. Eine vertiefte Studie mit einem 3D-Modell des ULPM muss zeigen, ob der CGH-Modus und der SITVC alle GNC-Operationen der CGRS-Y und -Yn-Triebwerke abdecken kann.
Zukünftige Untersuchungen können das Potential des DMTS auch für andere Nutzfälle aufdecken zum Beispiel für Kick-stages und wiederverwendbare und on-orbit Raumfahrzeuge.

Bibliography

[1] Zegler, F., "An Integrated Vehicle Propulsion and Power System for Long Duration Cryogenic Spaceflight," 09 2011, 10.2514/6.2011-7355, ISBN: 978-1-60086-953-2.

[2] Arianegroup Bremen, "Internal communication," 2019-2020.

[3] Napolitano, L., *Applications of Space Developments: Selected Papers from the XXXI International Astronautical Congress, Tokyo, 21 — 28 September 1980*, Elsevier Science, 2013, ISBN: 9781483159768.

[4] Rovey, J., Lyne, C., Mundahl, A., Rasmont, N., Glascock, M., Wainwright, M., and Berg, S., "Review of Chemical-Electric Multimode Space Propulsion," 08 2019, 10.2514/6.2019-4169.

[5] Bach, C., Schöngarth, S., Bust, B., Propst, M., Sieder-Katzmann, J., and Tajmar, M., "How to steer an aerospike," *69th International Astronautical Congress (IAC), Bremen, Germany*, October 2018, p. 29.

[6] Propst, M., Liebmann, V., Sieder-Katzmann, J., Bach, C., and Tajmar, M., "Maximizing side force generation in aerospike nozzles for attitude and trajectory control," 10 2018.

[7] Turner, M. J. L., *Rocket and Spacecraft Propulsion - Principles, Practice and New Developments*, Springer Science & Business Media, Berlin Heidelberg, 2nd ed., 2006, ISBN: 978-3-540-27041-6.

[8] Idelchik, I. and Steinberg, M., *Handbook of Hydraulic Resistance*, Begell House, 3rd ed., 1996, ISBN: 9781567000740.

[9] Arianegroup Bremen, "Classified internal documents," 2019-2020.

[10] Sutton, G. P. and Biblarz, O., *Rocket Propulsion Elements*, John Wiley & Sons, New York, 7th ed., 2011, ISBN: 978-1-118-17420-3.

[11] Huzel, D. K. and Huang, D. H., *Modern Engineering for Design of Liquid-Propellant Rocket Engines*, Vol. 147, American Institute of Aeronautics and Astronautics, 370 L'Enfant Promenade, SW, Washington DC, 20024-2518, 1992, ISBN: 1-65347-013-6.

[12] Eilers, S., *Development the Multiple Use Plug Hybrid for Nanosats (MUPHyN) Miniature Thruster*, Ph.D. thesis, Utah State University, USA, 2013.

[13] SPAID, F. W. and ZUKOSKI, E. E., "A study of the interaction of gaseous jets from transverse slots with supersonic external flows," *AIAA Journal*, Vol. 6, No. 2, 1968, pp. 205–212, 10.2514/3.4479.

[14] Spaid, F. W. and Zukoski, E., "Secondary injection of gases into a supersonic flow," *AIAA Journal*, Vol. 2, No. 10, 1964, pp. 1689–1696, 10.2514/3.2653.

[15] Silver, R., "Advanced aerodynamic spike configurations - hot firing investigations, Final Report," Tech. Rep. AFRPL-TR-67-246-Vol II AD-348 856, Rocketdyne, September 1964.

[16] Letchworth, G., "X-33 Reusable Launch Vehicle Demonstrator, Spaceport and Range, NASA Kennedy Space Center," 09 2011, 10.2514/6.2011-7314, ISBN: 978-1-60086-953-2.

[17] Arca Space Corporation, "Engineering the future," http://www.arcaspace.com/index.htm.

[18] Bui, T., Murray, J., Rogers, C., Bartel, S., Cesaroni, A., and Dennett, M., "Flight Research of an Aerospike Nozzle Using High Power Solid Rockets," *41st AIAA/ASME/SAE/ASEE Joint Propulsion Conference & Exhibit*, 2005, 10.2514/6.2005-3797.

[19] Besnard, E. and Garvey, J., "Development and Flight-Testing of Liquid Propellant Aerospike Engines," *40th AIAA/ASME/SAE/ASEE Joint Propulsion Conference and Exhibit*, 2004, 10.2514/6.2004-3354.

[20] Wisse, M., *An Asymptotic Analysis of compressible Base FLow and the Implementation into linear plug nozzles*, Ph.D. thesis, TU Delft, 2005.

[21] Eilers, S., Matthew, W., and Whitmore, S., "Analytical and Experimental Evaluation of Aerodynamic Thrust Vectoring on an Aerospike Nozzle," *AIAA Journal*, 2010, 10.2514/6.2010-6964.

[22] Eilers, S., Wilson, M., Whitmore, S., and Peterson, Z., "Side Force Amplification on an Aerodynamically Thrust Vectored Aerospike Nozzle," *47th AIAA/ASME/SAE/ASEE Joint Propulsion Conference & Exhibit*, 2011, 10.2514/6.2011-5531.

[23] Empresarios Agrupados Internacional, Magallanes, 3. 28015 Madrid, Spain, *EcoSimPro 5.0 Modelling and Simulation Software - User manual*, 2012.

[24] McBride, B. J. and Gordon, S., *Computer Program for Calculation of Complex Chemical Equilibrium Compositions and Applications - II. Users Manual and Program Description*, NASA Lewis Research Center, Cleveland, Ohio 44135, June 1996.

[25] Lemmon, E. W., Huber, M. L., and McLinden, M. O., *NIST Reference Fluid Thermodynamic and Transport Properties - REFPROP Version 9.1 User Guide*, Applied Chemicals and Materials Division National Institute of Standards and Technology, Boulder, Colorado 80305, April 2013.

[26] ESA, Magallanes, 3. 28015 Madrid, Spain, *ESPSS Version 3.2.2 EcosimPro Libraries User Manual (Volume 1)*, January 2017.

[27] TU Dresden, "Communication with project partners," 2019-2020.

[28] Humble, R. W., Henry, G. N., and Larson, W. J., *Space Propulsion Analysis and Design*, McGraw-Hill Companies,Incorporated, 1995, ISBN: 9780070313200.

[29] George, C., *Saturn V Flight Manual, SA 504*, Marshall Space Flight Center and United States. National Aeronautics and Space Administration, 1969.

[30] Davis, J. R., *Metals Handbook Desk Edition*, ASM International, 2nd ed., 1998, ISBN: 978-0-87170-654-6.

[31] Messerschmid, Ernst und Fasoulas, S., *Raumfahrtsysteme - Eine Einführung mit Übungen und Lösungen*, Springer-Verlag, Berlin Heidelberg, 2009, ISBN: 978-3-540-77699-4.

[32] Glassman, I., *Combustion*, ACADEMIC PRESS INC., San Diego, 3rd ed., 1996, ISBN: 9780122858529.

Appendix

A. Visio schematic of the line routing to the DMTS of the reference use-case

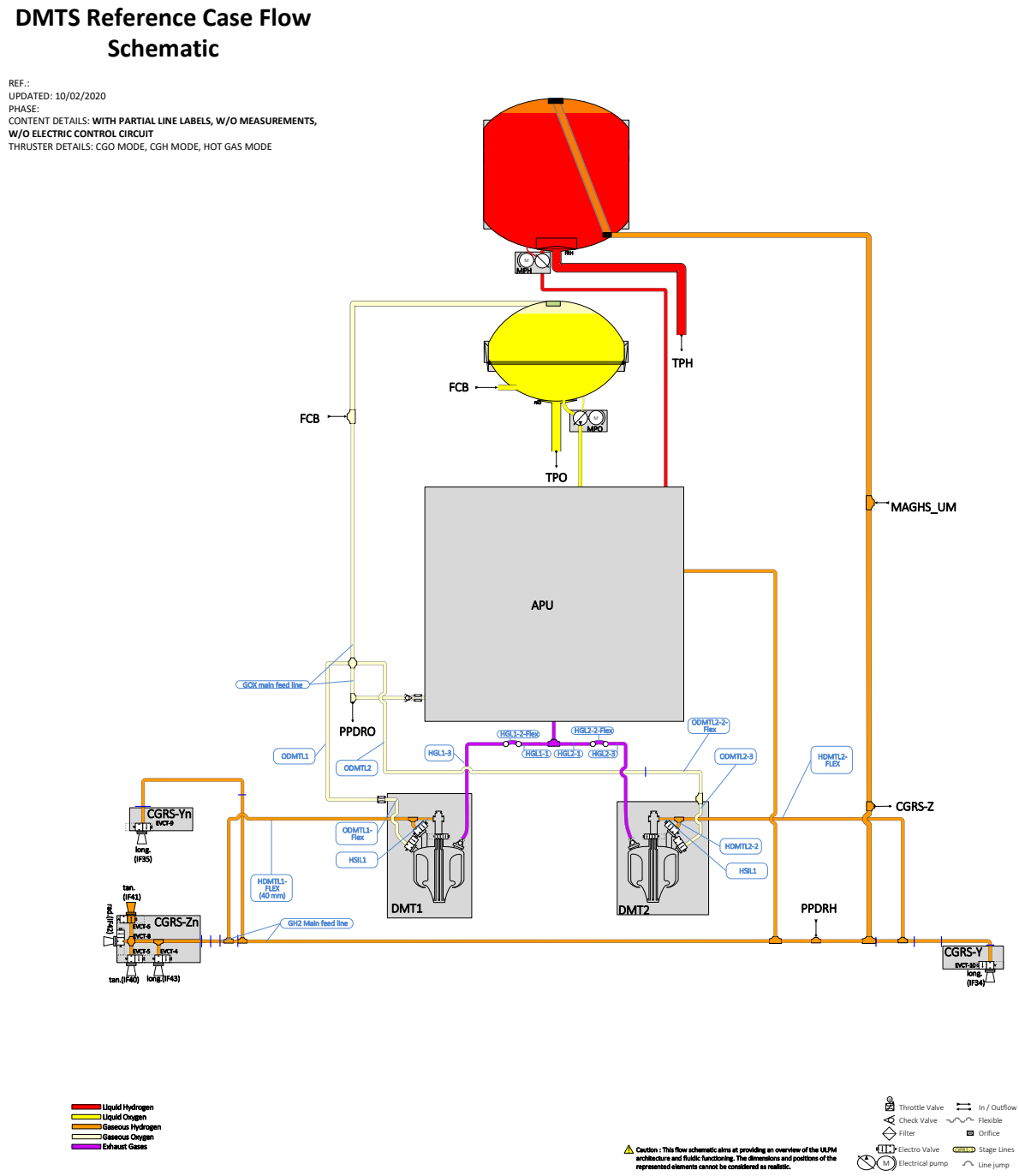

B. Detailed calculation of dry mass impact

B.1. Estimated dry mass of CGRS

Expandable Mass

		d [m]	L [m]	m [kg]	
	47.58% of HPR1		0.04	1.500	1.52
CGRS-Y	HPR6-Flex		0.04	1.179	3.17
	Flanges		0.04	-	0.80
	HPR1-1		0.04	0.823	0.83
	Flanges		0.04	-	0.80
	EVCT-10 + Th		0.04	-	4.60
	Brackets		0.04	-	1.10
CGRS-Yn	Terminal		0.04		4.40
	Flanges		0.04	-	0.80
	HPR2-Flex		0.04	1.184	3.18
	Flanges		0.04	-	0.80
	HPR2-1		0.04	0.823	0.83
	Flanges		0.04	-	0.80
	EVCT-9 + Thr		0.04	-	4.60
	Brackets		0.04	-	0.80
					29.04

Additional CGRS-Mass due to repositioning

Line extension of HPR4	1.52	same length as the one taken on the other side

B.2. Estimated dry mass of DMTS

H2-Side

	Additional Elements	Stk.	d [m]	L [m]	m [kg]	
	Terminal	1	0.04	-		4.4
	Flanges	2	0.04	-		0.8
Thruster 1	Flex-Line: HDMTL1-Flex	1	0.04		0.45	1.210
	Flanges	2	0.04	-		0.8
	GH2-Valve	1	0.04	-		4.3
	Terminal	0	0.04	-		0
	Flanges	0	0.04	-		0
Thruster 2	Flex-Line: HDMTL2-Flex	1	0.04		0.45	1.210
	Flanges	2	0.04			0.8
	GH2-Valve	1	0.04	-		4.3
Total						17.82

O2-Side

	Additional Elements	Stk.	d [m]	L [m]	m [kg]	
	4-way-Terminal	1	0.04	-		4.40
	Flanges	2	0.04	-		0.80
	Flex-Line: ODTML1-Flex	1	0.04		0.8	2.15
	Flanges	2	0.04	-		0.80
Thruster 1	Orifice	1	*0.04*		0.04	0.50
	GOX-Valve	1	0.04	-		4.30
	Rigid Line: ODTML2-1	1	0.04		6.35	6.42
	Flanges	2	0.04	-		0.80
Thruster 2	Flex-Line: ODTML2-2-Flex	1	0.04		0.45	1.21
	Flanges	2	0.04	-		0.80
	GOX-Valve	1	0.04	-		4.30
	Brackets, Mounts, etc.					1.53
Total						28.01

Hotgas-Side

	Additional Elements	Stk.	d [m]	L [m]	m [kg]	
	HG-CheckValve	2	0.025	-		2.6
Total						2.6

SITVC

	Additional Elements	Stk.	d [m]	L [m]	m [kg]	
	SITVC-Terminal	1	0.04	-		4.4
	SITVC-Terminal	*0*	*0.025*	-		*0*
Thruster 1	Rigid Line	1	0.01		0.1	0.027
	Flanges	2	0.01	-		0.2
	3-Way-Valve	1	0.01	-		4.3
Thruster 2						8.927
Total						17.9
Nozzle w/ SITVC dome		2				2
Total						68.3
Dry mass impact through removed TAPUs						63.1
Dry mass impact without Gox-Mode						35.1
Dry mass impact with removed Y- & Yn-CGRS						7.6

Elektrovalve n	4.3
Checkvalve m	1.3
Density steel	7850
wall thickness	0.001
Flange factor	10
Terminal factc	110
Flex line dens	20868.21806

C. Propellant mass calculation

C.1. Side force need calculation

M - Torque [Nm]	20
F_Primary [N]	150

Positions		**Angles**		
Nozzle flange x -position [mm]	995	beta	90	injection angle
Nozzle flange y -position [mm]	2306	delta	8	installation an
Distance CC - Orifice [mm]	80	alpha_3	8	
Orifice x -position [mm]	916			
Orifice y -position [mm]	2317			
Deviation of CoG from x-Axis[mm]	50			
y -distance CoG - Orifice L_y [mm]	2266.72719			

x_CoG,center	x_Cog,Vinci	L_x [mm]	F_side [N]	*alpha_1*	*L_side [mm]*
916.0677162	-4002	0	63.40	*8.0*	*2267*
1000	-4086	84	50.18	*10.1*	*2268*
2000	-5086	1084	14.40	*33.6*	*2513*
3000	-6086	2084	8.41	*50.6*	*3079*
4000	-7086	3084	5.94	*61.7*	*3827*
4490	-7576	3574	5.19	*65.6*	*4232*
5230	-8316	4314	4.36	*70.3*	*4873*
6000	-9086	5084	3.74	*74.0*	*5566*
6455	-9541	5539	3.45	*75.7*	*5985*
7000	-10086	6084	3.15	*77.6*	*6492*
7960	-11046	7044	2.74	*80.2*	*7400*
8000	-11086	7084	2.73	*80.3*	*7438*

Single Thrust through injection in xz-plane

L_CoG,x	L_x [mm]	F_side_tot [N]	F_side,1 [N]	F_side,2 [N]	
1000	84	238.29	120.42	117.87	
2000	1084	18.45	9.32	9.13	
3000	2084	9.60	4.85	4.75	
4000	3084	6.49	3.28	3.21	
4490	3574	5.60	2.83	2.77	2.80
5230	4314	4.64	2.34	2.29	
6000	5084	3.93	1.99	1.95	
6455	5539	3.61	1.82	1.79	
7000	6084	3.29	1.66	1.63	
7960	7044	2.84	1.43	1.40	
8000	7084	2.82	1.43	1.40	

CGRS		
x_position	2995	
Distance from center axis	2632	2785
F_long [N]	7.59878419	

CGRS

x_CoG,center	L_x [mm]	F_tan [N]	F_long [N]
1000	-1995	10.02506266	7.59878419
2000	-995	20.10050251	7.59878419
3000	5	4000	7.59878419
4000	1005	19.90049751	7.59878419
4490	1495	13.37792642	7.59878419
5230	2235	8.948545861	7.59878419
6000	3005	6.655574043	7.59878419
6455	3460	5.780346821	7.59878419
7000	4005	4.993757803	7.59878419
7960	4965	4.028197382	7.59878419
8000	5005	3.996003996	7.59878419

C.2. Exemplary propellant mass calculation at lowest CoG

M - Torque [Nm] 20

Positions

		Angles	
Nozzle flange x -p	995,2891617	beta	90 injection angle between thrust vector and side injection vector
Nozzle flange y -p	2305,59334	delta	8 installation angle of nozzle
Distance CC - Ori	80	alpha_3	8
Orifice x -position	916,0677162		
Orifice y -position	2316,727188		
Deviation of CoG	50		
y -distance CoG -	2266,727188		

x_CoG,center	x_CoG,Vinci	L_x [mm]	*alpha_1*	*L_side [mm]*	*F_side [N]*
4490	-7575,732284	3573,932284	*65,61553671*	*4232,144151*	*5,188580957*

		CGRS	Tank Pressure	Nozzle Inlet Press	Nozzle Inlet T	*Time_poly*	*Performance*	
Disturbance M	20	Highest performa	310000	236000	153	0	25062	OP1
Mission Time [s]	18000	Medium performa	130000	98968	46		19167	
		Lowest performa	92500	70419	35,6	1819	15503	OP2

	CGRS-long	DMT SITVC
R	2632	4232
Impuls need [Ns]	136778	93394

	Amp-Factor	D_throat [mm]	Pressure [Pa]	Temperature [K]	F [N]	Time [s]	m_dot [kg/s]	m [kg]	Abs Mass saving	% Propellant Mas	Check Mission Time
CGRS Y	-		310000	153		55,19	2478	0,03031	75,1	-	Within_Operational_Limit
	-	13,72	92500	35,6		16,46	8310	0,01889	157,0	-	Within_Operational_Limit
SITVC (GH2)	1		310000	153		8,65	10791	0,00568	61,3	13,8	18,4 Within_Operational_Limit
			92500	35,6		2,60	35954	0,00362	130,0	27,0	17,2 Outside_Operational_Limit
SITVC (GH2)	2	6	310000	153		17,31	5396	0,00568	30,7	44,5	59,2 Within_Operational_Limit
			92500	35,6		5,20	17977	0,00362	65,0	92,0	58,6 Within_Operational_Limit
SITVC (GH2)	3,5		310000	153		30,29	3083	0,00568	17,5	57,6	76,7 Within_Operational_Limit
			92500	35,6		9,09	10273	0,00362	37,1	119,8	76,3 Within_Operational_Limit
SITVC (Hotgas)	1					6,54	14280		42	33,1	78,9 Within_Operational_Limit
						6,54	14280		42	115,0	273,9 Within_Operational_Limit
SITVC (Hotgas)	2	3,385	621800	533		13,08	7140	0,00294	21	54,1	257,8 Within_Operational_Limit
						13,08	7140		21	136,0	647,8 Within_Operational_Limit
SITVC (Hotgas)	3,5					22,89	4080		12	63,1	526,2 Within_Operational_Limit
						22,89	4080		12	145,0	1208,7 Within_Operational_Limit

D. EcoSimPro files

D.1. Standard nozzle profile in EcoSimPro

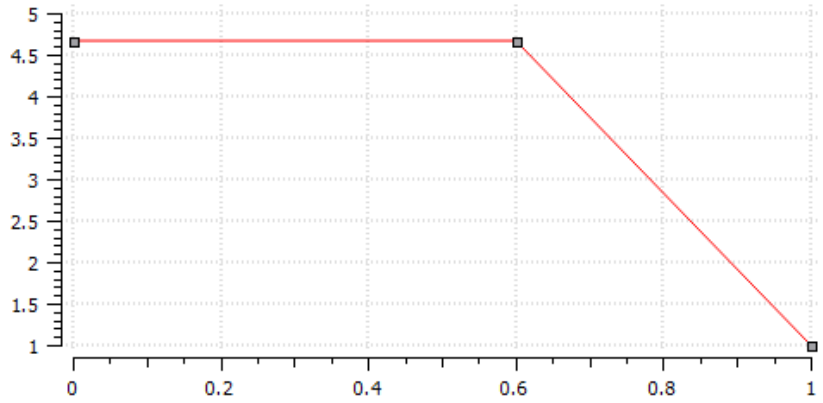

(a) Exemplary normalized profile for convergent nozzles part or gas generators

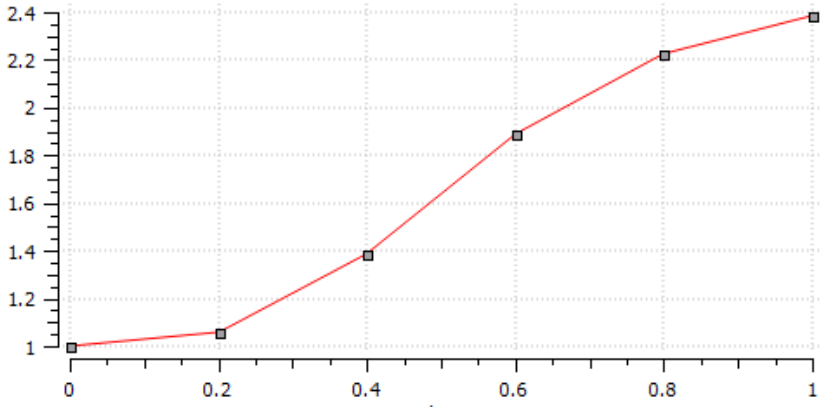

(b) Exemplary normalized profile for divergent nozzle part

D.2. Fully integrated DMTS model

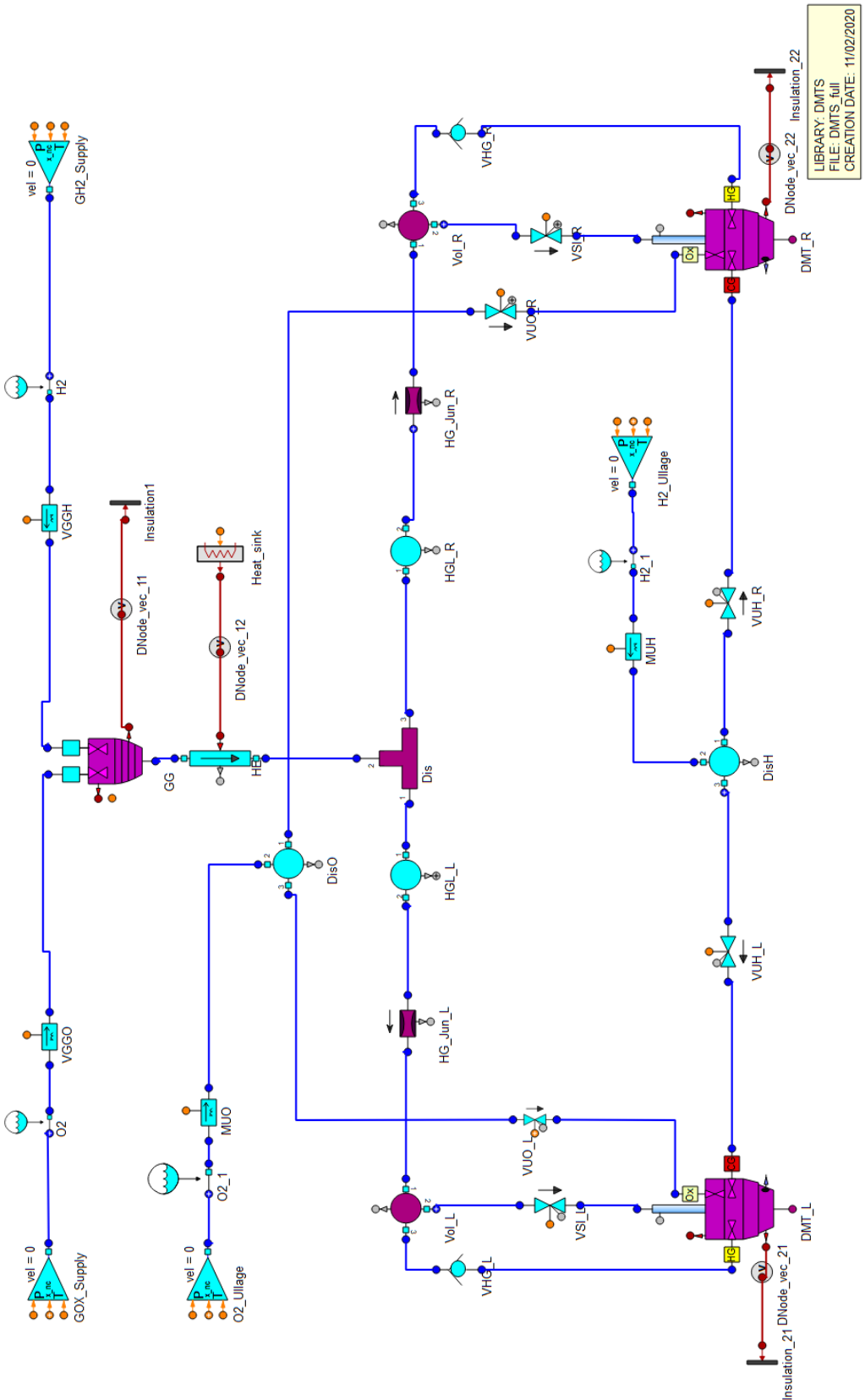

D.3. Experiment example: Performance calculation of the CGRS

```
/*------------------------------------------------------------------------------
LIBRARY: DMTS
COMPONENT: CGRS_Thruster
PARTITION: default
EXPERIMENT: exp_GH2_flow
TEMPLATE: TRANSIENT
CREATION DATE: 06/02/2020
------------------------------------------------------------------------------*/

EXPERIMENT exp_GH2_flow ON CGRS_Thruster.default
DECLS
REAL Isp UNITS "s"
REAL p[3] = {310000,92500,310000} --tank pressure for OP1, OP2, Reference
REAL T[3] = {153 +16, 35.6+18,150+16.5} --tank temperature for OP1, OP2, Reference +correction
    for loss between boundary and nozzle
INTEGER OP = 2
OBJECTS
INIT
-- initial values for state variables
Nozzle.Combustor.m_vf[1] = 0

BOUNDS
-- Set equations for boundaries: boundVar = f(TIME;...)
FLUID_FLOW_1D.Damp = 0.3
FLUID_FLOW_1D.GRAV = 9.806
FLUID_PROPERTIES.MinMolarFr = 1e-09
FLUID_PROPERTIES.VDW_option = 0
Nozzle.Combustor.IgnitFlag = 0
Nozzle.Combustor.f_v[1] = 1
Nozzle.Combustor.f_v[2] = 1
Nozzle.np_out.P = 10
VolPT_TMD_H2.s_temp.signal[1] = T[OP]
VolPT_TMD_H2.s_xNonCond.signal[1] = 0
Nozzle.tp_inj.q[1] = 0

BODY
Pres_val.Amp = p[OP]*2.36/3.1
Nozzle_inlet.Ao = PI * 0.25 * 0.025**2
Nozzle_inlet.zetaf = 0.0001 --9.96 actual valve value
Nozzle_inlet.zetab = Nozzle_inlet.zetaf
Nozzle.Eta = 1
Nozzle.AR_sup = 5.2

Nozzle.x_nco = 0
Nozzle.A_inj_red = 0.25*PI*0.025**2
Nozzle.zetaf_inj_red = 0.0001 --1.7194 --pressure loss coefficient from valve to nozzle

TIME = 0
TSTOP = 225
CINT = 1
INTEG()

WHILE (INTEG_CINT() != INTEG_END)
Isp = Nozzle.Nozzle.Ivac_nozzle[3] / 9.806
END WHILE
END EXPERIMENT
```

D.4. Iteration routine for obtaining heat extraction

```
/*-------------------------------------------------------------------------------
LIBRARY: LIBS_USER_STEADY
COMPONENT: STEADY_APU
PARTITION: Design
EXPERIMENT: exp_iter
TEMPLATE: STEADY
CREATION DATE: 30/10/2019
-------------------------------------------------------------------------------*/
EXPERIMENT exp_iter ON STEADY_APU.Design
--
...Experiment body
--

-- Call the steady state function
heat = heat_vec[iter_OP]
STEADY()
dm = m0 - GGAPU.Combustor.f_out.m

reduc = 0.2 --nicest values at 1.7
heat_old = heat
dm_old = dm
N_step = 30

FOR(i IN 1,N_step)
IF (dm_old * dm < 0) THEN
reduc = (reduc)/2
END IF

IF (sqrt(dm**2) > 0.00001) THEN
IF (m0 > GGAPU.Combustor.f_out.m) THEN
heat = heat_old * (1 + reduc) -- Increase heat extraction to increase nozzle mass flow
ELSE
heat = heat_old * (1 - reduc)
END IF
heat_old = heat
dm_old = dm
STEADY()
dm = m0 - GGAPU.Combustor.f_out.m
ELSE
WRITE("Target mass flow reached! \n")
END IF
END FOR
END EXPERIMENT
```

D.5. DMTS component coded in EL

```
    USE MATH
    USE PORTS_LIB
    USE FLUID_PROPERTIES
    USE THERMAL
    USE FLUID_FLOW_1D
    USE SATELLITE
    USE COMB_CHAMBERS
    USE THERMO_TABLE_INTERP

    COMPONENT DualModeThruster_comp( ENUM DropExchange GasLiqOption = UserDef "UserDef: user defined charactistic vaporization time",
    ENUM Hc_correl hc_correl=Bartz "heat transfer correlation option",
    BOOLEAN rateOption=FALSE "TRUE, burning rate model active",
    ENUM Scheme_comb scheme = centred "Numerical scheme used",
    SET_OF(Chemicals_full ) burnerGasesOptionP1 = noBurnGases "Select Chemicals, standard cold gas port",  -- GH2
    SET_OF(Chemicals_full ) burnerGasesOptionP2 = Chemicals "Select Chemicals, standard hot gas port",  -- HG
    SET_OF(Chemicals_full ) burnerGasesOptionP3 = noBurnGases "Select Chemicals, standard oxydizer port",  -- GOX
    SET_OF(Chemicals_full ) burnerGasesOptionSI = noBurnGases "Select Chemicals, Side injectant port",  -- Injectant
    INTEGER Nsub = 2 "Number of nodes in convergent part",
    INTEGER Nsup = 3 "Number of nodes in divergent part",
    --INTEGER Nodes = 3 "Number of injectant pipe nodes",
    ENUM NozzleType nozzle_type = NonIsentropic "Nozzle calculation option",
    REAL inst_angle = 90,
    REAL knee_radius = 0.005)

    PORTS
    IN FLUID_FLOW_1D.fluid (burnerGasesOption = burnerGasesOptionP1) GH2 CARDINALITY 1
    IN FLUID_FLOW_1D.fluid (burnerGasesOption = burnerGasesOptionP2) HG  CARDINALITY 1
    IN FLUID_FLOW_1D.fluid (burnerGasesOption = burnerGasesOptionP3) GOX CARDINALITY 1
    IN FLUID_FLOW_1D.fluid (burnerGasesOption = burnerGasesOptionSI) Injectant_fluid CARDINALITY 1
    --OUT SATELLITE.Forces Sideforce
    --OUT SATELLITE.Forces NozzleThrust
    OUT PORTS_LIB.thermal (n = Nsub+Nsup) tp
    OUT PORTS_LIB.thermal (n = 1) tp_inj
    OUT COMB_CHAMBERS.NozzlePort np_out
    OUT FLUID_FLOW_1D.jun_measure meas_out
    DATA
    -- Init for everything --
    REAL P_o = 100000 UNITS "Pa" "Initial pressure in elements"
    REAL T_o = 300 UNITS "K" "Initial temperature in elements"

    REAL m_o = 0 UNITS "kg/s" "Initial massflow in elements"
    ENUM PipeMat mat = None UNITS "-" "Material of nozzle"
    REAL rug = 5e-05 "rugiosity"
    REAL th_manifold = 0.005 UNITS "m" "Wall thickness of the chamber and manifolds"
    REAL k_w = 0.1  UNITS "W_mK" "Conductivity of material barrier if mat=None"
    REAL rho_w = 1000 UNITS "kg/m^3" "Density of material"
    REAL cp_w = 500 UNITS "J/(kg*K)" "Heat capacity at constant pressure of material"
    REAL Re_lam = 2000 UNITS "-" "Reynolds number"

    -- Reducer Manifold / Mixer --
    REAL V_cav_red = 0.3 UNITS "m^3" "Volume of mixer / manifold of the reducer components"
    REAL L_red_manifold = 0 UNITS "m" "Length of mixer / manifold of the reducer components"
    REAL A_inj_red = -- UNITS "m^2" "Injector area of reducer, for Dual-Mode use it has to be larger than the throat area"
    REAL zeta_inj_red = 1.7 UNITS "-" "Pressure loss coefficient of injector"

    -- Combustion chamber
    REAL x_nco = 0       UNITS no_units "Initial non-condensable mass fraction in cavities & combustor ; =0 --> red vapors in combustor; <0 --> oxy vapors in combustor"
```

```
58      REAL A_inj_oxy = -- UNITS u_m2 "Oxydiser effective injection area"
59      REAL zeta_inj_oxy=1.7  UNITS no_units "Oxi. injector forward pressure loss coefficient"
60      REAL V_cav_oxy = 0.000491 UNITS u_m3 "Oxydiser cavity volume"
61
62      REAL emiss = 0.01    UNITS no_units "Emissivity of the combustion gases; <0, calculated"
63      REAL Lrad = 0    UNITS u_m "Mean beam length; 0, calculated as 0.9*D"
64      REAL tau_v = 0.0001  UNITS u_s "Vaporization characteristic time. Only if GasLiqOption=UserDef"
65      REAL tau_c = 0.003  UNITS u_s "Combustion/ignition time delay"
66      REAL tau_b = 0.0003  UNITS u_s "Burning characteristic time"
67      REAL D_dr_fu = 0.00001 UNITS u_m "Fuel droplets size. Only if GasLiqOption=Advanced"
68      REAL D_dr_ox = 0.00001 UNITS u_m "Oxidizer droplets size. Only if GasLiqOption=Advanced"
69      REAL MR_ini= 0     UNITS no_units "Initial mixture ratio; > 0, ignited chamber initialisation"
70      REAL MR_min = 0.05  UNITS no_units "Minimum mixture ratio allowing ignition - /10 for extinction"
71      REAL MR_max = 20   UNITS no_units "Maximum mixture ratio allowing ignition - *10 for extinction"
72      BOOLEAN frozen_th = TRUE "Flag forcing frozen conditions in the throat"
73      BOOLEAN frozen_nz = TRUE "Flag forcing frozen conditions in the supersonic nozzle"
74      REAL Rcurv = 0.01    UNITS u_m "Curvature radius at throat"
75      REAL eta_c = 1     UNITS no_units "Combustor efficiency"
76      REAL eta_nz = 1  UNITS no_units "Nozzle efficiency"
77      REAL K_hc = 0.026    UNITS no_units "Correction factor for the heat transfer correlation"
78      REAL Lc  = --    UNITS u_m "Chamber length of subsonic part -also used to normalise 'Dc_vs_L'
            table"
79      REAL Dt  = --  UNITS u_m "Nozzle throat diameter - also used to normalise diameters"
80      TABLE_1D Dc_vs_L = {{ 0,0.6,1}, { 2,2,1}} \
81      UNITS no_units "Subsonic diameters normalized with Dt vs. axial position normalized with Lc"
82      BOOLEAN dxc_input= FALSE "FALSE, dxc_vs_L = weighting function for conv. mesh size distribution.
            TRUE, normalised node lengths vs node number"
83      TABLE_1D dxc_vs_L = {{ 0,0.6,1}, { 1,1,1}} \
84      UNITS no_units "Weighting function for subsonic mesh size distribution or normalised node lengths
             vs node number"
85      REAL Ld = --   UNITS u_m "Nozzle length to normalize 'Dd_vs_L' table"
86      REAL Ld2 = Ld    UNITS u_m "Length from throat to nozzle exit, <= Ld"
87      TABLE_1D Dd_vs_L = {{0,0.2,0.4,0.6,0.8,1}, {1,1.0555,1.3888,1.8888,2.2222,2.3888}} \
88      UNITS no_units "Supersonic diameters normalized with Dt vs. axial position normalized with Ld"
89      BOOLEAN dxd_input= FALSE "FALSE, dxd_vs_L = weighting function for div. mesh size distribution.
            TRUE, normalised node lengths vs node number"
90      TABLE_1D dxd_vs_L = {{ 0,0.6,1}, { 1,1,1}} \
91      UNITS no_units "Weighting function for supersonic mesh size distribution or normalised node
            lengths vs node number"
92      REAL AR_sup = 10   UNITS no_units "Nozzle exit/throat area ratio: 0, no Dd_vs_L profile
            modification"
93      REAL c_sf = 0      UNITS no_units "Summerfield coefficient; = 0, no Summerfield correction"
94      REAL cond = 10     UNITS u_W_K  "Chamber to cavities conductance"
95      REAL capa = 500    UNITS u_J_K  "Chamber to cavities heat capacity"
96      REAL GAM_ini = 1.3  UNITS no_units "Initial gamma value, only to initialise nozzle conditions"
97      REAL starter_y[Powder_gases] = {0.26, 0.19, 0.07, 0.21, 0.27, 0} UNITS no_units "Mass fractions -
            H2O,CO,CO2,N2,H2,He- of the starter gases"
98      REAL Floc[1,3]= {{0,0,0}}  UNITS u_m  "Location wrt the Mechanical Reference Frame centre O --i.e
            . wrt launcher interface at point O--"
99      REAL Forient[1,3]={{0,0,1}} UNITS no_units "Vector orientation not necessarily normalised"
100     REAL K_u = 0.25        "AUSM velocity diffusion term coeff. for interface pressure"
101     REAL K_p = 0.75        "AUSM pressure diffusion term coeff. for interface Mach"
102     --REAL sigma = 1         "AUSM pressure diffusion term param. for interface Mach"
103     ENUM Limiter lim = MinMod  "Limiter used"
104     ENUM Order order = first  "Precision order in the reconstruction"
105
106     REAL zeta_canal = 2.28 UNITS "-"
107     REAL D_canal = 0.008 UNITS "m" "Diameter of injection canal"
108     REAL D_ori = 0.006 UNITS "m" "Diameter of injection orifice"
109     REAL L_SIcanal = 0.2 UNITS "m" "Length of injection canal"
110     REAL L_SIori = 0.05 UNITS "m" "Length of the injection canal in divergent nozzle part"
111     REAL p_outlet = 10000 UNITS "Pa" RANGE 0,Inf "exit pressure at outlet orifice"
112     REAL th_canal = 0.005 UNITS "m" "Thickness of wall between chamber and SITVC canal"
113     REAL Amp = 1 UNITS "-" "Amplification factor of side injection"
114     DECLS
115     REAL F_i UNITS "N" "Pure injection momentum"
```

```
    REAL F_s UNITS "N" "Amplified side force"
    REAL m_i UNITS "kg/s" "Injection mass flow"

    TOPOLOGY

    COMB_CHAMBERS.ProdMixer_Tee (
    burnerGasesOptionP1 = burnerGasesOptionP1,
    burnerGasesOptionP2 = burnerGasesOptionP2
    ) Manifold (
    P_o = P_o,
    T_o = T_o,
    Vo = V_cav_red,
    L = L_red_manifold,
    Pw = 0,
    z_bottom = 0,
    rug = rug,
    fld_add = 0,
    mat = mat,
    th = th_manifold,
    rho_w = rho_w,
    cp_w = cp_w,
    Aout = A_inj_red,
    zeta_out = zeta_inj_red,
    Re_lam = Re_lam
    )

    COMB_CHAMBERS.CombustChamberNozzle (
    GasLiqOption = GasLiqOption,
    hc_correl = hc_correl,
    rateOption = rateOption,
    scheme = scheme,
    Inj_redGases = FLUID_PROPERTIES.Chemicals,  --always a chemical when downstream of a mixer
    Inj_oxyGases = burnerGasesOptionP3,
    Nsub = Nsub,
    Nsup = Nsup,
    nozzle_type = nozzle_type
    ) Thruster (
    P_o = P_o,
    T_o = T_o,
    P_ch = 100000,
    T_ch = 300,
    Tcav_oxy = T_o,
    Tcav_red = T_o,
    x_nco = x_nco,
    A_inj_oxy = A_inj_oxy,
    A_inj_red = A_inj_red,
    zetaf_inj_oxy = zeta_inj_oxy,
    zetaf_inj_red = 0.0001,
    V_cav_oxy = V_cav_oxy,
    V_cav_red = V_cav_red,
    emiss = emiss,
    Lrad = Lrad,
    tau_v = tau_v,
    tau_c = tau_c,
    tau_b = tau_b,
    D_dr_fu = D_dr_fu,
    D_dr_ox = D_dr_ox,
    MR_ini = MR_ini,
    MR_min = MR_min,
    MR_max = MR_max,
    frozen_th = frozen_th ,
    frozen_nz = frozen_nz ,
    Rcurv = Rcurv,
    eta = eta_c,
    Eta = eta_nz,
    K_hc = K_hc,
```

```
    Lc = Lc,
    Dt = Dt,
    Dc_vs_L = Dc_vs_L,
    dxc_input = dxc_input,
    dxc_vs_L = dxc_vs_L,
    Ld = Ld,
    Ld2 = Ld2,
    Dd_vs_L = Dd_vs_L,
    dxd_input = dxd_input ,
    dxd_vs_L = dxd_vs_L,
    AR_sup = AR_sup,
    c_sf = c_sf,
    cond = cond,
    capa = capa,
    GAM_ini = GAM_ini,
    starter_y = starter_y,
    Floc = Floc,
    Forient = Forient,
    K_u = K_u,
    K_p = K_p,
    lim = lim,
    order = order
    )

    COMB_CHAMBERS.Th_barrier (
    Nsub = Nsub,
    Nsup = Nsup
    ) Th_barrier_1 (
    th = th_canal,
    Lc = Lc,
    Dt = Dt,
    Dc_vs_L = Dc_vs_L,
    dxc_input = dxc_input,
    dxc_vs_L = dxc_vs_L,
    Ld = Ld,
    Ld1 = 0,
    Ld2 = L_SIori,   --needs to be tested, length of coating determines length position of SI orifice
         in nozzle
    Dd_vs_L = Dd_vs_L,
    dxd_input = dxd_input ,
    dxd_vs_L = dxd_vs_L,
    AR_sup = AR_sup,
    mat = mat,
    k = k_w,
    rho = rho_w,
    cp = cp_w,
    To = T_o
    )

    FLUID_FLOW_1D.Tube (
    burnerGasesOption = burnerGasesOptionSI,
    AbsorOption = noActive,
    nodes = Nsub + Nsup,
    n_bends = 1,
    scheme = centred
    ) SI_canal (
    num = 1,
    order = first,
    init_option = INIT_PT,
    P_o = P_o,
    T_o = T_o,
    x_o = 0,
    rho_o = 1,
    x_nco = x_nco,
    m_o = m_o,
    rug = rug,
```

```
    k_f = 1,
    k_d = 1,
    fld_add = 0,
    fld_nod = 0,
    alpha_bend = inst_angle,
    R_bend = knee_radius,
    fr_option = FR_tube_1ph,
    ht_option = HT_tube_1ph,
    hc_dat = 1,
    Isent_Correl = FALSE,
    entropy_fix = no_fix,
    entropy_fix_multiplier = 4,
    integration_rule = midpoint,
    dp_correction = FALSE,
    limiter = VanAlbada,
    preconditioner = unprecond,
    reconstructed_variables = primitive,
    central_reconstruction = TRUE,
    source_upwind_smoothing = 0,
    xd_nco = 0,
    Po_nc = 0,
    UserDefSolubData = TRUE,
    A_coef_sol = -521,
    B_coef_sol = 2.3874,
    TI = 0.03,
    Cd = 2,
    Ca = 0.1,
    tau_d = 0.3,
    tau_a = 2,
    Diff_Turb_Factor = 1,
    K_u = 0.25,
    K_p = 0.75,
    L = L_SIcanal,
    D = D_canal,
    D_vs_L = { { 0,0.5,1} ,{ 1,1,1} },
    dx_vs_L = { { 0,0.5,1} ,{ 1,1,1} }
    )

    FLUID_FLOW_1D.Junction (
    burnerGasesOption = burnerGasesOptionSI,
    CV_option = FALSE,
    choked_option = TRUE
    ) SI_junction (
    x_jun = 0,
    y_jun = 0,
    z_jun = 0,
    Gcr_ideal = FALSE,
    Ao =  0.25* PI * D_canal**2,
    zetaf = zeta_canal,
    zetab = 0.0001,
    m_o = m_o,
    Re_lam = Re_lam,
    x_t = 0.65,
    Cv = 0,
    F_p = 1
    )

    FLUID_FLOW_1D.Nozzle (
    burnerGasesOption = burnerGasesOptionSI,
    nodes = 2,
    scheme = centred
    ) SI_Orifice (
    num = 1,
    order = first,
    x_jun_out = 0,
    y_jun_out = 0,
```

```
    z_jun_out = 0,
    L = 0.001,
    D = D_ori,
    D_vs_L = { { 0,1} ,{ 1,1.0001} },
    dx_vs_L = { { 0,1} ,{ 1,1} },
    P_o = P_o,
    T_o = T_o,
    x_nco = 0,
    rug = rug,
    k_f = 1e-05,
    k_d = 1,
    fld_add = 0,
    ht_option = HT_constant,
    hc_dat = 1,
    Isent_Correl = FALSE,
    entropy_fix = no_fix,
    entropy_fix_multiplier = 4,
    integration_rule = midpoint,
    dp_correction = FALSE,
    limiter = VanAlbada,
    preconditioner = unprecond,
    reconstructed_variables = primitive,
    central_reconstruction = TRUE,
    source_upwind_smoothing = 0
    )

    COMB_CHAMBERS.DNode_vec (n = Nsub + Nsup) DNode_vec_1 (To = T_o, C = capa)
    COMB_CHAMBERS.DNode_vec (n = 1) DNode_vec_2 (To = T_o, C = capa)
    COMB_CHAMBERS.DNode_vec (n = 2) DNode_vec_3 (To = T_o,C = 5)
    THERMAL.Insulation (n = 2) Insulation_1

    CONNECT Manifold.fout TO Thruster.f_red
    CONNECT GOX TO Thruster.f_oxy
    CONNECT HG TO Manifold.f2
    CONNECT GH2 TO Manifold.f1
    CONNECT SI_junction.f1 TO SI_canal.f2
    CONNECT Th_barrier_1.tpr_out TO SI_canal.tp_in
    CONNECT SI_junction.f2 TO SI_Orifice.f1
    CONNECT Thruster.np_out TO np_out
    CONNECT Injectant_fluid TO SI_canal.f1
    CONNECT Thruster.tp TO DNode_vec_1.tp_in
    CONNECT DNode_vec_1.tp_in TO Th_barrier_1.tpr_in
    CONNECT Manifold.tp_in TO DNode_vec_2.tp_in
    CONNECT Thruster.tp_inj TO DNode_vec_2.tp_in
    CONNECT tp_inj TO DNode_vec_2.tp_in
    CONNECT tp TO DNode_vec_1.tp_in
    CONNECT SI_junction.meas_out TO meas_out
    CONNECT DNode_vec_3.tp_in TO Insulation_1.tp
    CONNECT DNode_vec_3.tp_in TO SI_Orifice.tp_in

    DISCRETE

    CONTINUOUS
    SI_Orifice.s_pres.signal[1] = p_outlet
    F_i = SI_Orifice.Thrust
    F_s = F_i * Amp
    m_i = SI_junction.m

    END COMPONENT
```